Aus der Klinik für Neurologie mit experimenteller Neurologie
der Medizinischen Fakultät Charité – Universitätsmedizin Berlin

DISSERTATION

RNA-edited glycine receptors in temporal lobe epilepsy

zur Erlangung des akademischen Grades
Doctor of Philosophy (PhD)

vorgelegt der Medizinischen Fakultät
Charité – Universitätsmedizin Berlin

Von

Larissa Kraus

aus Gladbeck, Deutschland

Datum der Promotion: 18.09.2020

Contents

1. Abstract

C-to-U RNA editing has been implicated as possibly either adaptive or maladaptive mechanism in temporal lobe epilepsy (TLE), the most common form of focal epilepsy with a persistently high rate of pharmacoresistance, despite an abundance of available antiepileptic drugs. C-to-U RNA-edited glycine receptors (edGlyR) might present a novel drug target for treatment of pharmacoresistant TLE. Previous studies have shown elevated expression of edGlyR in resected hippocampi of TLE patients, which correlated with the degree of hippocampal sclerosis. C-to-U RNA editing of GlyR mRNA leads to a gain of function, resulting in an increased affinity for glycine. edGlyR act predominantly in presynaptic compartments, where they facilitate neurotransmitter release and, depending on neuron type afflicted with edGlyR expression, induce network hyper- or hypoexcitability. C-to-U RNA editing of GlyR mRNA could therefore contribute to seizure generation or represent an adaptive mechanism to decrease hyperexcitability.

The aim of this thesis was to identify specific edGlyR antagonists and investigate their effect on epileptic activity in human brain *ex vivo*, as well as identify the neuronal cell type expressing edGlyR using a novel RNAediting sensor tool in human brain slice cultures. Using high-throughput screening methods and database research, I was unable to identify a specific edGlyR antagonist. However, one of the molecules tested as a potential edGlyR antagonist, dimethylethanolamine (DMEA), has been tested as treatment option for different neurological disorders, although detailed functional mechanisms are still unknown. Here, I showed that DMEA decreased spontaneous activity in primary neuronal cultures and displayed an antiepileptic effect in patient-derived brain tissue *ex vivo*. In addition, I established stable viral mediated expression of the RNA-editing sensor tool in human brain slice cultures and showed neuron-specific expression.

I propose that application of DMEA as well as identification of RNA-editing on single cell level in human brain tissue present valuable tools for the development of novel therapeutic options in patients with pharmacoresistant TLE.

2. Zusammenfassung

C-zu-U RNA-Editierung wurde sowohl als adaptiver als auch maladaptiver Prozess bei Temporallappenepilepsie (TLE) beschrieben. TLE ist die häufigste Form der fokalen Epilepsie, mit einem hohen Anteil an pharmakoresistenten Verläufen, trotz einer Vielzahl an verfügbaren antiepileptischen Substanzen. Einen neuen potentiell antiepileptischen Mechanismus stellen RNA-editierte Glyzinrezeptoren (edGlyR) dar. Hippocampi von Patienten mit pharmakoresistenter TLE zeigen eine Überexpression von edGlyR mRNA, welche mit der Schwere der Hippocampus-Sklerose korreliert. C-zu-U RNA-Editierung der GlyR mRNA führt zu einem Funktionsgewinn und zu einer erhöhten Affinität für Glyzin. edGlyR wirken überwiegend präsynaptisch, wo sie die Freisetzung von Neurotransmittern erhöhen und bedingt durch die Lokalisation auf inhibitorischen oder exzitatorischen Neuronen zu einer verstärkten oder verminderten neuronalen Erregbarkeit führen. Die C-zu-U RNA-Editierung der GlyR mRNA könnte daher zur Anfallsgenerierung beitragen oder einen adaptiven Mechanismus zur Verringerung der Übererregbarkeit darstellen.

Ziel dieser Arbeit war es, spezifische edGlyR-Antagonisten zu identifizieren und ihren Einfluss auf epileptische Aktivität im humanen Gehirn *ex vivo* zu untersuchen sowie mit Hilfe eines RNA-Editierungssensors das Expressionsmuster von edGlyR auf Einzelzellebene in humanen Hirnschnittkulturen zu identifizieren. Weder mittels high-throughput Screening noch strukturbasierter Datenbankanalyse konnten jedoch in dieser Arbeit spezifische Antagonisten für edGlyR identifiziert werden. Eine der getesteten potentiellen edGlyR Antagonisten, Dimethylethanolamin (DMEA), wurde bereits in diversen präklinischen und klinischen Studien als Therapie für neurologische Erkrankungen getestet, jedoch ohne detailliertes Wissen über den Wirkmechanismus. In dieser Arbeit konnte ich zeigen, dass DMEA die spontane Aktivität von primären neuronalen Kulturen reduziert sowie antiepileptische Effekte in reseziertem humanem Hirngewebe von TLE Patienten aufweist. Zudem konnte ich eine stabile viral-vermittelte Expression des RNA-Editierungssensors spezifisch in Neuronen von humanen Hirnschnittkulturen zeigen.

Die Anwendung von DMEA als antiepileptische Substanz sowie die Identifizierung von RNA-Editierung auf Einzelzellenebene stellen essentielle Werkzeuge für die Entwicklung neuartiger antiepileptischer Therapieansätze für Patienten mit pharmakoresistenter TLE dar.

3. Introduction

Epilepsy is a life-altering neurological disorder affecting up to 1% of the world population[1,2]. Epilepsy types can be classified as generalized or focal by the type of seizure onset; generalized seizures show an onset in networks of both hemispheres whereas focal seizures originate from one hemisphere[3]. 30-40% of patients diagnosed with focal epilepsy develop pharmacoresistance and do not respond to currently available antiepileptic drugs (AEDs) despite treatments with multiple AEDs at high dosages[4].

Ketogenic diet and deep brain stimulation have been investigated in detail as alternative therapies to reduce seizure burden in such patients[5–7]. Ketogenic diet is mostly effective in children, and is also able to reduce seizure frequency in adults, but this approach is not standard of care for adult epilepsy patients[8,9]. Deep brain stimulation is still part of ongoing investigations, as it has been shown to be promising in terms of seizure reduction in patients with pharmacoresistant epilepsy[10]. Nevertheless, selection of targeted brain regions and prospective trials are still lacking. Finally, surgical resection of the epileptic focus is a successful treatment option[11,12]. 60-70% of resected patients have a positive outcome with seizure freedom or substantial reduction of seizure burden (International League Against Epilepsy Outcome Scale 1-2), while no effective therapy exists for the remaining patients[13]. Given these numbers, it is of vital importance to investigate new treatment options against focal pharmacoresistant epilepsy.

In temporal lobe epilepsy (TLE), the most common form of focal epilepsy in humans[14], RNA-editing has been suggested as a key mechanism during epileptogenesis. RNA editing is a posttranscriptional modification that results in sequence changes of RNA transcripts and thus increases the transcriptome size[15,16]. Upregulation of RNA editing in TLE has been described for several targets[17–20]. In a mouse model of TLE, RNA editing of epilepsy-related genes was not only upregulated but also positively correlated with seizure frequency[17], indicating the functional relevance of this mechanism.

Glycine receptor (GlyR) RNA was previously identified as a target of RNA editing in TLE[18,21]. Upregulation of C-to-U RNA editing of GlyR was demonstrated in resected hippocampal tissue of TLE patients, and the degree of editing positively correlated with the degree of hippocampal sclerosis[18]. On a functional level, C-to-U edited GlyR (edGlyR) display increased affinity for glycine[18,21] and an altered presynaptic function. Similar to presynaptically expressed unedited GlyR or GABAR, edGlyRs are considered to contribute to changes of network excitability in epilepsy due to high chloride concentration in the presynaptic compartment[22–25]. Here, edGlyR facilitate neurotransmitter release resulting in increased neuronal gain and, depending on the neuron type afflicted with edGlyR function, network hyper- or hypoexcitability[19,26]. As demonstrated in neuron type-specific mouse models[19,26], edGlyR function in glutamatergic neurons leads to increased network excitability and cognitive dysfunctions whereas their function

in parvalbumin-positive GABAergic interneurons decreases network excitability and facilitates persistence of contextual fear memory. Thus, depending on the neuronal cell type involved, RNA editing of GlyR could increase or decrease seizure threshold in TLE. To test this hypothesis, specific tools that analyze edGlyR expression patterns are required.

Unedited GlyRs have been investigated as possible antiepileptic targets in the past. Kirchner et al. (2003) reported bimodal effects of glycine on epileptic activity *in vitro*: while high concentration of glycine increased frequency of epileptic activity, low concentrations delayed its onset[27]. The opposite was reported by Chen et al. (2014), who observed that 100 µM glycine attenuate epileptic activity by activation of somatodendritic GlyR and enhanced tonic inhibition, but 10 µM enhance epileptic activity presumably by activation of presynaptic GlyR expressed at glutamatergic terminals[28]. In a different approach, increase of endogenous glycine concentration by pharmacological block or genetic ablation of the sodium/chloride/glycine symporter GlyT1 resulted in a decrease of acute and chronic seizure activity in rodent models of TLE[29]. Irrespective of the reported effects, clinical application of glycine for antiepileptic purposes is limited, as it would also affect GlyR mediated inhibition in the spinal cord and brain stem. Even more importantly, regulation of endogenous glycine is not expected to affect spontaneous edGlyR activity[19]. Thus, in patients with TLE, rather specific edGlyR modulation might be effective.

The aim of my thesis was to identify and characterize specific edGlyR antagonists in cell culture experiments and investigate their effect regarding seizure-like activity in human epileptic tissue *ex vivo.* In addition, I aimed to establish a RNA-editing sensor tool in human brain slice culture with the goal to identify RNA-editing competed neurons on single cell level.

4. Material and Methods

HEK 293T cell culture and transfection

Human embryonal kidney-derived cells (HEK293T) were maintained in DMEM (Invitrogen, Carlsbad CA, USA) supplemented with 10% fetal bovine serum (Biochrom) and penicillin (100 U/ml) / streptomycin (100 mg/ml) (Invitrogen, Carlsbad CA, USA) and cultured at 37°C, 5% CO_2 in a humidified incubator.

For high-throughput screening, cells were transfected with a total of 4 µg cDNA per 6 cm dish using 25 µl PolyFect transfection reagent (Qiagen, Hilden, Germany) according to the manufacturer's instructions. HEK cells were co-transfected with GlyR subunits and chloride indicator YFPI152L (ratio 1:1). 24 h after transfection 2.5x 10^4 cells were plated into each well of a transparent 96-well plate (TPP) and fluorescence imaging experiments were carried out on the following day[30].

For patch clamp experiments, HEK cells were transfected with a total of 1 µg GlyR α2 or α3 coding plasmid DNA using FuGENE® HD transfection reagent (catalog no. 04 709 705 001, Roche Applied Science) according to the manufacturer's instructions. GlyR α2 constructs were cotransfected with 0.1 µg of an N1-EGFP-containing plasmid. On the following day, HEK293T cells were seeded onto polyornithine-coated glass coverslips (diameter 13 mm, Hecht Assistant, Germany; 0.1% poly-dl-ornithine hydrobromide, catalog no. P8638-100MG, Sigma). Before electrophysiological recordings cells were allowed to adhere for at least 1 h.

Primary rat hippocampal neuronal cell culture

Primary neuronal cell cultures were prepared from E18 Wistar rat embryos as previously described[19]. Permit was given by the Animal Care Committee of the Technical University Braunschweig (Zentrale Einrichtung für Tierhaltung der TU Braunschweig, §4 10.15.M TSB TU BS). Cultures were maintained in Neurobasal medium supplemented with B27 and 1% FCS and subjected to whole cell patch clamp analysis at DIV13-16 to ensure that the cultures were mature enough to display synaptic activity[31].

High-throughput screening HEK 293T cells

Approximately 1 h prior to experiments, culture medium was replaced by 50 µl control solution, containing (in mM): NaCl (140), KCl (5), $CaCl_2$ (2), $MgCl_2$ (1), HEPES (10), and glucose (10) (pH 7.4, NaOH). The 96-well plates were placed onto the 3D printed motorized stage of an in house-built imaging system including an autosampler for liquid handling (HTS PAL, CTC Analytics, Switzerland), an inverted digital fluorescence microscope (Thorlabs, USA) with 10x objective (Olympus, Japan), CCD camera (Point Grey Research Inc., USA) and LED light source (LUMITRONIX, Germany). Cells were imaged in 50 µl control solution (control image) and again 8 sec after injection of 100 µl test solution (test image). Test solution was automatically

applied and contained (in mM): NaI (140), KCl (5), $CaCl_2$ (2), $MgCl_2$ (1), HEPES (10), glucose (10) (pH 7.4, NaOH). To determine EC50 of all tested glycine subunits in our experimental setup the applied test solution contained increasing concentrations of glycine. The fluorescence signal of identified cells was measured in control and test images as the mean of all pixel values within the area of a cell. '% fluorescence quench' in chloride imaging experiments was defined as

$$\%\text{fluorescence quench} = (F_{init} - F_{final}) * 100 / F_{init}$$

where F_{init} and F_{final} are the initial (of control image) and final (of test image) values of fluorescence, respectively[30,32].

For high-throughput screening experiments, control solution was supplemented with compounds of the NIH Clinical Collection small molecule compound libraries (I & II) and test solution was supplemented with identified EC50 for the each GlyR subunit from the prior experiment. All drugs were diluted from stocks at the day of the experiment and added in a final concentration of 10 µM. All experiments were conducted at room temperature.

Whole cell patch clamp recordings

For whole cell patch clamp recordings in HEK cells and cultured neurons, pipettes were made from borosilicate glass (Science Products, Hofheim, Germany), with a resistances of 4-7 MΩ and filled with the intracellular solution containing (in mM): CsCl (130), NaCl (5), CaCl2 (0.5), MgCl2 (1), EGTA (5) and HEPES (30), pH 7.2 (CsOH). Extracellular solution was supplied by gravity using a perfusion pencil (Automate Scientific, Inc. Berkeley, USA) for fast solution exchange. HEK cells were perfused with extracellular solution E1 containing (in mM): NaCl (140), KCl (5), MgCl2 (1), CaCl2 (2), HEPES-NaOH (10) and glucose (10), pH 7.4 (NaOH). For neuronal experiments, we applied carbongenated aCSF containing (in mM): NaCl (125), KCl (2), MgCl2 (1), CaCl2 (2), NaHCO3 (25), NaH2PO4 (1.25) and glucose (10), pH 7.4. Signals were recoded using a EPC-7 amplifier (List-Medical, Darmstadt, Germany), ITC-18 interface and Patchmaster software (both HEKA, Lamprecht, Germany).

All cells were first clamped at a holding potential of -50 mV. Series resistances (Rs) were monitored by 5 mV voltage pulses (50 ms) applied every 5 s and varied between 20 MΩ and 40 MΩ for HEK293T cells and 10 MΩ and 30 MΩ for cultured hippocampal neurons. Data was acquired with a sampling rate of 20 kHz and filtered at 2.8 kHz. All experiments were carried out at 24°C.

HEK cells were visualized using a Zeiss Axioscope 10 (Carl Zeiss, Jena, Germany) equipped with a 40x objective, a custom made eGFP filter set (Chroma Technology GmbH), an Uniblitz electronic shutter and a Spot Pursuit 2 M pixel monochrome CCD camera. HEK cells were recorded in voltage clamp mode for recording of current responses to glycine application (1 mM for unedited GlyR, 100 µM glycine for the edGlyR). Potential antagonists (DMEA, sarcosine and

methylamine hydrochloride, all from Sigma-Aldrich Sigma-Aldrich, Munich, Germany) were added to E1 and co-applied with glycine to record dose-response curves (0.1 mM to 50 mM of the tested molecule). The following sequence was applied to test effects on glycine mediated currents: 5 s glycine, 5 s glycine + test molecule, 5 s glycine, following wash out for 45 s with E1, before additional applications. In this way, the tested molecules were applied during steady state phase of glycine evoked currents. DMEA increases pH of extracellular solutions, therefore recordings with and without adjusting pH using 100% acetic acid (final pH 7.4) were performed.

The effect of DMEA on spontaneous neuronal activity was tested in current clamp mode, and membrane potentials were held around -50 mV by steady current injection, which never exceeded 150 pA. DMEA was applied for 60 s to investigate effects on spontaneous activity, following 3-5 min wash-out with aCSF before stepwise increase of DMEA concentration (0.5, 2, 5 or 10 mM). Action potential (AP) threshold was investigated by short current injections of 10 pA steps with or without application of DMEA. AP threshold was determined as the mean of the minimum membrane potential necessary for AP generation and membrane potential of the previous step current[31].

Human tissue transport and preparation for acute recordings

Human hippocampal tissue was collected from 12 TLE patients, who all gave written consent prior to the procedure. Experiments were approved by the Ethics Committee of Charité-Universitätsmedizin Berlin on 01.11.2014 (EA2/111/14) and performed in agreement with the Declaration of Helsinki. For details on tissue transport and preparation, see Kraus et al., 2019[31]. Shortly, tissue was transported from the operation room in chilled carbogenated transport solution and cut to 400 µm slices using a vibratome (Leica VT1200S, Wetzlar, Germany) for minimal tissue damage. Slices were stored in an interface chamber and continuously perfused (1.6 ml/min) with carbogenated aCSF (32°C) until recording.

For electrophysiological recording, slices were transferred to submerged-type recording chamber with high flow rates (10 ml/min) to assure optimal oxygenation and drug application. Epileptic activity was induced by elevation of KCl concentration to 8 mM and application of K-channel blocker 4-aminopyridine (4-AP, 100 µM, Sigma, Munich, Germany). Epileptiform activity was recorded for at least 20 min before 20 min of drug application, following 20 min wash out. For control of hyperosmotic effects, the recording sequence stated above was modified and consisted of the following steps: 1) baseline with stable epileptiform activity (≥ 10 min); 2) 10 mM sucrose (≥ 20 min), 3) wash-out sucrose (≥ 10 min), 4) 10 mM DMEA (≥ 20 min), 5) wash-out DMEA (≥ 20 min). Applied substances were the following: DMEA (Sigma-Aldrich, Munich, Germany), lacosamide (100 µM, Biozol, Eching, Germany), sucrose (10 mM, Sigma-Aldrich, Munich, Germany)[31].

Human organotypic brain slice cultures and AAV transduction

Tissue preparation was performed at the Cortex & Epilepsie group of Richard Miles at the Inserm, Paris. Human cortical slice cultures were prepared from surgically excised tissue blocks of human temporal lobe and peri-tumoral or dysplasic cortex. All patients gave their written, informed consent and procedures were approved by the Comité de protection des personnes, Ile de France 1 (C16-16, 20152482) and the Consultatif National d'Ethique.

For details on transport and tissue preparation, see Le Duigou et al, 2018[33]. Shortly, tissue was transported and sliced to 300 µm slices in chilled, carbogenated sucrose aCSF. After cutting, slices were washed in carbogenated Hanks balanced salt solution (HBSS, Invitrogen, Carlsbad CA, USA) with 20 mM HEPES (Invitrogen, Carlsbad CA, USA) for 15 min at room temperature. Preparation was performed under sterile conditions to prevent contaminations. Slices were finally placed on cell culture insert (30 mm, Merck-Millipore, Darmstadt, Germany) in a 6-well plate with 1 ml of organotypic slice culture medium (OSCM) with 20 mM HEPES. OSCM was prepared according to previous publication[34] and contained various added substances as well as Antibiotic-Antimycotic mix (Invitrogen, Carlsbad CA, USA). OSCM was exchanged after 1 h to OSCM without HEPES and exchanged daily. Antibiotics were omitted from OSCM after one week. Slices were cultured in humidified incubator with 5% CO2 at 37°C.

Adeno-associated virus (AAV) transduction of RNAed sensor (fusion protein with mCherry, for details on plasmid see Kankowski et al., 2018[35]) was performed on the day of culture preparation (day in-vitro 1, DIV-1). AAV was applied in small drops on top of the slices using a micro-pipette to cover the whole slice.

Antibody staining and microscopy

For immunohistochemistry, cultured human slices were fixed for 24 h in 4% paraformaldehyde in phosphate buffered saline (PBS, pH 7.3) at 4°C before transfer to a 30% sucrose in PBS overnight. Following 3 freeze-thaw cycles using dry ice, slices were incubated in blocking solution (PBS, 10% normal donkey serum, 0.5% Triton X-100, 2% milk powder) for 2 h. Slices were stained with NeuN (Millipore MAB377, monoclonal, mouse, dilution 1:250) primary antibody 48 h at 4°C, followed by several washing steps in PBS and overnight incubation at 4°C with donkey-anti-mouse Alexa Fluor 488 (dilution 1:500; Invitrogen, Carlsbad CA, USA) secondary antibody. Sections were counterstained with the nuclear stain DAPI (10 µg/ml, 15 min) and mounted on glass slides with ProLong Gold Antifade Reagent (Life Technologies, Carlsbad CA, USA).

Confocal images were acquired with an inverted confocal laser scanning microscope LSM700 (Zeiss, Oberkochen, Germany). Z-stacks were acquired with 0.5 µm lateral and 4 µm axial pixel size to identify individual nuclei and cells. A 405 nm laser (set at 2%) was used for excitation of DAPI. A 639nm laser (set at 2.9%) was used for detection of NeuN (Cy5). A 555 nm laser (set at 3%) was used for excitation of mCherry.

Data analysis and statistics

Toxfinder data of high throughput screening were annotated in Microsoft Excel and analyzed using Origin 7 G (OriginLab Corporation, Northampton MU, USA)[30].

Electrophysiological data recorded in HEK cells and primary neuronal cell cultures was quantified and measured using an IGOR Pro (Version 6.3.7.2, Wavemetrics Inc., Oregon, USA) procedure written by Dr. Marcus Semtner (MDC Berlin) and the extension PatchersPowerTools[31].

For analysis of human recordings, signals were band pass filtered (1-1000 Hz) and last 5 min of each application (300 s of each application phase) were analyzed with Clampfit 10.7 threshold analysis (Molecular Devices, Sunnyvale, CA, USA). All events visually identified as burst activity (defined by biphasic, positive and negative deflection and a duration ≥ 100 ms) were manually indicated for further analysis of event frequency (inter-event-interval, IEI), amplitude and total number of events during the analyzed time frame[31]. Interictal spikes (defined by exclusive negative deflections and a duration <10 ms) were not analyzed. According to literature, interictal spikes, although pathologically relevant, are not significantly affected by AEDs[36,37].

Data of patch clamp and field potential recordings were analyzed with GraphPad Prism 5 (GraphPad Software, Inc., San Diego, CA, USA). Data were subjected to D'Agostino and Pearson omnibus normality test and analyzed accordingly. In cases where sample size of tested groups was too small for evaluation of data distribution, data was analyzed using non-parametric tests[31]. Details on statistical analysis are described in Kraus et al (2019)[31].

5. Results

Screening for potential edGlyR antagonists (Schneidereit et al., 2017[30])

To identify specific edGlyR antagonists, I performed a high-throughput screening with a fluorescence-based approach using a chloride-sensitive dye in HEK293T cells overexpressing unedited GlyR or edGlyR[38,39]. I used the NIH Clinical Collection small molecule compound libraries (I & II) to test approximately 800 substances for their antagonist potential against edGlyR. Although in this first screening line I was unable to validate promising candidates for edGlyRs (data not shown or published), we were successful in developing a novel, low-cost pharmacological screening tool based on an in house-build automated XY-stage. We published a detailed description and instructions for easy reproducibility[30].

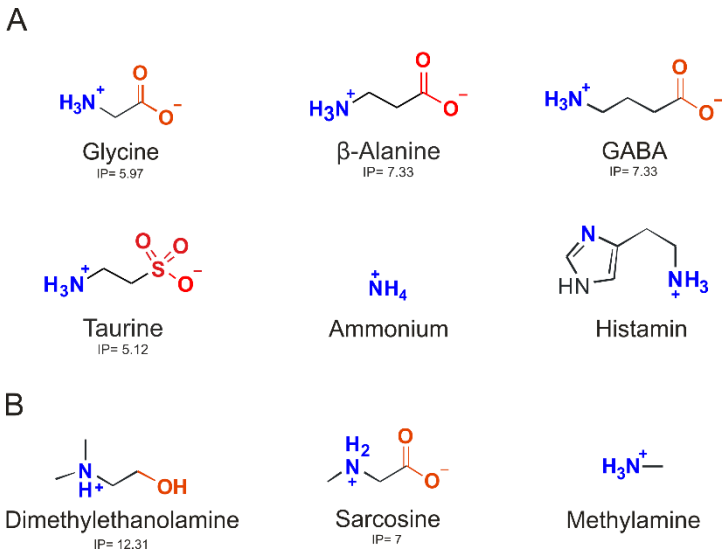

Figure 1 Structures of known and possible ligands for edGlyR
Selected ligands and possible edGlyR targets including positive and negative charges. Carboxyl and ethyl groups are marked in red. Ammonium is marked in blue. (A) Substances known to act on edGlyR. (B) Candidates for antagonists of edGlyR: dimethylethanolamine, sarcosine and methylamine. IP: isoelectric point.

While library screens have the advantage to cover a broad spectrum of possible ligands, they do not focus on structural similarities of derivatives of known ligands. In a next step, we therefore compared chemical structures of GlyR agonists and antagonists (Fig. 1A). More specifically, glycine, β-alanine, taurine, GABA, and ammonium are known agonists of GlyR or edGlyR[35,40,41], whereas histamine was recently identified as an inverse agonist of GlyR and edGlyR[42]. We considered three substances that shared similarities to, and exhibited differences with, known edGlyR agonists or antagonists: dimethylethanolamine (DMEA), sarcosine and methylamine (Fig. 1B).

To test the correlation between structural similarities of potential edGlyR ligands and their function, we assessed the effects of DMEA, methylamine and sarcosine on edited and non-edited GlyR currents. For this purpose, we performed whole-cell patch clamp recordings in HEK293T cells overexpressing edited and non-edited homomeric α2B or α3L GlyR, which are prevalent edGlyR variants in TLE[18]. In all investigated cells, glycine evoked stable current responses with a peak and a steady-state current component (Fig. 2). During the steady state phase of glycine-evoked currents, application of up to 25 mM sarcosine or methylamine did not affect GlyR or edGlyR activity, independently of the tested subunit (data not shown), suggesting that these two compounds do not act as GlyR ligands. For both unedited and edited GlyR α3L and GlyR α2B 5-10 mM DMEA was able to inhibit glycine evoked currents (Fig. 2).

Since application of DMEA increased pH of our HEPES buffered extracellular solution (10mM DMEA corresponds to ~pH 10), I performed additional experiments with physiological pH 7.4 using saturating concentrations of DMEA. I found that our initial effect on GlyR and edGlyR currents was purely pH dependent, as application of DMEA at physiological pH did not affect GlyR or edGlyR currents (Fig. 2).

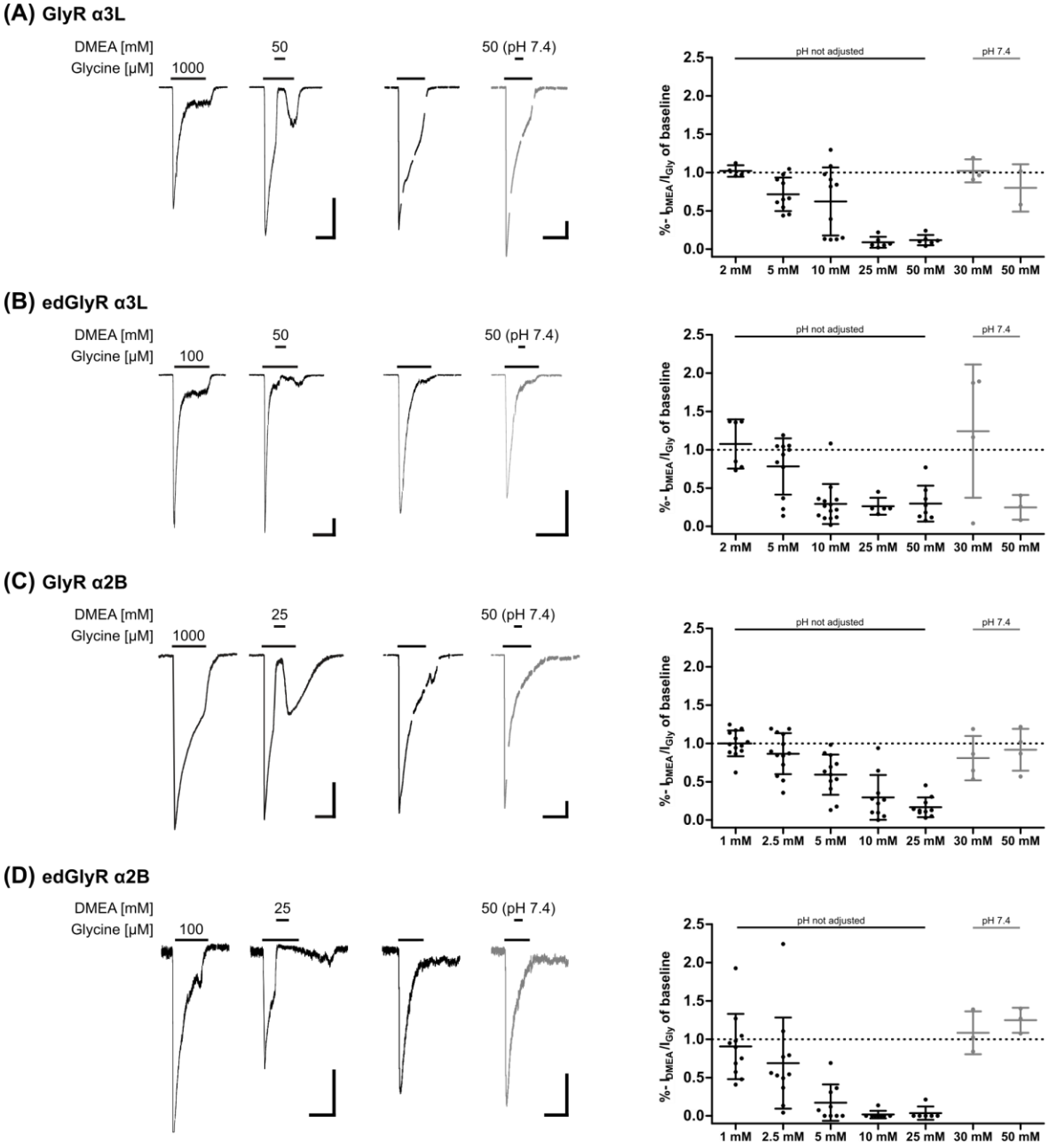

Figure 2: Effect of DMEA on activation of unedited and edited GlyR by glycine.
Activation of all tested edGlyR subunits was blocked by high concentrations DMEA only when pH was not adjusted. Adjusting pH of extracellular solutions containing DMEA to pH 7.4, abolished effects on glycine evoked currents in most of the GlyR subunits. **(A-D, left)** Example traces from patch-clamp recordings in HEK cells overexpressing unedited GlyR α3L **(A),** edGlyR α3L **(B)**, unedited GlyR α2B **(C)** or edGlyR α2B **(D)**. **(A-D, right)** Ratio of current amplitude before and at the end of DMEA application was normalized to ratio of current amplitude without DMEA application (baseline, only glycine) in the same cell. DMEA was applied during steady state of GlyR activation by glycine. Scale bars: 0.5 nA, 10 s. mean ± SEM; data is purely descriptive and no statistical analysis was performed due to low n in some of the experimental groups. Experiments without adjusted pH were performed by Nikolai Dorka (TU Braunschweig, Lab of Prof. Jochen Meier, TU Braunschweig, Germany), control experiments with adjusted pH and data analysis of all experiments were performed by me.

Effects of DMEA in neuronal cultures and resected human brain tissue (Kraus et al., 2019[31])

DMEA has been applied as therapy for different neurological disorders, though molecular targets are still unknown[43–48]. We therefore continued to investigate in more detail functional mechanisms of DMEA action, although we could not confirm the antagonist effect of DMEA on edGlyR currents.

We first analyzed DMEA effects in primary neuronal cell cultures, to investigate, 1) whether DMEA affects spontaneous neuronal activity and 2) affects intrinsic properties of neurons (see Fig. 1 of Kraus et al., 2019[31]). Using a buffered solution at a pH of 7.4, we observed a decrease of spontaneous neuronal activity without affecting the resting membrane potential (RMP), the latter suggesting little effect on intrinsic properties of neurons. We showed full block of spontaneous activity at 2 mM DMEA without increased effect at higher concentrations. Due to this promising effect on neuronal activity, I investigated potential antiepileptic effects of DMEA in resected human brain tissue of TLE patients.

To investigate DMEA effects on epileptiform activity in resected human brain tissue, I first established stable recording conditions for human hippocampal brain slices in our experimental setup with a novel submerged type recording chamber. Application of 8mM K^+ and 4-AP induced two types of activity: interictal spikes and burst activity. Since interictal spikes are considered to be insensitive to established antiepileptic drugs, I focused my analysis on burst activity. I was able to show fast induction of burst events, which were stable for long periods and in addition sensitive to the clinically approved AED lacosamide. Using this established recording procedure, I then investigated effects of 5 and 10 mM DMEA on epileptiform activity. I found 5 mM to show only a mild effect compared to 10 mM DMEA in tissue of the first six patients and continued to apply only 10 mM DMEA in tissue of the following five patients[31]. DMEA showed heterologous effects on burst activity, ranging from no effect to a full block of activity in three patients. Overall, DMEA significantly decreased the number of burst events exhibiting antiepileptic effects in most slices (see Fig. 4A of Kraus et al., 2019[31]).

C-to-U RNA editing tool in human brain slice cultures (Le Duigou et al., 2018[33])

edGlyR function can have a bimodal effect on the neuronal network, depending on neuronal cell type inflicted with edGlyR expression[19,26]. Unfortunately, so far little is known about the expression pattern of edGlyR in TLE patients. To further investigate C-to-U RNA editing on single cell level, I aimed to apply a recently developed RNA-editing sensor (RNAed sensor) tool to human organotypic brain slice cultures of TLE patients. The RNAed sensor is capable of identifying C-to-U RNA editing on a single cell basis and has been established for cell culture and primary neuronal culture systems [35]. In cells capable of C-to-U RNA editing, the sensor element will be edited to a stop codon. Once the stop codon is introduced to the sequence, the dominant cytosol-trafficking sequence is no longer synthesized, leading to translocation of the reporter

protein mCherry to the nucleus by the now dominant nucleus targeting domain. For successful expression of our RNAed sensor, we used an AAV2/9 viral system for transduction of human brain slices. In cooperation with Prof. Richard Miles, I analysed neuronal specificity of our viral system in human organotypic brain slice cultures (see suppl. Fig. 1F of Le Duigou et al., 2018[33]). In the first set of experiments, I was able to show specific neuronal expression of the RNAed sensor in human neurons as visible by co-localization of neuronal marker NeuN and mCherry expression.

This proof of principle work will enable the use of the RNAed sensor tool to better understand mechanisms of C-to-U RNA editing in TLE on single cell level in future experiments.

6. Discussion

Focal epilepsy is pharmacoresistant in 30-40% of patients[4], and all new AEDs which had been developed over the last decades did not result in seizure freedom in these patients. Despite the abundance of > 20 AEDs, pharmacoresistance in TLE remains a challenge and therefore calls for the development of new, individual therapeutic options.

In the present thesis, I focused on edGlyRs as a potential novel target for individual antiepileptic therapy. Using high-throughput screening methods and structural analysis of known GlyR ligands, I identified three possible edGlyR antagonists: methylamine, sarcosine and DMEA. While neither methylamine nor sarcosine showed any effects on GlyR or edGlyR currents in a heterologous expression system, DMEA decreased glycine evoked currents of unedited and edGlyR in a concentration-dependent manner. Further control experiments revealed a decrease of GlyR activity indirectly by increase of pH affecting cell viability rather than by specific function of DMEA on GlyR. Independently of the non-specific effect of DMEA on edGlyR currents, we continued to investigate DMEA as a potential antiepileptic molecule. Indeed, DMEA had been investigated as a therapy for different neurological diseases in the past[43–45,47,48], without detailed knowledge on specific targets of action.

DMEA shares structural similarities with choline and was first hypothesized to be a precursor for acetylcholine (ACh). *In vivo* experiments indeed showed that DMEA increases plasma and brain choline, though brain ACh levels remained unaffected[49,50]. The proposed correlation of DMEA to the cholinergic system had led to multiple clinical trials, in which DMEA was tested as treatment for tardive dyskinesia (TD)[43,44,47]. Later, systematic reviews could not confirm positive effects of DMEA or other cholinergic compounds in patients with TD[46,51], questioning any functional impact of DMEA on the cholinergic system. Surprisingly, in both acute and chronic seizure models, a conjugate of DMEA and valproate was shown to be more potent compared to valproate alone. This may be explained by a DMEA-induced increase in uptake of valproate through the blood

brain barrier[52]. However, Shekh-Ahmad and colleagues did not evaluate the effect of DMEA alone, and until now, targets of DMEA action have not been identified.

We investigated the effect of DMEA on spontaneous activity in untransfected neuronal cultures and on epileptiform activity in resected human brain tissue. Indeed, we were able to show a decrease of spontaneous activity in neuronal cultures while resting membrane potential and action potential threshold remained largely unaffected, suggesting no effect on intrinsic but rather synaptic excitability[31]. In resected human brain tissue, DMEA displayed strong antiepileptic effects in the majority of investigated human slices, including a full block of epileptiform activity in slices of three out of 11 patients. The observed complete block of activity could not be reproduced in tissue of all patients, implying differences in expression patterns of molecular DMEA targets among patients.

In this thesis, I was unable to identify targets of DMEA action, though due to above-mentioned similarities with ACh and choline, M2 and M3 muscarinic ACh receptors (mAChRs) present potential targets. Choline and Ach have both been identified as M2 and M3 ligands[53,54]. The $G_{ßγ}$-subunit of M2 and M3 mAChRs increases the open probability of G-protein coupled inwardly rectifying potassium (GIRK) channels, specifically GIRK1 and GIRK4 subunits[55]. Both GIRK1 and GIRK4 are expressed in the hippocampus[56–58] and activation of GIRK was described to have anticonvulsant effects *in vitro* and *in vivo*[59]. For these reasons, M2 or M3 mAChRs and GIRK channels present a possible mechanism for DMEA action and will have to be investigated in more detail in future experiments.

DMEA has been tested in healthy volunteers as well as patients suffering from different neurological disorders. First application of DMEA to human healthy volunteers dates back to the 1960s, when DMEA was reported to exert stimulating effects comparable to amphetamine[60,61]. Murphree et al. (1960) described improved concentration, increased muscle tone and changed sleeping habits in healthy males (21-26 years) with an intake of 10-20 mg DMEA (or Deanol) daily for 2-3 weeks compared to a placebo group[61]. Though this observation was subjective and the cohort small, they also reported no change in heart rate, body weight, muscle power, hand steadiness or vital capacity. In contrast, two double-blinded, placebo-controlled studies reported side effects of DMEA in TD patients such as lethargy, drowsiness and a mild but significant increase in the schizophrenia score[43,44]. However, a review comparing multiple studies was not able to confirm an increased risk for psychosis in TD patients when treated with DMEA[46]. In addition, severe neurological and cardiovascular side effects (apathy, motor retardation, increased confusion associated with rise in systolic and diastolic blood pressure) were reported in two AD patients when treated with 1,800 mg DMEA daily[48]. In contrast to Murphree et al. (1960)[61], the abovementioned studies reporting severe side effects administered DMEA in a

100fold higher daily dosage (1,000-2,000 mg vs. 10-20 mg). The reported side effects of DMEA application in patients calls for the need to investigate DMEA action in more detail.

Although in this thesis, I clearly demonstrate an antiepileptic effect of DMEA, the applied high concentrations of DMEA, the variability of underlying pathologies and unknown molecular mechanism of action present substantial limitations.

The applied high concentration of DMEA presents two limitations: first, the observed increase of pH in the presented HEK cell experiments. Alkaline shift of pH by 0.2 was reported to increase neuronal hyperexcitabilty, in contrast to antiepileptic effects shown by acidic shift[62]. For this thesis, all experiments in neurons and human tissue were performed using bicarbonate buffered aCSF with a stable pH of 7.4 and a maximum alkaline shift in pH of 0.2. The clear antiepileptic effects of DMEA can therefore not be explained by potential acidic changes of pH. Second, addition of DMEA to our extracellular solution increased osmolarity by up to 10 mOsm, possibly affecting the observed antiepileptic effect. Previous studies have reported a decrease of neuronal excitability and epileptic activity upon application of hyperosmolar solutions (5 mOsm and above). In most cases, 30 mOsm and more was necessary to induce these effects[63–65]. As shown by Rosen and Andrew (1990), an increase of extracellular osmolarity by 10 mOsm might result in a 10% decrease of EPSC amplitude in CA1 pyramidal neurons, though the effects of such EPSC alteration on network activity were not investigated[64]. I was able to show that an increase in osmolarity of the extracellular solution does not result in a decrease of epileptiform activity, indicating that the antiepileptic effects of DMEA are not primarily mediated by changes in osmolarity[31].

Differences in neuronal survival and the degree of hippocampal sclerosis could possibly contribute to the observed interindividual effect of DMEA between patients. Neuronal survival or tissue quality could have been influenced differentially by the transportation solutions (NMDG vs choline-based aCSF). We cannot exclude differences in neuronal survival depending on transport solution, though in all slices included in this project, epileptiform activity was induced within a few minutes following the application of 8mM K^+ and 4-AP and was stable in most slices, indicating no differences in tissue quality between different transport conditions.

Epileptiform activity is highly variable in frequency, spike pattern and amplitude depending on the induction method, recording conditions and recorded brain area. In rodent slices, epileptiform activity can be induced by inhibition of potassium channels by 4-AP alone[66–68]. However, in human brain tissue, only application of 4-AP in combination with electrical stimulation or elevated extracellular potassium was shown to induce stable epileptiform activity[31,69,70]. Gabriel *et al.* (2004) showed a high variability of epileptiform activity between patients, with highest occurrence of seizure-like events in the dentate gyrus of patients with hippocampal sclerosis[69]. In this study by Gabriel and colleagues and in other studies concerning epileptiform activity in resected human

brain tissue, field potential recordings were performed using an interface type recordings chamber[69,71–74]. For this thesis, I recorded field potentials using a modified submerged chamber and observed mostly burst activity (spike and burst activity) described before as interictal-like[69,72,73,75], in contrast to ictal discharges lasting > 10 s recorded in interface type recording chambers. The predictive value of this interictal-like activity for drug development in an *ex vivo* setting is still unclear. Brückner and Heinemann (2000) suggested that only seizure-like ictal activity is sensitive to AED application in brain slices (of non-epileptic animals)[76]. Other studies, however, demonstrated a robust decrease in interictal activity in the hippocampus upon AED application[77–79]. In this thesis, I was able to demonstrate stable induction of the observed burst activity in all recorded slices and a sensitivity of this burst activity to the approved antiepileptic drug lacosamide, indicating that my experimental setting is capable of validating and possibly predicting antiepileptic efficacy for drug development.

In a separate project, I further aimed to investigate the functional mechanisms of edGlyR function on TLE. Considering excitatory and inhibitory neurons as the major neuronal populations, two effects of edGlyR inhibition are possible as suggested recently[80]. In case of excitatory neurons, edGlyR inhibition could lead to a reduced glutamate release and reduction of hyperexcitability, thus acting in an antiepileptic manner[19]. In contrast, inhibition of edGlyR expressed in inhibitory neurons is expected to result in network disinhibition and consequently an increase of epileptic activity[26]. So far, it is not known which neuronal cell type is inflicted with edGlyR expression or how edGlyR contribute to epilepsy onset or epileptogenesis. In this thesis, I established a recently developed C-to-U RNA editing sensor for the use in human organotypic brain slice cultures. I was able to show neuron-specific viral transfection using an AAV2/9 based expression system and a ubiquitous promotor for expression of the RNA-editing sensor tool. The RNA-editing sensor tool can be useful in the future to identify the neuronal cell type inflicted with C-to-U RNA-editing of GlyR mRNA and help to identify the function of edGlyR in TLE in more detail.

The consistently high rate of pharmacoresistance in TLE and the failure of new AEDs in clinical trials increase the need for novel treatment approaches in this common form of epilepsy. Here, I demonstrated antiepileptic properties of DMEA in resected hippocampal tissue from TLE patients, indicating its potential to act as a novel AED. I propose that research focused on possible new antiepileptic mechanisms as well as TLE-associated modification of GlyR-coding gene transcripts can be useful for the identification of affected neuron types in pharmacoresistant TLE and may provide new personalized treatment options against maladaptive neuronal plasticity in TLE.

7. References

1. Ngugi, A. K., Bottomley, C., Kleinschmidt, I., Sander, J. W. & Newton, C. R. Estimation of the burden of active and life-time epilepsy: a meta-analytic approach. *Epilepsia* **51,** 883–90 (2010).

2. Hirtz, D., Thurman, D. J., Gwinn-Hardy, K., Mohamed, M., Chaudhuri, A. R. & Zalutsky, R. How common are the "common" neurologic disorders? *Neurology* **68,** 326–37 (2007).

3. Fisher, R. S., Cross, J. H., French, J. A., Higurashi, N., Hirsch, E., Jansen, F. E., Lagae, L., Moshé, S. L., Peltola, J., Roulet Perez, E., Scheffer, I. E. & Zuberi, S. M. Operational classification of seizure types by the International League Against Epilepsy: Position Paper of the ILAE Commission for Classification and Terminology. *Epilepsia* **58,** 522–530 (2017).

4. Stephen, L. J., Kwan, P. & Brodie, M. J. Does the cause of localisation-related epilepsy influence the response to antiepileptic drug treatment? *Epilepsia* **42,** 357–62 (2001).

5. Dibué-Adjei, M., Brigo, F., Yamamoto, T., Vonck, K. & Trinka, E. Vagus nerve stimulation in refractory and super-refractory status epilepticus - A systematic review. *Brain Stimul.* **0,** (2019).

6. Giordano, C., Marchiò, M., Timofeeva, E. & Biagini, G. Neuroactive peptides as putative mediators of antiepileptic ketogenic diets. *Front. Neurol.* **5,** 63 (2014).

7. Kowski, A. B., Voges, J., Heinze, H.-J., Oltmanns, F., Holtkamp, M. & Schmitt, F. C. Nucleus accumbens stimulation in partial epilepsy-A randomized controlled case series. *Epilepsia* **56,** e78–e82 (2015).

8. Falco-Walter, J. J., Roehl, K., Ouyang, B. & Balabanov, A. Do certain subpopulations of adults with drug-resistant epilepsy respond better to modified ketogenic diet treatments? Evaluation based on prior resective surgery, type of epilepsy, imaging abnormalities, and vagal nerve stimulation. *Epilepsy Behav.* **93,** 119–124 (2019).

9. Hallböök, T., Sjölander, A., Åmark, P., Miranda, M., Bjurulf, B. & Dahlin, M. Effectiveness of the ketogenic diet used to treat resistant childhood epilepsy in Scandinavia. *Eur. J. Paediatr. Neurol.* **19,** 29–36 (2015).

10. Zangiabadi, N., Ladino, L. D., Sina, F., Orozco-Hernández, J. P., Carter, A. & Téllez-Zenteno, J. F. Deep Brain Stimulation and Drug-Resistant Epilepsy: A Review of the Literature. *Front. Neurol.* **10,** 601 (2019).

11. Engel, J., Wiebe, S., French, J., Sperling, M., Williamson, P., Spencer, D., Gumnit, R., Zahn, C., Westbrook, E. & Enos, B. Practice parameter: Temporal lobe and localized neocortical resections for epilepsy. *Contin. Lifelong Learn. Neurol.* **13,** 225–234 (2007).

12. Wiebe, S., Blume, W. T., Girvin, J. P., Eliasziw, M. & Effectiveness and Efficiency of Surgery for Temporal Lobe Epilepsy Study Group. A randomized, controlled trial of surgery for temporal-lobe epilepsy. *N. Engl. J. Med.* **345,** 311–8 (2001).

13. Mohan, M., Keller, S., Nicolson, A., Biswas, S., Smith, D., Osman Farah, J., Eldridge, P. & Wieshmann, U. The long-term outcomes of epilepsy surgery. *PLoS One* **13,** e0196274 (2018).

14. Semah, F., Picot, M. C., Adam, C., Broglin, D., Arzimanoglou, A., Bazin, B., Cavalcanti, D. & Baulac, M. Is the underlying cause of epilepsy a major prognostic factor for recurrence? *Neurology* **51,** 1256–62 (1998).

15. Meier, J. C., Kankowski, S., Krestel, H. & Hetsch, F. RNA Editing-Systemic Relevance and Clue to Disease Mechanisms? *Front. Mol. Neurosci.* **9,** 124 (2016).

16. Tomaselli, S., Locatelli, F. & Gallo, A. The RNA editing enzymes ADARs: mechanism of action and human disease. *Cell Tissue Res.* **356,** 527–532 (2014).

17. Srivastava, P. K., Bagnati, M., Delahaye-Duriez, A., Ko, J.-H., Rotival, M., Langley, S. R., Shkura, K., Mazzuferi, M., Danis, B., van Eyll, J., Foerch, P., Behmoaras, J., Kaminski, R. M., Petretto, E. & Johnson, M. R. Genome-wide analysis of differential RNA editing in epilepsy. *Genome Res.* **27,** 440–450 (2017).

18. Eichler, S. A., Kirischuk, S., Jüttner, R., Schafermeier, P. K., Legendre, P., Lehmann, T.-N., Gloveli, T., Grantyn, R. & Meier, J. C. Glycinergic tonic inhibition of hippocampal neurons with depolarizing GABAergic transmission elicits histopathological signs of temporal lobe epilepsy. *J. Cell. Mol. Med.* **12,** 2848–66 (2008).

19. Winkelmann, A., Maggio, N., Eller, J., Caliskan, G., Semtner, M., Häussler, U., Jüttner, R., Dugladze, T., Smolinsky, B., Kowalczyk, S., Chronowska, E., Schwarz, G., Rathjen, F. G., Rechavi, G., Haas, C. A., Kulik, A., Gloveli, T., Heinemann, U. & Meier, J. C. Changes in neural network homeostasis trigger neuropsychiatric symptoms. *J. Clin. Invest.* **124,** 696–711 (2014).

20. Krestel, H., Raffel, S., von Lehe, M., Jagella, C., Moskau-Hartmann, S., Becker, A., Elger, C. E., Seeburg, P. H. & Nirkko, A. Differences between RNA and DNA due to RNA editing in temporal lobe epilepsy. *Neurobiol. Dis.* **56,** 66–73 (2013).

21. Meier, J. C., Henneberger, C., Melnick, I., Racca, C., Harvey, R. J., Heinemann, U., Schmieden, V. & Grantyn, R. RNA editing produces glycine receptor alpha3(P185L), resulting in high agonist potency. *Nat. Neurosci.* **8,** 736–744 (2005).

22. Jang, I.-S., Nakamura, M., Ito, Y. & Akaike, N. Presynaptic GABAA receptors facilitate spontaneous glutamate release from presynaptic terminals on mechanically dissociated rat CA3 pyramidal neurons. *Neuroscience* **138,** 25–35 (2006).

23. Waseem, T. V. & Fedorovich, S. V. Presynaptic glycine receptors influence plasma membrane potential and glutamate release. *Neurochem. Res.* **35,** 1188–95 (2010).

24. Ruiz, A., Campanac, E., Scott, R. S., Rusakov, D. A. & Kullmann, D. M. Presynaptic GABAA receptors enhance transmission and LTP induction at hippocampal mossy fiber synapses. *Nat. Neurosci.* **13,** 431–8 (2010).

25. Kubota, H., Alle, H., Betz, H. & Geiger, J. R. P. Presynaptic glycine receptors on hippocampal mossy fibers. *Biochem. Biophys. Res. Commun.* **393,** 587–91 (2010).

26. Çalışkan, G., Müller, I., Semtner, M., Winkelmann, A., Raza, A. S., Hollnagel, J. O., Rösler, A., Heinemann, U., Stork, O. & Meier, J. C. Identification of Parvalbumin Interneurons as Cellular Substrate of Fear Memory Persistence. *Cereb. Cortex* **26,** 2325–40 (2016).

27. Kirchner, A., Breustedt, J., Rosche, B., Heinemann, U. F. & Schmieden, V. Effects of taurine and glycine on epileptiform activity induced by removal of Mg2+ in combined rat entorhinal cortex-hippocampal slices. *Epilepsia* **44,** 1145–52 (2003).

28. Chen, R., Okabe, A., Sun, H., Sharopov, S., Hanganu-Opatz, I. L., Kolbaev, S. N., Fukuda, A., Luhmann, H. J. & Kilb, W. Activation of glycine receptors modulates spontaneous epileptiform activity in the immature rat hippocampus. *J. Physiol.* **592,** 2153–2168 (2014).

29. Shen, H.-Y., Van Vliet, E. A., Bright, K.-A., Hanthorn, M., Lytle, N. K., Gorter, J., Aronica, E. & Boison, D. Glycine transporter 1 is a target for the treatment of epilepsy. *Neuropharmacology* **99,** 554–565 (2015).

30. Schneidereit, D., Kraus, L., Meier, J. C., Friedrich, O. & Gilbert, D. F. Step-by-step guide to building an inexpensive 3D printed motorized positioning stage for automated high-

content screening microscopy. *Biosens. Bioelectron.* **92,** 472–481 (2017).

31. Kraus, L., Hetsch, F., Schneider, U. C., Radbruch, H., Holtkamp, M., Meier, J. C. & Fidzinski, P. Dimethylethanolamine Decreases Epileptiform Activity in Acute Human Hippocampal Slices in vitro. *Front. Mol. Neurosci.* **12,** 209 (2019).

32. Talwar, S., Lynch, J. W., Gilbert, D. F. & Attali, B. Fluorescence-Based High-Throughput Functional Profiling of Ligand-Gated Ion Channels at the Level of Single Cells. *PLoS One* **8,** e58479 (2013).

33. Le Duigou, C., Savary, E., Morin-Brureau, M., Gomez-Dominguez, D., Sobczyk, A., Chali, F., Milior, G., Kraus, L., Meier, J. C., Kullmann, D. M., Mathon, B., de la Prida, L. M., Dorfmuller, G., Pallud, J., Eugène, E., Clemenceau, S. & Miles, R. Imaging pathological activities of human brain tissue in organotypic culture. *J. Neurosci. Methods* **298,** 33–44 (2018).

34. Eugène, E., Cluzeaud, F., Cifuentes-Diaz, C., Fricker, D., Le Duigou, C., Clemenceau, S., Baulac, M., Poncer, J.-C. & Miles, R. An organotypic brain slice preparation from adult patients with temporal lobe epilepsy. *J. Neurosci. Methods* **235,** 234–44 (2014).

35. Kankowski, S., Förstera, B., Winkelmann, A., Knauff, P., Wanker, E. E., You, X. A., Semtner, M., Hetsch, F. & Meier, J. C. A Novel RNA Editing Sensor Tool and a Specific Agonist Determine Neuronal Protein Expression of RNA-Edited Glycine Receptors and Identify a Genomic APOBEC1 Dimorphism as a New Genetic Risk Factor of Epilepsy. *Front. Mol. Neurosci.* **10,** 439 (2018).

36. D'Antuono, M., Köhling, R., Ricalzone, S., Gotman, J., Biagini, G. & Avoli, M. Antiepileptic drugs abolish ictal but not interictal epileptiform discharges in vitro. *Epilepsia* **51,** 423–31 (2010).

37. Spencer, S. S., Goncharova, I. I., Duckrow, R. B., Novotny, E. J. & Zaveri, H. P. Interictal spikes on intracranial recording: Behavior, physiology, and implications. *Epilepsia* **49,** 1881–1892 (2008).

38. Galietta, L. J. ., Haggie, P. M. & Verkman, A. S. Green fluorescent protein-based halide indicators with improved chloride and iodide affinities. *FEBS Lett.* **499,** 220–4 (2001).

39. Lynch, J. W., Zhang, Y., Talwar, S. & Estrada-Mondragon, A. in 225–253 (2017). doi:10.1016/bs.apha.2017.01.003

40. Legendre, P., Förstera, B., Jüttner, R. & Meier, J. C. Glycine Receptors Caught between Genome and Proteome - Functional Implications of RNA Editing and Splicing. *Front. Mol. Neurosci.* **2,** 23 (2009).

41. Schmieden, V., Kuhse, J. & Betz, H. Agonist pharmacology of neonatal and adult glycine receptor alpha subunits: identification of amino acid residues involved in taurine activation. *EMBO J.* **11,** 2025–32 (1992).

42. Kletke, O., Sergeeva, O. A., Lorenz, P., Oberland, S., Meier, J. C., Hatt, H. & Gisselmann, G. New insights in endogenous modulation of ligand-gated ion channels: Histamine is an inverse agonist at strychnine sensitive glycine receptors. *Eur. J. Pharmacol.* **710,** 59–66 (2013).

43. George, J., Pridmore, S. & Aldous, D. Double Blind Controlled Trial of Deanol in Tardive Dyskinesia. *Aust. New Zeal. J. Psychiatry* **15,** 68–71 (1981).

44. de Montigny, C., Chouinard, G. & Annable, L. Ineffectiveness of deanol in tardive dyskinesia: A placebo controlled study. *Psychopharmacology (Berl).* **65,** 219–223 (1979).

45. Ferris, S. H., Sathananthan, G., Gershon, S. & Clark, C. Senile Dementia: Treatment with Deanol†. *J. Am. Geriatr. Soc.* **25,** 241–244 (1977).

46. Tammenmaa, I. A., Sailas, E., McGrath, J. J., Soares-Weiser, K. & Wahlbeck, K. Systematic review of cholinergic drugs for neuroleptic-induced tardive dyskinesia: a meta-analysis of randomized controlled trials. *Prog. Neuro-Psychopharmacology Biol. Psychiatry* **28,** 1099–1107 (2004).

47. Penovich, P., Morgan, J. P., Kerzner, B., Karch, F. & Goldblatt, D. Double-Blind Evaluation of Deanol in Tardive Dyskinesia. *JAMA J. Am. Med. Assoc.* **239,** 1997 (1978).

48. Fisman, M., Mersky, H. & Helmes, E. Double-blind trial of 2-dimethylaminoethanol in Alzheimer's disease. *Am. J. Psychiatry* **138,** 970–2 (1981).

49. Millington, W. R., McCall, A. L. & Wurtman, R. J. Deanol acetamidobenzoate inhibits the blood brain barrier transport of choline. *Ann. Neurol.* (1978). doi:10.1002/ana.410040403

50. Jope, R. S. & Jenden, D. J. Dimethylaminoethanol (Deanol) Metabolism in Rat Brain and its Effect on Acetyicholine Synthesis1. *J. Pharmacol. Exp. Ther* **211,** 472–479 (1979).

51. Cornett, E. M., Novitch, M., Kaye, A. D., Kata, V. & Kaye, A. M. Medication-Induced Tardive Dyskinesia: A Review and Update. *Ochsner J.* **17,** 162–174 (2017).

52. Shekh-Ahmad, T., Bialer, M. & Yavin, E. Synthesis and anticonvulsant evaluation of dimethylethanolamine analogues of valproic acid and its tetramethylcyclopropyl analogue. *Epilepsy Res.* (2012). doi:10.1016/j.eplepsyres.2011.10.005

53. Shi, H., Wang, H., Yang, B., Xu, D. & Wang, Z. The M3 receptor-mediated K(+) current (IKM3), a G(q) protein-coupled K(+) channel. *J. Biol. Chem.* **279,** 21774–8 (2004).

54. Moreno-Galindo, E. G., Sanchez-Chapula, J. A., Tristani-Firouzi, M. & Navarro-Polanco, R. A. Pharmacological Conversion of a Cardiac Inward Rectifier into an Outward Rectifier Potassium Channel. *Mol. Pharmacol. Mol Pharmacol* **90,** 334–340 (2016).

55. Nemec, J., Wickman, K. & Clapham, D. E. Gbetagamma binding increases the open time of IKACh: kinetic evidence for multiple Gbetagamma binding sites. *Biophys. J.* **76,** 246–52 (1999).

56. Murer, G., Adelbrecht, C., Lauritzen, I., Lesage, F., Lazdunski, M., Agid, Y. & Raisman-Vozari, R. An immunocytochemical study on the distribution of two G-protein-gated inward rectifier potassium channels (GIRK2 and GIRK4) in the adult rat brain. *Neuroscience* **80,** 345–357 (1997).

57. Miyashita, T. & Kubo, Y. Localization and developmental changes of the expression of two inward rectifying K+-channel proteins in the rat brain. *Brain Res.* **750,** 251–263 (1997).

58. Cea-del Rio, C. A., Lawrence, J. J., Tricoire, L., Erdelyi, F., Szabo, G. & McBain, C. J. M3 muscarinic acetylcholine receptor expression confers differential cholinergic modulation to neurochemically distinct hippocampal basket cell subtypes. *J. Neurosci.* **30,** 6011–24 (2010).

59. Kaufmann, K., Romaine, I., Days, E., Pascual, C., Malik, A., Yang, L., Zou, B., Du, Y., Sliwoski, G., Morrison, R. D., Denton, J., Niswender, C. M., Daniels, J. S., Sulikowski, G. A., Xie, X. S., Lindsley, C. W. & Weaver, C. D. ML297 (VU0456810), the first potent and selective activator of the GIRK potassium channel, displays antiepileptic properties in mice. *ACS Chem. Neurosci.* **4,** 1278–86 (2013).

60. Pfeiffer, C. C., Goldstein, L., Munoz, C., Murphree, H. B. & Jenney, E. H. Quantitative comparisons of the electroencephalographic stimulant effects of deanol, choline, and amphetamine. *Clin. Pharmacol. Ther.* **4,** 461–6 (1963).

61. Murphree, H. B., Pfeiffer, C. C. & Backerman, I. A. The stimulant effect of 2-dimethylaminoethanol (deanol) in human volunteer subiects. *Clin. Pharmacol. Ther.* **1,**

303–310 (1960).

62. Aram, J. A. & Lodge, D. Epileptiform activity induced by alkalosis in rat neocortical slices: Block by antagonists of N-methyl-d-aspartate. *Neurosci. Lett.* **83,** 345–350 (1987).

63. Dudek, F. E., Obenaus, A. & Tasker, J. G. Osmolality-induced changes in extracellular volume alter epileptiform bursts independent of chemical synapses in the rat: Importance of non-synaptic mechanisms in hippocampal epileptogenesis. *Neurosci. Lett.* **120,** 267–270 (1990).

64. Rosen, A. S. & Andrew, R. D. Osmotic effects upon excitability in rat neocortical slices. *Neuroscience* **38,** 579–590 (1990).

65. Traynelis, S. F. & Dingledine, R. Role of extracellular space in hyperosmotic suppression of potassium-induced electrographic seizures. *J. Neurophysiol.* **61,** 927–38 (1989).

66. Perreault, P. & Avoli, M. Physiology and pharmacology of epileptiform activity induced by 4-aminopyridine in rat hippocampal slices. *J. Neurophysiol.* **65,** 771–85 (1991).

67. Avoli, M., D'Antuono, M., Louvel, J., Köhling, R., Biagini, G., Pumain, R., D'Arcangelo, G. & Tancredi, V. Network and pharmacological mechanisms leading to epileptiform synchronization in the limbic system in vitro. *Prog. Neurobiol.* **68,** 167–207 (2002).

68. Heuzeroth, H., Wawra, M., Fidzinski, P., Dag, R. & Holtkamp, M. The 4-Aminopyridine Model of Acute Seizures in vitro Elucidates Efficacy of New Antiepileptic Drugs. *Front. Neurosci.* **13,** 677 (2019).

69. Gabriel, S., Njunting, M., Pomper, J. K., Merschhemke, M., Sanabria, E. R. G., Eilers, A., Kivi, A., Zeller, M., Meencke, H.-J., Cavalheiro, E. A., Heinemann, U. & Lehmann, T.-N. Stimulus and Potassium-Induced Epileptiform Activity in the Human Dentate Gyrus from Patients with and without Hippocampal Sclerosis. *J. Neurosci.* **24,** 10416–10430 (2004).

70. Antonio, L. L., Anderson, M. L., Angamo, E. A., Gabriel, S., Klaft, Z. J., Liotta, A., Salar, S., Sandow, N. & Heinemann, U. In vitro seizure like events and changes in ionic concentration. *J. Neurosci. Methods* (2016). doi:10.1016/j.jneumeth.2015.08.014

71. Klaft, Z.-J., Hollnagel, J.-O., Salar, S., Calişkan, G., Schulz, S. B., Schneider, U. C., Horn, P., Koch, A., Holtkamp, M., Gabriel, S., Gerevich, Z. & Heinemann, U. Adenosine A_1 receptor-mediated suppression of carbamazepine-resistant seizure-like events in human neocortical slices. *Epilepsia* **57,** 746–756 (2016).

72. Sandow, N., Kim, S., Raue, C., Päsler, D., Klaft, Z.-J., Antonio, L. L., Hollnagel, J. O., Kovacs, R., Kann, O., Horn, P., Vajkoczy, P., Holtkamp, M., Meencke, H.-J., Cavalheiro, E. A., Pragst, F., Gabriel, S., Lehmann, T.-N. & Heinemann, U. Drug resistance in cortical and hippocampal slices from resected tissue of epilepsy patients: no significant impact of p-glycoprotein and multidrug resistance-associated proteins. *Front. Neurol.* **6,** 30 (2015).

73. Remy, S., Gabriel, S., Urban, B. W., Dietrich, D., Lehmann, T. N., Elger, C. E., Heinemann, U. & Beck, H. A novel mechanism underlying drug resistance in chronic epilepsy. *Ann. Neurol.* **53,** 469–479 (2003).

74. Jandová, K., Päsler, D., Antonio, L. L., Raue, C., Ji, S., Njunting, M., Kann, O., Kovács, R., Meencke, H.-J., Cavalheiro, E. A., Heinemann, U., Gabriel, S. & Lehmann, T.-N. Carbamazepine-resistance in the epileptic dentate gyrus of human hippocampal slices. *Brain* **129,** 3290–306 (2006).

75. Reyes-Garcia, S. Z., Scorza, C. A., Araújo, N. S., Ortiz-Villatoro, N. N., Jardim, A. P., Centeno, R., Yacubian, E. M. T., Faber, J. & Cavalheiro, E. A. Different patterns of epileptiform-like activity are generated in the sclerotic hippocampus from patients with drug-resistant temporal lobe epilepsy. *Sci. Rep.* **8,** 7116 (2018).

76. Brückner, C. & Heinemann, U. Effects of standard anticonvulsant drugs on different patterns of epileptiform discharges induced by 4-aminopyridine in combined entorhinal cortex–hippocampal slices. *Brain Res.* **859,** 15–20 (2000).

77. Fueta, Y. & Avoli, M. *Effects of antiepileptic drugs on 4-aminopyridine-induced epileptiform activity in young and adult rat hippocampus*. *Epilepsy Res.* **12,** (1992).

78. Holtkamp, D., Opitz, T., Niespodziany, I., Wolff, C. & Beck, H. Activity of the anticonvulsant lacosamide in experimental and human epilepsy via selective effects on slow Na^+ channel inactivation. *Epilepsia* **58,** 27–41 (2017).

79. Taing, K. D., O'Brien, T. J., Williams, D. A. & French, C. R. Anti-Epileptic Drug Combination Efficacy in an In Vitro Seizure Model - Phenytoin and Valproate, Lamotrigine and Valproate. *PLoS One* **12,** e0169974 (2017).

80. Meier, J. C., Meier, J. C., Semtner, M., Winkelmann, A. & Wolfart, J. Presynaptic mechanisms of neuronal plasticity and their role in epilepsy. *Front. Cell. Neurosci.* **8,** 164 (2014).

8. Statutory Declaration

I,Larissa Kraus, by personally signing this document in lieu of an oath, hereby affirm that I prepared the submitted dissertation on the topic RNA-edited glycine receptors in temporal lobe epilepsy, independently and without the support of third parties, and that I used no other sources and aids than those stated.

All parts which are based on the publications or presentations of other authors, either in letter or in spirit, are specified as such in accordance with the citing guidelines. The sections on methodology (in particular regarding practical work, laboratory regulations, statistical processing) and results (in particular regarding figures, charts and tables) are exclusively my responsibility.

Furthermore, I declare that I have correctly marked all of the data, the analyses, and the conclusions generated from data obtained in collaboration with other persons, and that I have correctly marked my own contribution and the contributions of other persons (cf. declaration of contribution). I have correctly marked all texts or parts of texts that were generated in collaboration with other persons.

My contributions to any publications to this dissertation correspond to those stated in the below joint declaration made together with the supervisor. All publications created within the scope of the dissertation comply with the guidelines of the ICMJE (International Committee of Medical Journal Editors; www.icmje.org) on authorship. In addition, I declare that I shall comply with the regulations of Charité – Universitätsmedizin Berlin on ensuring good scientific practice.

I declare that I have not yet submitted this dissertation in identical or similar form to another Faculty.

The significance of this statutory declaration and the consequences of a false statutory declaration under criminal law (Sections 156, 161 of the German Criminal Code) are known to me."

Date Signature

9. Declaration of own contribution to the publications

Larissa Kraus contributed the following to the below listed publications:

Publication 1:
Schneidereit D, **Kraus L**, Meier JC, Friedrich O, Gilbert DF. Step-by-step guide to building an inexpensive 3D printed motorized positioning stage for automated high-content screening microscopy. Biosens Bioelectron. 2017
Contribution in detail: I prepared and performed HEK cell experiments and analysed data shown in figure 3, 4a and b of the manuscript.

Publication 2:
Kraus L, Hetsch F, Schneider UC, Radbruch H, Holtkamp M, Meier JC, Fidzinski P. Dimethylethanolamine Decreases Epileptiform Activity in Acute Human Hippocampal Slices in vitro. Front Mol Neurosci. 2019
Contribution in detail: I performed all experiments and data analysis concerning resected human brain tissue (figure 2, 3, 4 and suppl. figure 2, 3 and suppl. table 1, 2) and performed analysis of raw data shown in figure 1 and suppl. figure 1. I wrote the manuscript together with the senior author Pawel Fidzinski.

Publication 3:
Le Duigou C, Savary E, Morin-Brureau M, Gomez-Dominguez D, Sobczyk A, Chali F, Milior G, **Kraus L**, Meier JC, Kullmann DM, Mathon B, de la Prida LM, Dorfmuller G, Pallud J, Eugène E, Clemenceau S, Miles R. Imaging pathological activities of human brain tissue in organotypic culture. J Neurosci Methods. 2018
Contribution in detail: I helped preparing the tissue and performed slice culture experiments involving tissue used for transduction with AAV9 (with CMV promotor and mCherry fluorescent reporter). I performed antibody staining and analysis on neuronal specificity of the used viral expression system. Results are seen in suppl. Fig. 1F of the manuscript. For readability, details on RNA editing sensor included in this thesis were not included in the publication.

Signature, date and stamp of first supervising university professor / lecturer

Signature of doctoral candidate

10. Selected publications

Publication 1: Schneidereit et al., 2017

Schneidereit D, **Kraus L**, Meier JC, Friedrich O, Gilbert DF. Step-by-step guide to building an inexpensive 3D printed motorized positioning stage for automated high-content screening microscopy. Biosens Bioelectron. 2017

Biosensors and Bioelectronics 92 (2017) 472–481

Contents lists available at ScienceDirect

Biosensors and Bioelectronics

Step-by-step guide to building an inexpensive 3D printed motorized positioning stage for automated high-content screening microscopy

Dominik Schneidereit[a,b], Larissa Kraus[a,d,e], Jochen C. Meier[c], Oliver Friedrich[a,b], Daniel F. Gilbert[a,b,*]

[a] Institute of Medical Biotechnology, Friedrich-Alexander-Universität Erlangen-Nürnberg, Erlangen, Germany
[b] Erlangen Graduate School in Advanced Optical Technologies (SAOT), Friedrich-Alexander-Universität Erlangen-Nürnberg Erlangen, Germany
[c] Zoological Institute, Cell Physiology, Technical University Braunschweig, Braunschweig, Germany
[d] Department of Neurology, Clinical and Experimental Epileptology, Charité - Universitätsmedizin Berlin, Berlin, Germany
[e] Berlin Institute of Health (BIH), Berlin, Germany

ARTICLEINFO

Keywords:
3D desktop printing
Arduino
High-content screening
Cell viability
YFPI152L
Glycine receptor
TRPV1
Fluo-4 AM

ABSTRACT

High-content screening microscopy relies on automation infrastructure that is typically proprietary, non-customizable, costly and requires a high level of skill to use and maintain. The increasing availability of rapid prototyping technology makes it possible to quickly engineer alternatives to conventional automation infrastructure that are low-cost and user-friendly. Here, we describe a 3D printed inexpensive open source and scalable motorized positioning stage for automated high-content screening microscopy and provide detailed step-by-step instructions to re-building the device, including a comprehensive parts list, 3D design files in STEP (Standard for the Exchange of Product model data) and STL (Standard Tessellation Language) format, electronic circuits and wiring diagrams as well as software code. System assembly including 3D printing requires approx. 30 h. The fully assembled device is light-weight (1.1 kg), small (33×20×8 cm) and extremely low-cost (approx. EUR 250). We describe positioning characteristics of the stage, including spatial resolution, accuracy and repeatability, compare imaging data generated with our device to data obtained using a commercially available microplate reader, demonstrate its suitability to high-content microscopy in 96-well high-throughput screening format and validate its applicability to automated functional Cl^-- and Ca^{2+}-imaging with recombinant HEK293 cells as a model system. A time-lapse video of the stage during operation and as part of a custom assembled screening robot can be found at https://vimeo.com/158813199.

1. Introduction

Over the past two decades, automated high-content screening (HCS) microscopy has become an indispensable method in cell biology with applications in an almost infinite variety of scientific fields including cancer research and neurosciences.

Conventional HCS systems are typically made up of a fully automated inverted microscope as a central component and a motorized stage mounted on top of the microscope's chassis. The microscope, usually equipped with exchangeable objectives, focusing mechanics, a digital camera and infrastructure allowing for fluorescence or luminescence microscopy, is used for visualization of biological probes at the microscopic level. The motorized stage enables inspection of specimen larger than the field of view of the objective and automatic positioning of biological samples, cultured e.g. in multititer plates, during operation in high-throughput screening mode. Besides these components, conventional HCS devices are equipped with additional parts, such as an incubator, capable of maintaining optimal conditions necessary for culturing cells, liquid-handling systems or robotics for operation in almost autonomous high- or ultrahigh-throughput screening mode.

Commercially available motorized positioning stages are characterized by high-speed scanning capabilities and high positional accuracy in the micro- or sub-micrometer range, achieved through e.g. stable closed-loop control systems. These stages are claimed ideal for manually or automatically positioning a wide range of specimens and samples in many types of microscopy or imaging techniques and applications but are typically proprietary and thus disadvantageous for a number of reasons. First, installation of commercially available positioning devices or integration with existing equipment as well as application and maintenance requires a high level of product-specific skill and hence, is resource-intensive and not user friendly or straightforward. Second, options for interfacing with third-party systems are

* Corresponding author at: Institute of Medical Biotechnology, Friedrich-Alexander-Universität Erlangen-Nürnberg, Erlangen, Germany.
E-mail address: daniel.gilbert@fau.de (D.F. Gilbert).

http://dx.doi.org/10.1016/j.bios.2016.10.078
Received 9 August 2016; Received in revised form 21 October 2016; Accepted 25 October 2016
Available online 02 November 2016

often limited at both hard- and software levels, e.g. because available I/O (input/output) ports are not documented and thus, virtually not available to users, software code is closed source or the command set is not provided. Third, customization of conventional positioning stages is hampered for the sake of protection of proprietary hard- and software. For example, hardware modification is typically not permis- sible and will result in the loss of the warranty and exclusion of liability. Furthermore, proprietary commercial systems are typically cost-intensive and not readily applicable to a broad range of laboratories in low-resource settings or for educational purposes, e.g. in schools or universities.

Despite the fact that there are examples on low-cost 3D printed technologies for cell-based high-content imaging (Campbell et al., 2014; Walzik et al., 2015; Wardyn et al., 2015) and high-throughput screening (Berg et al., 2015; Gregory and Veeman, 2013; Spivey et al., 2014), a positioning stage for automated high-content screening microscopy that is fully open source, scalable and low-cost has not been reported yet. The recent availability of rapid prototyping technology, including 3D desktop printing, open source microcontroller boards and inexpensive consumer electronics, mechanics and robotics parts - also adopted by the 'Maker' movement, a culture of do-it-yourself (DIY) product design (Editorial, 2013; Landrain et al., 2013; Seyfried et al., 2014) - makes it possible to quickly engineer and share user-friendly equipment of reduced cost and complexity.

To overcome the limitations of proprietary technology described above we aimed to develop a motorized stage based on a 'Makers' approach that is fully open source, customizable, robust, affordable to a broad range of research labs and could rapidly and easily be re-built e.g. in so called *fab labs* (fabrication laboratories) and - at the same time - is sufficiently accurate for automated high-content screening microscopy. To this end we aimed to use off-the-shelf electronic components as well as 3D-desktop printing and low-cost open-source microcontroller architecture, both being increasingly used in the development of scientific devices (D'Ausilio, 2012; Frame and Leach, 2014; Leeuw et al., 2013; Pineño, 2014; Schubert et al., 2013; Starosolski et al., 2014; Stokes et al., 2013; Wittbrodt et al., 2014) and proven valuable in the design of technology suitable to educational purposes (Marzullo and Gage, 2012; Shannon et al., 2014; Walzik et al., 2015). We further aimed to evaluate the stage with regard to its positioning characteristics including spatial resolution, accuracy and repeatability and to provide one example each for applications in cancer research and in neurosciences i.e. for high-content imaging in high-throughput screening mode, e.g. for cell fitness screening, and for functional imaging of ion channels, respectively.

In cancer research, high-content imaging in high-throughput screening mode is applied for example in the context of cell viability or fitness screening to identify novel chemotherapeutics. Cellular fitness is indicated by various physiological indicators which are partially and indirectly assessable using fluorescence-based assaying methods and is often measured by quantifying cell number using e.g. fluorescent proteins (Gilbert et al., 2011). In order to demonstrate the applicability of the motorized stage to quantifying cellular fitness, we intended to apply the technology with recombinant human embryo-derived (HEK293$^{YFPI_{152L}}$) cells, stably expressing YFPI152L, an engineered variant of yellow fluorescent protein (YFP) and to compare data obtained from the custom device with data from a commercial high-end microplate reader.

In neuroscience, high-content imaging, also referred to as functional imaging, has become an integral part for evaluating the biophysical and pharmacological properties of ion channels - pore-forming membrane proteins involved in most physiological and disease processes and considered highly attractive drug targets for therapeutic intervention (Alexander et al., 2015; Braat and Kooy, 2015; Meier et al., 2014; Ortega-Guerrero et al., 2016; Talwar et al., 2013). In functional imaging experiments, the activity of ion channels is mostly assessed indirectly using ion-selective indicators such as loadable or genetically encoded fluorescence dyes that report an ion channel-induced change in intracellular ion concentration via varying fluorescence intensity. For assessing the suitability of the low cost device for functional imaging of ion channels, we aimed to conduct agonist and antagonist concentration-response experiments with glycine receptor (GlyR) chloride channels in combination with YFPI152L as fluorescence probe and with transient receptor vanilloid receptor type 1 (TRPV1) cation channels in combination with Fluo-4 AM as fluorescence indicator.

GlyRs are ligand-gated ionotropic receptors that mediate inhibitory neurotransmission in the central nervous system and conduct an anion current, mainly carried by chloride (Cl^-) upon activation by the amino acid glycine. The channels can be selectively blocked by the high-affinity competitive antagonist strychnine (Lynch et al., 1997). Functional GlyRs are formed from a total of five subunits (α1– α4, β) which assemble either as α homomeric or αβ heteromeric channels (Lynch, 2009). GlyR-activation can be monitored by fluorescence imaging using YFPI152L. YFPI152L, an engineered variant of YFP with greatly enhanced anion sensitivity, is quenched by small anions and is thus suited to reporting anionic influx into cells (Galietta et al., 2001). It has proven useful in screening compounds against many chloride channel types (Balansa et al., 2010, 2013a, 2013b; , 2011, 2009c; , 2011, 2009c; Kruger et al., 2005; Kuenzel et al., 2016).

TRPV1 is a non-selective cation channel that mediates pain perception in nociceptive somatosensory neurons. It is activated by temperatures exceeding 43 °C, by a drop in pH below 6.8 and by capsaicin, the main pungent ingredient in chili peppers (Caterina and Julius, 2001). When activated, the channels conduct a depolarizing cation current, partly carried by Ca^{2+}, leading to an increase in intracellular calcium concentration $[Ca^{2+}]_i$. Capsaicin-induced activation is antagonized by the competitive antagonist capsazepine, a synthetic analogue of capsaicin (Bevan et al., 1992). Activation of TRPV1 and increase of the intracellular Ca^{2+} concentration $[Ca^{2+}]_i$ can be assessed using Ca^{2+} selective fluorophores, such as Fluo-4 AM. Fluo-4 AM is a non-ratiometric, high-affinity fluorescent dye for quantifying $[Ca^{2+}]_i$ within a large dynamic range, around a Kd(Ca^{2+}) of 345 nM (Gee et al., 2000). Its fluorescence intensity increases with increasing $[Ca^{2+}]_i$.

Finally, we aimed to create and to provide detailed step-by-step instructions to re-building the stage and to evaluate it with regard to the time required for production and installation.

2. Materials and methods

2.1. Pharmacological reagents

Glycine, strychnine, capsaicin and capsazepine were obtained from Sigma-Aldrich. Glycine was prepared as a 1 M stock in water, strychnine was prepared as 10 mM stock in dimethylsulphoxide (DMSO). Capsaicin and capsazepine were prepared as 100 mM stocks in DMSO. All stocks were frozen at −20 °C. From these stocks, solutions for experiments were prepared on the day of recording.

2.2. Calcium indicator

Fluo-4 AM was obtained from Molecular Probes and was prepared as 10 mM stock in DMSO. Fluo-4 AM stocks were frozen at −20 °C. From these stocks, solutions for calcium imaging experiments were prepared on the day of recording.

2.3. Cell lines

Human embryonal kidney-derived cells (HEK293, CRL-1573) were purchased from *The American Type Culture Collection* (ATCC). The HEK293$^{YFPI_{152L}}$ cell line was generated as described in (Walzik et al., 2015).

2.4. Cell culture

Cells were maintained in DMEM (Invitrogen) supplemented with 10% fetal bovine serum (Biochrom) and penicillin (100 U/ml)/streptomycin (100 mg/ml) (Invitrogen) and were cultured in T75 flasks (TPP) at 37 °C, 5% CO_2 in a humidified incubator according to standard procedures. Cells were passaged every 2–3 days and used in experiments when approximately 80–90% confluent.

2.5. Low-cost 3D printed stage

The stage in its current design is made up of a total of sixteen 3D printed parts (14 individual designs), two orthogonally positioned bipolar stepper motors (200 Steps/Rev, NEMA 8, Watterott, Germany) each attached to a threaded spindle with lead screw (1 mm pitch, Misumi, Japan) and terminally centered using ball bearings (Kugellager Shop, Germany), six linear bearings (Misumi, Japan), four M4 brass guide rods (OBI, Germany), two pairs of end switches (ZF Electronics, Germany) and a total of 65 standard M2-4 screws and nuts. The stepper motors are controlled via L293DNE H-bridge motor drivers (Texas Instruments, USA) mounted to a custom created Arduino UNO-compatible actuator shield, i.e. a printed circuit board (PCB), designed in Fritzing 0.9.2b/64 bit (Interaction Design Lab Potsdam, Germany) which plugs directly into Arduino UNO pin-headers. To limit the traveling path of the stage and to allow zero-point calibration at the start of an experiment each of the two axes is equipped with a pair of end switches (ZF Electronics, Germany) connected to the shield.

The stage is orchestrated by one Arduino UNO open-source electronics prototyping board (Arduino, Italy) based on the ATmega328 microcontroller programmed using the Arduino open-source integrated development environment (IDE). The NI *LabVIEW Interface for Arduino Toolkit* (National Instruments, Ireland) was used for interfacing the Arduino board with LabVIEW 2014 through a serial connection. A user interface for parametrization, calibration and application of the device was written in LabVIEW 2014 for use with a standard laptop or personal computer with e.g. Windows 7 operating System (Microsoft Corporation, USA) or any other device running LabVIEW software.

2.6. Custom built robot

The imaging system is made-up of an autosampler for liquid handling (HTS PAL, CTC Analytics, Switzerland), a miniaturized low-cost inverted digital fluorescence microscope (Thorlabs, USA) with 10x objective (Olympus, Japan), CCD camera (Point Grey Research Inc., USA) and LED light source (LUMITRONIX, Germany) and in house built autofocussing mechanics - all orchestrated by Arduino (Arduino, Italy) and LabVIEW software (National Instruments, Ireland).

2.7. Preparation of cells for Example I experiments

The day before imaging experiments HEK293^{YFPI152L} cells, previously dislodged from a T75 flask (TPP, Switzerland) using 0.25% trypsin–EDTA solution (Gibco BRL) and resuspended into DMEM, were counted using a haemocytometer (LO Laboroptik GmbH, Germany) and were seeded into the wells of a 96-well plate at 5000 (row A–H, column 1–2), 10000 (row A–H, column 3–4), 15000 (row A–H, column 5–6), 20000 (row A–H, column 7–8), 25000 (row A-H, column 9–10) and 30000 (row A-H, column 11–12) cells per well in 16 replicates each. Cells were cultured overnight at 37 °C, 5% CO_2 in a humidified incubator according to standard procedures. The next day, the medium was replaced by 50 µl standard control solution, which contained (in mM) NaCl 140, KCl 5, CaCl2 2, MgCl2 1, HEPES 10, and glucose 10 (pH 7.4, NaOH) and fluorescence intensity of cells was measured first using a VICTOR X4 plate reader (Perkin Elmer) with YFP filter set (exposure time: 0.5 s) and subsequently using the custom built robot.

2.8. Example I experiments with custom built robot

The 96-well plates were placed onto the 3D printed motorized stage of the in house-built imaging system and cells were imaged with a 10× objective (Plan Achromat, 0.25 NA, 10.6 mm WD, Olympus, Japan). Illumination from an LED (Nichia NCSE119A 98 lm, LUMITRONIX LED-Technik GmbH) passing through an excitation filter (EX 497/16, MDF-YFP, Thorlabs) and fluorescence light passing through emission and dichroic filters (BA 535/22, DM 515, MDF-YFP, Thorlabs) was imaged by a CCD camera (1.3 MP Chameleon, 1/3" CCD, Point Grey Research Inc.) and digitized to disk onto a personal computer with Windows operating System (Microsoft Corporation). The primary resolution of the camera was 1280×960 pixel, although images were binned (2×2), resulting in a resolution of 640×480 pixels. Each image typically contained 50–250 cells. The CCD image acquisition time was 2 s. These experiments were conducted at room temperature.

2.9. Transient transfection of HEK293 cells for Example II experiments

Approx. 24 h prior to transfection, cells were seeded into 6 cm dishes (TPP) at a concentration of 10^6 cells per dish. GlyR chloride channel subunits (Kuhse et al., 1990; Legendre et al., 2009), YFPI152L (Galietta et al., 2001) and TRPV1 were transfected with a total cDNA quantity of 4 µg per 6 cm dish. Cells were transfected using 30 µl PolyFect Transfection Reagent (Qiagen) according to the manufacturer's instructions. We have published a detailed comparison of five transient transfection methods employed routinely for this purpose (Gilbert et al., 2009a).

2.10. Preparation of cells for Example II experiments

Following termination of transfection, cells were trypsinized by adding 0.3 ml of 0.25% trypsin–EDTA solution (Gibco BRL), resuspended into DMEM, and 3×10^4 cells, suspended in 200 µl DMEM, and were plated into each well of a transparent 96-well plate (TPP) for fluorescence imaging experiments. Cells were used in experiments 24 h later. Individual wells typically contained $3–5\times10^4$ cells at the time of the experiment. Approximately 1 h prior to commencement of experiments, culture medium in 96-well plates was entirely removed by turning the plate upside-down onto a stack of tissue and plates were left for approximately 30 s until culture media was entirely removed from the wells. The medium was replaced by 50 µl standard control solution, which contained (in mM) NaCl 140, KCl 5, $CaCl_2$ 2, $MgCl_2$ 1, HEPES 10, and glucose 10 (pH 7.4, NaOH) upon washing the cells once in 50 µl standard control solution.

For chloride imaging experiments, the agonist NaI test solution was supplemented with 3 mM glycine and serially diluted with NaI test solution to obtain agonist solutions containing 3, 10, 30, 100, 300, 1000 and 3000 µM final glycine concentration. For antagonist concentration response experiments with GlyR α3 expressing cells, the control solution was supplemented with 0.1, 0.3, 1, 3, 10, 30, 100 µM final strychnine concentration and pre-incubated prior to functional imaging for approx. 30 min.

For calcium imaging experiments, cells were incubated in 50 µl standard control solution supplemented with 1 µM Pluronic F-127 (Life Technologies) and 5 µM Fluo-4 AM (Molecular Probes) final concentrations for 1 h at 37 °C, 5% CO_2 and staining solution was replaced by 50 µl control solution. For TrpV1 receptor stimulation, the control solution was supplemented with 0.1, 0.1, 1, 10, 100, 1000, 10000 and 100000 nM final capsaicin concentrations. For TRPV1 antagonist concentration response experiments, the agonist solution containing 1 µM capsaicin was supplemented with 0.01, 0.1, 1, 10, 100,

1000 and 10000 nM capsazepine (Sigma) final concentration. For TrpV1 receptor stimulation, the control solution was supplemented with 0.01, 0.03, 0.1, 0.3, 1, 3, 10, 30, 100, 300, 1000 and 3000 µM final capsaicin concentrations.

All drugs were diluted from stocks at the day of the experiment and experiments were conducted at room temperature.

2.11. Example II experiments

Imaging experiments were conducted as explained in section *Example experiments I* with the difference that the experimental protocol involved imaging each well twice: once in 50 µl control solution and once 8 s after the injection of 100 µl agonist solution. Liquid handling was performed with the autosampler described above. Solutions were applied to cells at a rate of 0.6 ml/min.

2.12. Evaluation of positioning characteristics

Images acquired for calculation of spatial resolution, accuracy and repeatability were aligned with ImageJ (National Institutes of Health) using the plugin *Register Virtual Stack Slices* (Arganda-Carreras et al., 2006) (for documentation see http://fiji.sc/wiki/Register_Virtual_Stack_Slices). Bi-directional registration information (in pixels) was extracted from so called *transforms* *.xlm-files provided by the plugin and converted into micrometers based on a previously determined factuator. The conversion factuator was calculated from images of a *1951 USAF test target* consisting of reference line patterns with well-defined dimensions.

2.13. Image registration

Images acquired with the automated high-content screening system were spatially aligned with LabVIEW (National Instruments) and ImageJ (National Institutes of Health) using the plugin *Register Virtual Stack Slices* (Arganda-Carreras et al., 2006). For automated registration of large sets of image pairs, we created a LabVIEW virtual instrument (VI) which dynamically generates jython scripts and calls the *Register Virtual Stack Slices* plugin via the command line in ImageJ headless mode in a non-interactive fashion. Resulting transforms are saved in XML format and are used by the VI for extraction of matching image regions in the original image pairs which are copied to a new subdirectory in TIFF format and enable single cell or image-based quantitative image analysis.

2.14. Single cell-based quantitative image analysis

Registered images of fluorescent cells were segmented and quantitatively analyzed using a modified version of DetecTiff software (Gilbert et al., 2009b). The fluorescence signal of identified cells was measured in images acquired before and after the addition of agonist solution as the mean of all pixel values within the area of a cell. '% fluorescence quench' in chloride imaging experiments is defined as:

$$(1)\ \%\ \mathit{fluorescence\ quench} = (F_{init} - F_{final}) * 100 / F_{init}.$$

and '% fluorescence change' in calcium imaging experiments is defined as:

$$(2)\ \%\ \mathit{fluorescence\ change} = (F_{final} / F_{init}) - 1 * 100,$$

where F_{init} and F_{final} are the initial and final values of fluorescence, respectively.

2.15. Image-based intensity analysis

Mean fluorescence intensity (MPI) of all pixels within one image acquired with the custom-designed automated high-content screening system was quantitatively analyzed using a modified version of DetecTiff software.

2.16. Calculation of concentration-response relationships

Individual concentration responses were constructed by pooling results from approx. 100–300 cells in one well exposed to agonist solution. Concentration-response relationships were fitted with the following equation:

$$(3)\ F = F_{init} / (1 + (EC_{50} / [Agonist])^{nH}).$$

where F is the fluorescence corresponding to a particular agonist concentration, $[Agonist]$; F_{init} is the initial fluorescence value; EC_{50} is the concentration that elicits half-maximal activation; and nH is the Hill coefficient. Curve fits were performed using a least squares fitting routine (Origin 7 G, OriginLab Corporation). All averaged results are expressed as mean ± SD.

2.17. Data analysis and visualization

Plate reader data were annotated in Microsoft Excel and analyzed using Origin 7 G (OriginLab Corporation). Heat maps of normalized imaging results were generated using LabVIEW 2014.

3. Results

We have developed an inexpensive motorized positioning stage that can easily be reconstructed within a few hours using 3D desktop printing and off-the-shelf components. To demonstrate its applicability to automated high-content microscopy in high-throughput screening mode, we integrated the stage into a custom built imaging robot (see Methods for details). Schematics and images of the stage as well as of the robot are shown in Fig. 1. We describe positioning characteristics of the stage, including spatial resolution, accuracy and repeatability, compare imaging data generated with our platform to data obtained using a commercially available microplate reader, demonstrate its suitability to high-content microscopy in 96-well high-throughput screening format and validate its applicability to automated functional Cl^-- and Ca^{2+}-imaging with recombinant HEK293 cells as a model system. We further provide detailed step-by-step instructions to re-building the stage including a comprehensive parts list, 3D design files, electronic circuits and wiring diagrams as well as software code, and we give examples for customization, e.g. for use with various culture plastic ware such as 40 and 60 mm dishes, T25 and T75 tissue culture flasks and standard 76×26 mm (3×1 in.) microscope slides. System assembly including printing of plastic parts requires approx. 30 h. The fully assembled device is light-weight (1.1 kg), small (33×20×8 cm) and extremely low-cost (approx. EUR 250). A time-lapse video of the stage and custom built robot during operation can be found at https://vimeo.com/158813199.

3.1. 3D-design, mechatronics, software & development process

As a starting point towards designing a low-cost positioning stage we modified a miniaturized and motorized webcam-microscope stage previously developed in our lab (Walzik et al., 2015) to fit the dimensions of a standard, e.g. 24-, 96-, 384- or 1536-well multititer plate using commercial computer assisted design (CAD) software (Autodesk Inventor 2013, Autodesk, Inc., USA). In a next step, we optimized the design to ensure robustness in everyday use, and at the same time, minimize space and resource requirements. Images of the initial and modified up-scaled stages, respectively, are shown in Fig. 1a and b-d, demonstrating the versatility of 3D printed infrastructure with regard to customization. The stage in its current design is made up of a total of sixteen 3D printed parts (14 individual designs), printed during an overall time of < 23 h from approx. 250 g black acrylonitrile butadiene styrene filament (ABS, MakerBot Industries, USA) using a consumer grade 3D printer (MakerBot Replicator, MakerBot Industries, USA). For details on the mechanical and electronic components please refer to the methods section.

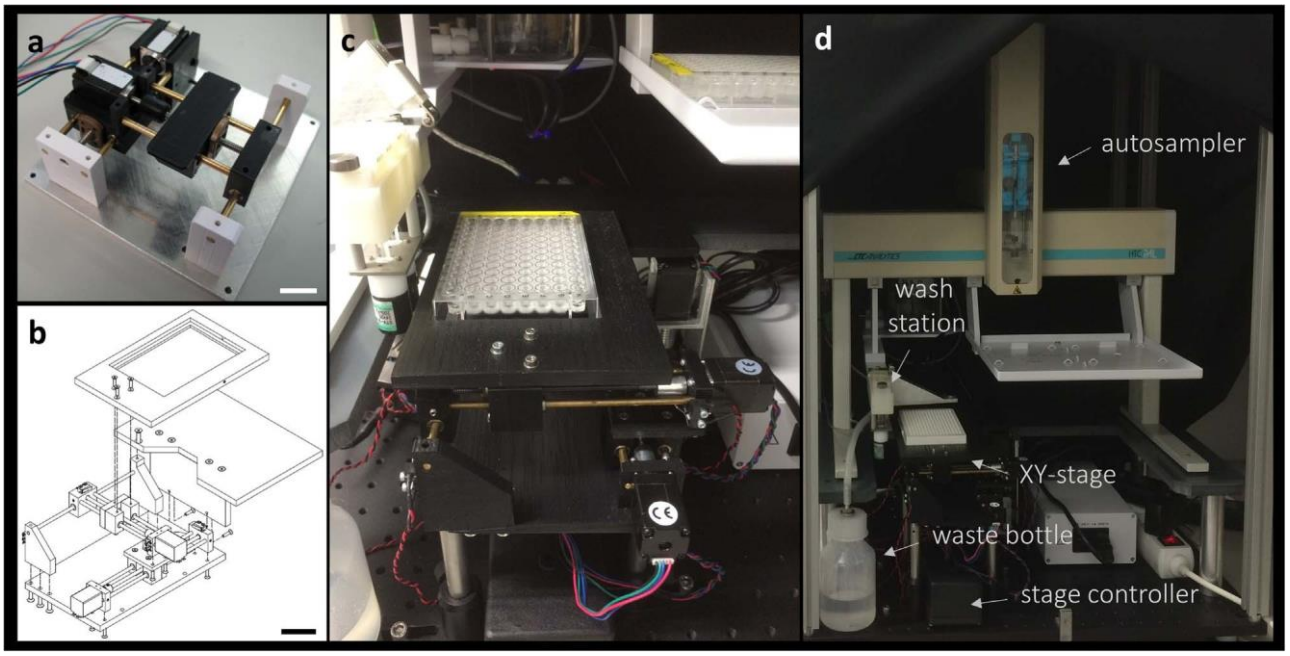

Fig. 1. The open source motorized microscope stage is customizable and can be modified to fit any conventional or custom assembled hardware. (a) Previously developed low-cost stage for a motorized webcam-based digital microscope serving as a starting point for designing the low-cost open source positioning system. Scale bar: 2 cm. (b) Assembly drawing of the stage indicating its simple design and modifiability. Scale bar: 5 cm. (c) Close-up view of the stage, integrated into a custom built screening robot. (d) Custom built screening robot with integrated stage.

The stage is orchestrated by one Arduino UNO open-source electronics prototyping board (Arduino, Italy), the NI *LabVIEW Interface for Arduino Toolkit* (National Instruments, Ireland) and LabVIEW 2014 through a serial connection. The device was prototyped during a period of approx. 6 months, which can be divided into three phases. In the initial phase (2 months), the required electronic components were researched, ordered and assembled and preliminary circuits and software were developed. In the second phase (1 month) the motorized stage was engineered and proof-of-concept experiments were carried out and in the final stage (3 months), hard- and software were optimized and benchmarking with conventional technology was conducted.

All mechanical and electronical hardware components, 3D design files, PCB sketch and software code as well as additional information required to re-building and applying the stage are summarized in the Supplementary Table S1.

3.2. Positioning characteristics

The usability of a motorized positioning system for microscopic applications is limited by a variety of parameters, including (1.) its overall travel range, (2.) its spatial resolution, i.e. the smallest traveling distance of the positioning stage in X- and Y-direction, (3.) its accuracy, the difference between the actual position in space and the position as quantified by a measurement device and (4.) its repeatability, i.e. the range of positions attained when the system is repeatedly commanded to one location under identical conditions (Conrad et al., 2000). Generally speaking, the larger the travel range, the smaller the spatial resolution; the higher the accuracy and the better the repeatability, the larger is the spectrum of potential applications. In the current configuration, the travel range is approx. 120×80 mm. The spatial resolution of the positioning stage is defined by the following equation.

(4) $X,\ Y\ Resolution\ (\mu m) = Pitch_{spindle} / No.\ of\ steps_{motor}$, where $Pitch_{spindle}$ is the incline of the spindle per revolution (1000 µm) and $No.\ of\ steps_{motor}$ is the total number of steps per revolution of the stepper motor (200 steps). To evaluate whether the calculated spatial resolution of 5 µm equals the practical resolution, we set the controlling software to repeatedly move one axis by a single step and to subsequently acquire an image of an *USAF 1951 test target*. This procedure was repeated 50 times for both axes in positive and negative direction each. The practical resolution was quantified by measuring the drift of the *USAF 1951 test target*-structures in recurrently acquired images using the ImageJ plugin *Register Virtual Stack*. For methodological details refer to methods section. The relation of set point positions to associated measured positions for both axes is displayed in the graphs in Fig. 2A and B (X-axis, black; Y-axis, grey). From these data, we calculated the average step size (n = 50, mean ± SD,) for positively and negatively directed movements of the X- (5.1 ± 1.8 µm; −4.9 ± 1.9 µm) and Y-axis (3.5 ± 2.2 µm; −5.0 ± 1.1 µm), respectively, as shown in the histogram insets in Fig. 2a and b. The grey (Y-axis) and black (X-axis) dots in Fig. 2a and b, respectively, represent measured positions of the axis perpendicular to the actively moving axis and indicate a passively occurring offset that was not further quantified.

These results demonstrate excellent correlation of practical resolution to calculated theoretical resolution but at the same time also reflect moderate accuracy as indicated by the high standard deviation (X: ± 1.8 and ± 1.9 µm; Y: ± 2.2 and ± 1.1 µm) at the resolution limit of the stage as well as a passively occurring offset at the axis perpendicular to the actively moving axis.

For assessing repeatability of the stage, we parametrized the controlling software to repeatedly capture a single image at the same position of a *USAF 1951 test target*, defined by a fixed number of steps (well D4 of 96-well plate, corresponding to 6900 and 6200 single X- and Y-axis motor steps, respectively) to be executed by the stepper motors upon zero-point calibration. The repeatability was quantified by measuring the deviation from the original position using the ImageJ plugin *Register Virtual Stack*. Fig. 2c shows single data points and box plots of the deviation from the original position in X- and Y-direction. The minimal and maximal deviations from the origin vary between −92.6 and 94.5 µm for the X-axis and −29.2 and 108.8 µm for the Y-axis. The average repeatability and standard deviation for X-(black, 3.9 ± 48.3 µm) and Y-directions (grey, 5.4 ± 28.9 µm) calculated from a total of 19 repeats each are represented by open circles and error bars.

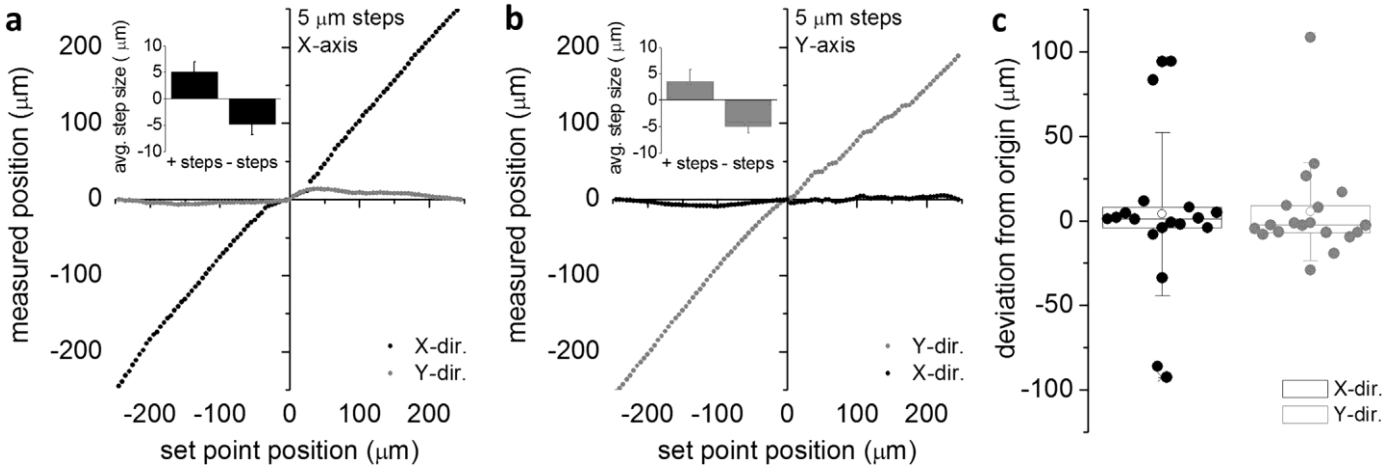

Fig. 2. The spatial resolution, accuracy and repeatability of the positioning system is sufficient to microscopic applications. (a) and (b) Correlation plots of set point position to associated measured position of the X- (black) and Y-axis (grey) when either the X- (a) or Y-axis (b) is moved. The histogram-insets depict the average resolution (mean ± SD, n=50) and reflect moderate accuracy as indicated by high standard deviation as well as a passively occurring offset at the axis perpendicular to the actively moving axis (see grey dots in (a) and black dots in (b)). (c) The bi-directional repeatability range was assessed by repetitively commanding the device to the same location and measures approx. ± 5 µm.

The solid line in the box mark the median value, upper and lower box-margins indicate 75th and 25th percentiles, respectively.

These data demonstrate the suitability of the stage to microscopic applications which require a mean bi-directional repeatability range of approx. ± 5 µm.

3.3. Example I (Cancer research): high-throughput cell viability screening

In order to assess the applicability of the presented positioning device to automated high-content microscopy in high-throughput mode, we imaged HEK293^{YFPI152L} cells, recombinantly expressing a cytosolic fluorescence marker and seeded at densities between 5000 and 30,000 cells per well with our custom built robot and compared quantification data of cell number to those generated with a microplate reader. Plate reader-based quantification typically delivers low-resolution data within short time (here: approx. three minutes per 96-well plate), i.e. a single data point per well of a multititer plate that is usually expressed as relative fluorescence unit (RFU). Microscopy-based quantification is more time consuming (here: approx. one hour per 96-well plate) but in turn provides data of high content and allows characterization of fluorescence signal and cell number at both single cell and population-based level, typically expressed as cells per image or mean pixel intensity (MPI). Fig. 3a shows images of HEK293^{YFPI152L} cells acquired using the custom built system. Fig. 3b shows color maps of data generated with the plate reader (left) and the custom robot (middle, right) with cold and warm colors representing low and high values, respectively. For quantification of the cells per image and MPI, images were segmented and quantitatively analyzed using a modified version of DetecTiff software (see methods section for details). Fig. 3c and d show correlation plots of averaged values for 5000, 10000, 15000, 20000, 25000 and 30000 seeded cells per well (n =16 wells, error bars: ± SD) reflected by RFU from plate reader-based quantification (11024 ± 233, 13343 ± 606, 16120 ± 1630, 18377 ± 1402, 20385 ± 1207 and 22776 ± 1912) versus MPI (9.9 ± 0.7, 12.8 ± 1.6, 15.4 ± 1.1, 18.6 ± 1.1, 20.9 ± 1.6 and 21.4 ± 2.3) and cells per image (94 ± 25, 235 ± 43, 366 ± 39, 520 ± 50, 590 ± 53 and 604 ± 74) calculated from data obtained using the custom built robot. Regression analysis (dashed lines) of quantification data obtained with the custom built system including the low-cost positioning stage revealed excellent correlation with data from conventional technology (Fig. 3c, R^2=0.98 ± 0.79; Fig. 3d, R^2=0.97 ± 47.8). Thus, data generated in high-throughput screening experiments using our platform compares well with data from conventional technology.

These results clearly demonstrate that the low cost positioning device is suitable to application for high-content imaging in high-throughput screening mode.

3.4. Example II (Neurosciences): high-content functional chloride- and calcium-imaging

In order to assess whether the motorized stage as a key element of our custom built robot enables fluorescence-based functional imaging of ion channels in high-throughput mode, we conducted automated agonist and antagonist concentration-response experiments with glycine receptor (GlyR) chloride channels and transient receptor potential vanilloid receptor type 1 (TRPV1) cation channels using the fluorescence indicators YFPI152L and Fluo-4 AM, respectively.

For Cl^- imaging experiments with GlyRs, we co-transfected HEK293 cells with YFPI152L and α3 GlyR cDNA and seeded the cells at defined density of 3×10^4 cells in each well of a 96-well plate. The next day and approximately 1 h prior to imaging, the culture medium was completely removed and was replaced by 50 µl NaCl control solution. The standard NaCl control solution contained (in mM): NaCl 140, KCl 5, $CaCl_2$ 2, $MgCl_2$ 1, HEPES 10, glucose 10, pH 7.4 using NaOH. The 96-well plate was placed onto the motorized stage of our in house-built imaging system and cells were imaged once in control solution or in control solution supplemented with increasing concentrations (0.1–100 µM) of the competitive antagonist strychnine (STR) to record cellular YFP fluorescence in unquenched state. As YFPI152L is almost insensitive to chloride, its fluorescence intensity is highest in NaCl solution allowing for optimal focussing into the optical layer of cells. Subsequently, cells were perfused with 100 µl NaI test solution containing either increasing (3–3000 µM, Fig. 4a) or a single concentration of glycine (GLY, 65 µM, Fig. 4b) and were imaged again. The NaI test solution was similar to NaCl control solution except that the NaCl was replaced by equimolar NaI. Fluorescence quench was calculated at single cell level by quantitative analysis of image pairs as described in the methods section. Sample images of HEK293 cells transfected with both YFPI152L and the GlyR α3 subunit are shown in Fig. 4a and b. Average (mean ± SD) agonist and antagonist dose–responses were constructed by pooling results from wells exposed to different solutions and subsequent averaging from replicate experiments (Fig. 4a: n =8; Fig. 4b: n =3). Calculated half-maximal activation or inhibition concentration (EC_{50}, IC_{50}) for glycine (63.7 ± 7.3 µM) and strychnine (3.3 ± 0.7 µM) correspond well with data from functional Cl^- imaging and electrophysiology previously reported in the literature (Meier et al., 2005; Talwar et al., 2013) and demonstrate that the

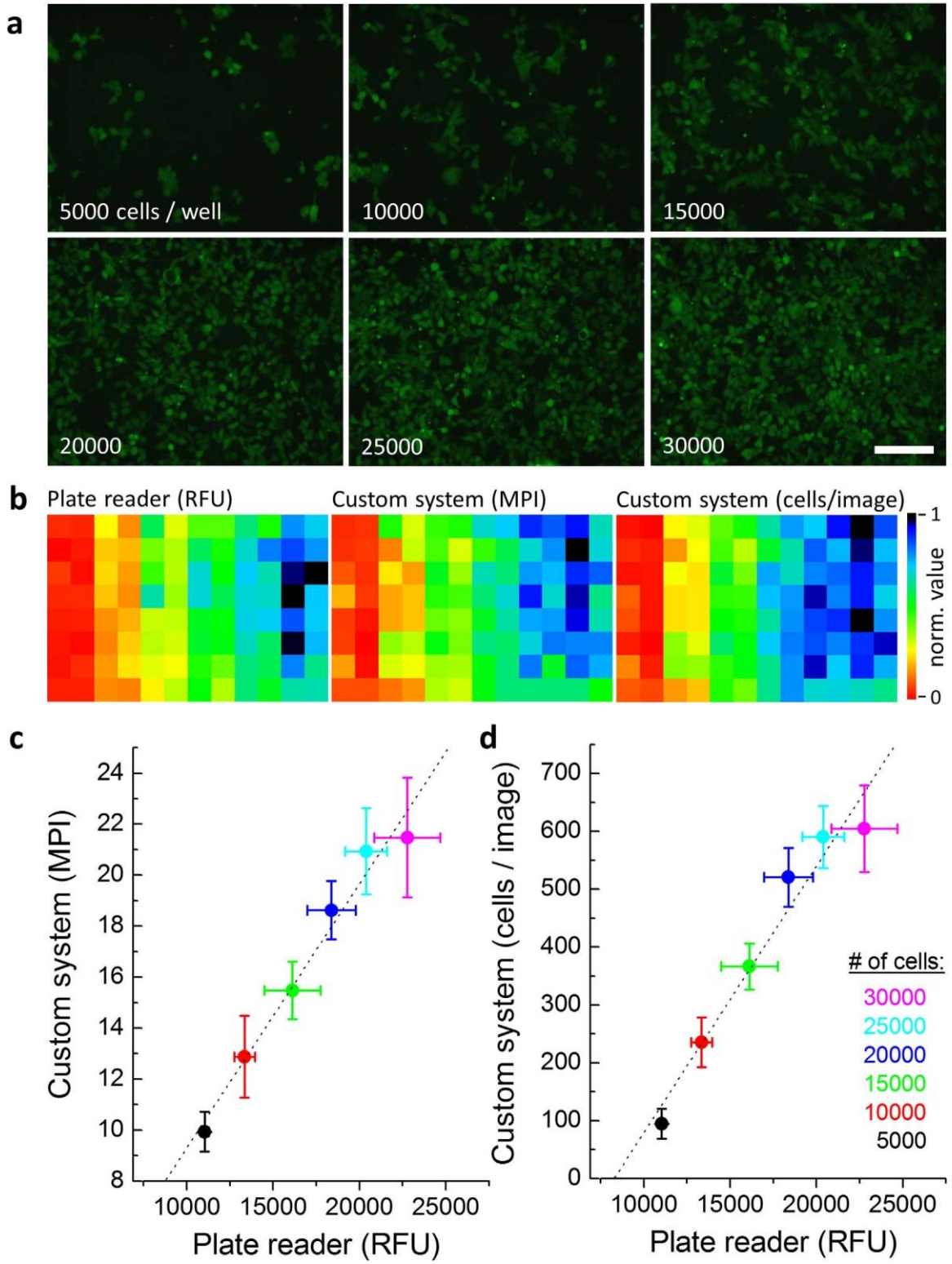

Fig. 3. High-content imaging data acquired in high-throughput screening mode compare well with data from conventional technology. (a) Images of HEK293$^{YFP_{I152L}}$-cells seeded at different densities and acquired using the custom built system. Scale bar: 200 µm. (b) Color maps of data generated with a plate reader (left, population-based analysis) and the custom robot (middle, population-based analysis; right, single cell-based analysis) with cold and warm colors representing low and high values, respectively. (c) and (d) Correlation plots of averaged values for cells seeded at different densities (n =16 wells, error bars: ± SD) and regression analysis (dashed lines) of quantification data obtained with the custom built system and conventional technology demonstrating that the low-cost positioning device is suitable to application for high-content imaging in high-throughput screening mode.

motorized stage enables automated fluorescence-based functional imaging of GlyRs.

For Ca^{2+} imaging experiments with TRPV1 channels, HEK293 cells were transiently transfected with TRPV1 cDNA and seeded the cells at defined density of 2.5×10^4 cells in each well of a 96-well plate. The next day and approximately 1.5 h prior to imaging, the cells were incubated in Fluo-4 AM calcium indicator as described in the methods section and cells were imaged once in control solution using the custom-built

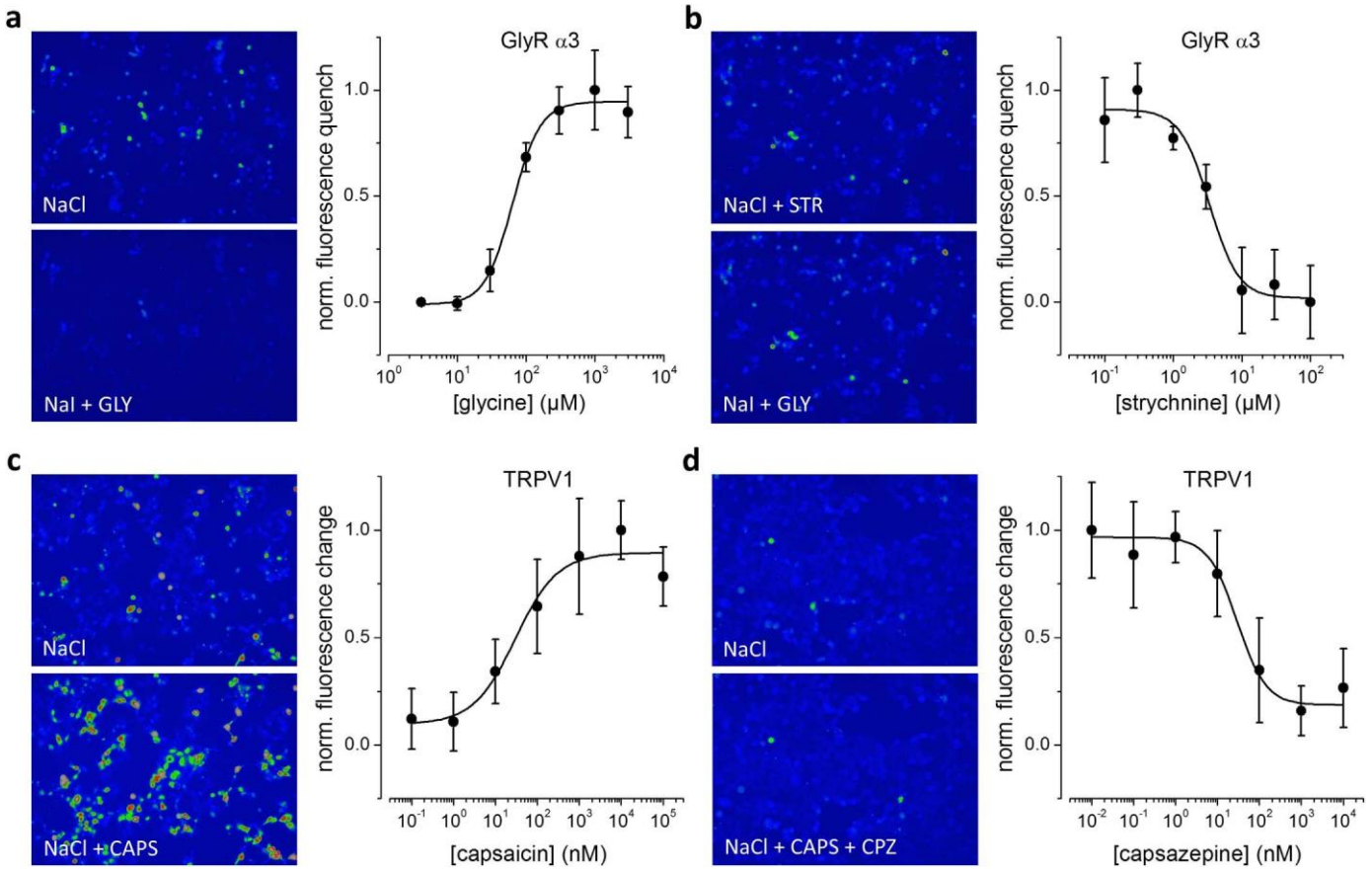

Fig. 4. The positioning device enables high-throughput functional Cl^- and Ca^{2+} imaging for evaluating the physiological and pharmacological characteristics of ion channels. (a, left) Images of HEK293 cells transiently transfected with GlyR α3 and YFPI152l, incubated in NaCl control solution (top) and NaI test solution containing 100 μM glycine (GLY, bottom). (a, right) Dose-response experiment with increasing glycine concentrations. (b, left) Images of HEK293 cells transfected as in (a) but incubated in NaCl control solution containing 100 μM strychnine (STR, top) and upon addition of NaI test solution containing 100 μM glycine (GLY, bottom). (b, right) Concentration-response experiment with constant glycine but increasing strychnine concentrations. (c, left) Images of HEK293 cells transiently transfected with TRPV1 cDNA, incubated in NaCl control solution (top) and NaCl test solution supplemented with 10 μM capsaicine (CAPS, bottom). (c, right) Dose-response experiment with increasing capsaicin concentrations. (d, left) Images of HEK293 cells transiently transfected as in (c) but incubated in NaCl control solution (top) and NaCl test solution supplemented with 1 μM capsaicine and 100 nM capsazepine (CPZ, bottom). (b, right) Dose-response experiment with constant capsaicine (1 μM) but increasing capsazepine concentrations. These data correspond well to data available in the literature and validate the applicability of the positioning stage as a central and key component of a low-cost screening device for automated physiological and pharmacological profiling of ion channels in high throughput mode.

robot. Subsequently, cells were perfused with 100 μl NaCl agonist solution containing either increasing concentrations (0.1–100000 nM, Fig. 4c) or a single concentration of capsaicin (CAPS, 1 μm, Fig. 4d), supplemented with increasing concentrations (0.01–10000 nM) of the competitive antagonist capsazepine (CPZ). Fluorescence change was calculated as described in the methods section. Sample images of HEK293 cells transfected with TRPV1 and loaded with the calcium probe Fluo-4 AM are shown in Fig. 4c and d. Average (mean ± SD) agonist and antagonist dose–responses are shown in Fig. 4c (n =4) and Fig. 4d. (n =3). Calculated half-maximal activation or inhibition concentration (EC_{50}, IC_{50}) for capsaicin (29.7 ± 33.7 nM) and capsazepine (29.3 ± 35.0 nM) basically correspond to data reported in the literature (Bevan et al., 1992) and further validate applicability of the positioning system for automated functional imaging, i.e. for evaluating the physiological and pharmacological characteristics of ion channels in high throughput mode.

Detailed instructions to re-building the device can be found in the Supplementary Step-by-Step instructions.pdf file in the archive *Supplements.zip*.

4. Discussion

To overcome the limitations of commercially available positioning technology suitable for automated high-content microscopy, we have developed a system that is advantageous for several reasons. First, with a footprint of 33×20 cm and a mass of 1.1 kg, including controller and power supply, the device is smaller and lighter compared to conventional technology (e.g. Nikon TI-SH-U or Prior Scientific H107/HLD117), allowing for mobile application. The device requires a USB connection as well as 5 V DC that could either be provided by a 220V-powered supply or even a battery further supporting mobile applicability. No specific cabling or connectors are needed and operation using a laptop and any other handheld device is sufficient. Second, with EUR 250 costs of material, the system is approx. 40–80 times less expensive compared to commercially available devices and is readily applicable to a broad range of laboratories in various fields of research and educational institutions. Despite its extremely low costs, the positioning characteristics in general and the repeatability in particular, compares well with commercially available systems (3.9–5.4 μm vs. 1 μm for Prior Scientific H107), that could be further improved by using e.g. stable closed-loop positioning feedback control systems, spindles of smaller pitch as well as by operating the stepper motors in half or micro-stepping mode, resulting in finer resolution and higher repeatability. Third, the device was prototyped based on a 'Makers' approach and can easily and quickly be re-built in so called 'Fab labs' (fabrication laboratories) based on the information provided in the paper including supplementary files. Fab labs are small-scale workshops, virtually accessible to anyone and available in many cities and

countries (for a list see e.g. https://www.fablabs.io/labs), which are increasingly being adopted by schools and universities as platforms for project-based, hands-on STEM (science, technology, engineering and mathematics) education. Furthermore, as STL and STEP files are provided for all 3D printable components it is possible to simply and quickly modify individual parts and even the complete stage to meet specific requirements. In contrast, hardware modification and customization of conventional positioning stages is typically not permissible and will result in the loss of warranty and exclusion of liability. Additionally, in case of defective hardware, even within the warranty period, it typically takes several weeks and even up to months until the issue is identified and fixed. Beyond the warranty period, replacement of defective parts presumably takes even longer and might also generate disproportionately high costs. All 3D printed parts and off-the-shelf components of the presented device can easily be replaced within the same day. For modification of the provided 3D design files, there is a variety of free 3D design software available on the internet including, e.g. SketchUp Make or FreeCAD. Although building the positioning stage based on 3D printed parts is probably the quickest and most inexpensive way, the device could also be constructed from more durable machined components using different and more robust material including injection molding. Fourth, the positioning stage presented in this paper is completely open source as we also provide any software required to operating the device including Arduino- and LabVIEW-based software code. Both programming environments are comprehensively documented and support is provided in user forums, via tutorials and with a large spectrum of examples allowing the user to quickly interface the stage with third-party soft- and hardware without being a specialist. For example, most commercial stages are optionally equipped with a joystick or related hardware for manual control that – with a few thousand euros cost – is typically prohibitively expensive for many labs. The presented positioning system could be easily extended for manual control using e.g. a few buttons on the computer keyboard or a simple joystick for less than a euro as typically implemented in conventional gaming controllers. Finally, the device in its current configuration is straightforward, easy to use and does not require highly skilled staff for application and maintenance as well as expensive service contracts thus, further highlighting the applicability in a large spectrum of scientific or educational fields.

Despite the above mentioned advantages over conventional positioning stages, the inexpensive open source microscope stage has also potential for improvement. For example, all plastic parts were printed with a relatively low infill value of 30%, leading to light weight but also fragile components. Although in our laboratory the stage has been intensively used on a daily basis and for months without functional impairment, increasing the fill value may result in increased robustness and reliability in long-term applications. In high-throughput screening experiments, hardware speed is one of the most important throughput-limiting factors. Commercially available positioning devices specify the maximal scanning speed with values from 40 (e.g. Prior Scientific H107) to 300 mm/s (e.g. Prior Scientific HLD117). Due to LabVIEW-related speed limitations for communication with the Arduino board via the serial port, the maximum scanning speed of the low-cost device is currently limited to 5 mm/s, reducing the achievable experimental throughput compared to commercially available high-end motorized microscope stages. Some manufacturers indicate the flatness of the complete stage (e.g. 5 µm for Prior Scientific H107) as it influences the maximally achievable experimental throughput via a given minimal range required for autofocussing. The flatness of the low cost device was not determined but is presumably in the range of hundreds of micro meters.

Although the system is currently set up for application with multititer plates it could easily be extended for use with standard cell or tissue culture plastic or glass ware without the need for the device to be re-designed. We have created a range of adapters allowing the positioning system to be used with standard 26×76 mm glass slides, 40 and 60 mm dishes as well as T25 and T75 tissue culture flasks. Associated 3D design files in STL and STEP format can be found in the supplements subfolder named *Misc*.

While controlling of the presented device is orchestrated by an Arduino microcontroller board and its IDE as well as – optionally - LabVIEW, system control could also be realized by other microcontroller prototyping boards such as Raspberry Pi or BeagleBone and associated programming languages and operating systems.

Imaging data generated with our device compares well with data obtained using a commercially available microplate reader, demonstrating its suitability to high-content microscopy in high-throughput screening format and validating its applicability to automated functional Cl^-- and Ca^{2+}-imaging with recombinant HEK293 cells as a model system.

Although this work focusses on automated high-content imaging in high-throughput mode, the presented technology could also be extended by implementation of further instrumentation including incubator infrastructure, capable of maintaining optimal conditions necessary for culturing organisms such as temperature and carbon dioxide or oxygen concentration as well as humidity of the atmosphere or other biosensor technology to suit the requirements for a vast variety of fields of research including life and even material sciences.

In summary, the 3D printed motorized positioning stage presented in this article improves the classical technologies in terms of portability, customizability, user-friendliness and cost and provides an example of open source low-cost technology that is compatible with fast and resource-efficient prototype optimization. Altogether, this work contributes to furthering the applicability and availability of commercially viable automated high-content imaging devices for use in biomedical research and education.

Conflict of interest statement

The authors declare no conflict of interest.

Author contributions

O.F. and D.F.G. conceived the project. D.S. created 3D CAD models. L.K. and D.F.G. conducted experiments. J.C.M. provided GlyR cDNA and contributed to supervision of L.K.. D.F.G. designed electrical circuits, developed and employed software code, assembled the system, analyzed and displayed the data and wrote the paper.

Supplementary information

The *Supplements.zip* archive includes, 1. Step-by-Step Instructions, 2. 3D design files in STL and STEP format, 3. Illustrated assembly instructions organized in a total of five modules (Module A – E), 4. A PCB design file (PCB_Stepper.fzz) 5. Software code (Arduino and LabVIEW), 6. Parts list Table S1.

Acknowledgements

We thank Dr. M. Tominaga (Okazaki Institute for Integrative Biosc Jence, Okazaki, Japan) for TRPV1-DNA (Genbank accession number AF029310) and J.W. Lynch for YFPI152L. We thank O. Oppermann for video post-processing and C. Detmers for helpful discussions. The authors gratefully acknowledge funding of the Erlangen Graduate School in Advanced Optical Technologies (SAOT) by the German Research Foundation (DFG) in the framework of the German excellence initiative. This work was also supported by the Bundesministerium für Bildung und Forschung BMBF (Era-Net NEURON II CIPRESS to J.C.M.) and the Deutsche Forschungsgemeinschaft DFG (Priority Programme SPP 1784 ME2075/7-1 to J.C.M.). L.K. was supported by a PhD grant from the Berlin Institute of Health (BIH). The funders had no role in study

design, data collection and analysis, decision to publish, or preparation of the manuscript.

Appendix A. Supplementary material

Supplementary data associated with this article can be found in the online version at http://dx.doi.org/10.1016/j.bios.2016.10.078.

References

Alexander, S.P., Kelly, E., Marrion, N., Peters, J.A., Benson, H.E., Faccenda, E., Pawson, A.J., Sharman, J.L., Southan, C., Buneman, O.P., Catterall, W.A., Cidlowski, J.A., Davenport, A.P., Fabbro, D., Fan, G., McGrath, J.C., Spedding, M., Davies, J.A., 2015. The concise guide to PHARMACOLOGY 2015/16: overview. Br. J. Pharmacol. 172 (24), 5729–5743.

Arganda-Carreras, I., Sorzano, C.S., Marabini, R., Carazo, J., Ortiz-de-Solorzano, C., Kybic, J., 2006. Consistent and elastic registration of histological sections using vector-spline regularization. In: Beichel, R., Sonka, M. (Eds.), Computer Vision Approaches to Medical Image Analysis. Springer Berlin Heidelberg, 85–95.

Balansa, W., Islam, R., Fontaine, F., Piggott, A.M., Zhang, H., Webb, T.I., Gilbert, D.F., Lynch, J.W., Capon, R.J., 2010. Ircinialactams: subunit-selective glycine receptor modulators from Australian sponges of the family Irciniidae. Bioorg. Med. Chem. 18 (8), 2912–2919.

Balansa, W., Islam, R., Fontaine, F., Piggott, A.M., Zhang, H., Xiao, X., Webb, T.I., Gilbert, D.F., Lynch, J.W., Capon, R.J., 2013a. Sesterterpene glycinyl-lactams: a new class of glycine receptor modulator from Australian marine sponges of the genus Psammocinia. Org. Biomol. Chem. 11 (28), 4695–4701.

Balansa, W., Islam, R., Gilbert, D.F., Fontaine, F., Xiao, X., Zhang, H., Piggott, A.M., Lynch, J.W., Capon, R.J., 2013b. Australian marine sponge alkaloids as a new class of glycine-gated chloride channel receptor modulator. Bioorg. Med. Chem. 21 (14), 4420–4425.

Berg, B., Cortazar, B., Tseng, D., Ozkan, H., Feng, S., Wei, Q., Chan, R.Y., Burbano, J., Farooqui, Q., Lewinski, M., Di Carlo, D., Garner, O.B., Ozcan, A., 2015. Cellphone-based hand-held microplate reader for point-of-care testing of enzyme-linked immunosorbent assays. ACS Nano 9 (8), 7857–7866.

Bevan, S., Hothi, S., Hughes, G., James, I.F., Rang, H.P., Shah, K., Walpole, C.S., Yeats, J.C., 1992. Capsazepine: a competitive antagonist of the sensory neurone excitant capsaicin. Br. J. Pharmacol. 107 (2), 544–552.

Braat, S., Kooy, R.F., 2015. The GABAA receptor as a therapeutic target for neurodevelopmental disorders. Neuron 86 (5), 1119–1130.

Campbell, R.A., Eifert, R.W., Turner, G.C., 2014. OpenStage: a low-cost motorized microscope stage with sub-micron positioning accuracy. PloS One 9 (2), e88977.

Caterina, M.J., Julius, D., 2001. The vanilloid receptor: a molecular gateway to the pain pathway. Annu. Rev. Neurosci. 24, 487–517.

Conrad, K.L., Shiakolas, P.S., Yih, T., 2000. Robotic calibration issues: Accuracy, repeatability and calibration. In: Proceedings of the 8th Mediterranean Conference on Control and Automation (MED2000).

D'Ausilio, A., 2012. Arduino: a low-cost multipurpose lab equipment. Behav. Res. Methods 44 (2), 305–313.

Editorial, 2013. The DIY dilemma. Nature 503 (7477), 437–438.

Frame, M., Leach, W., 2014. DIY 3D printing of custom orthopaedic implants: a proof of concept study. Surg. Technol. Int 24, 314–318.

Galietta, L.J., Haggie, P.M., Verkman, A.S., 2001. Green fluorescent protein-based halide indicators with improved chloride and iodide affinities. FEBS Lett. 499 (3), 220–224.

Gee, K.R., Brown, K.A., Chen, W.N., Bishop-Stewart, J., Gray, D., Johnson, I., 2000. Chemical and physiological characterization of fluo-4 Ca(2+)-indicator dyes. Cell Calcium 27 (2), 97–106.

Gilbert, D., Esmaeili, A., Lynch, J.W., 2009a. Optimizing the expression of recombinant alphabetagamma GABAA receptors in HEK293 cells for high-throughput screening. J. Biomol. Screen. 14 (1), 86–91.

Gilbert, D.F., Erdmann, G., Zhang, X., Fritzsche, A., Demir, K., Jaedicke, A., Muehlenberg, K., Wanker, E.E., Boutros, M., 2011. A novel multiplex cell viability assay for high-throughput RNAi screening. PloS One 6 (12), e28338.

Gilbert, D.F., Islam, R., Lynagh, T., Lynch, J.W., Webb, T.I., 2009a. High throughput techniques for discovering new glycine receptor modulators and their binding sites. Front. Mol. Neurosci. 2, 17.

Gilbert, D.F., Meinhof, T., Pepperkok, R., Runz, H., 2009b. DetecTiff: a novel image analysis routine for high-content screening microscopy. J. Biomol. Screen. 14 (8), 944–955.

Gilbert, D.F., Wilson, J.C., Nink, V., Lynch, J.W., Osborne, G.W., 2009c. Multiplexed labeling of viable cells for high-throughput analysis of glycine receptor function using flow cytometry. Cytom. Part A: J. Int. Soc. Anal. Cytol. 75 (5), 440–449.

Gregory, C., Veeman, M., 2013. 3D-printed microwell arrays for Ciona microinjection and timelapse imaging. PloS One 8 (12), e82307.

Kruger, W., Gilbert, D., Hawthorne, R., Hryciw, D.H., Frings, S., Poronnik, P., Lynch, J.W., 2005. A yellow fluorescent protein-based assay for high-throughput screening of glycine and GABAA receptor chloride channels. Neurosci. Lett. 380 (3), 340–345.

Kuenzel, K., Friedrich, O., Gilbert, D.F., 2016. A recombinant human pluripotent stem cell line stably expressing halide-sensitive YFP-I152L for GABAAR and GlyR-targeted high-throughput drug screening and toxicity testing. Front. Mol. Neurosci., 9.

Kuhse, J., Schmieden, V., Betz, H., 1990. Identification and functional expression of a novel ligand binding subunit of the inhibitory glycine receptor. J. Biol. Chem. 265 (36), 22317–22320.

Landrain, T., Meyer, M., Perez, A.M., Sussan, R., 2013. Do-it-yourself biology: challenges and promises for an open science and technology movement. Syst. Synth. Biol. 7 (3), 115–126.

Leeuw, T., Boss, E.S., Wright, D.L., 2013. In situ measurements of phytoplankton fluorescence using low cost electronics. Sensors 13 (6), 7872–7883.

Legendre, P., Forstera, B., Juttner, R., Meier, J.C., 2009. Glycine receptors caught between genome and proteome - functional implications of RNA editing and splicing. Front. Mol. Neurosci. 2, 23.

Lynch, J.W., 2009. Native glycine receptor subtypes and their physiological roles. Neuropharmacology 56 (1), 303–309.

Lynch, J.W., Rajendra, S., Pierce, K.D., Handford, C.A., Barry, P.H., Schofield, P.R., 1997. Identification of intracellular and extracellular domains mediating signal transduction in the inhibitory glycine receptor chloride channel. EMBO J. 16 (1), 110–120.

Marzullo, T.C., Gage, G.J., 2012. The SpikerBox: a low cost, open-source bioamplifier for increasing public participation in neuroscience inquiry. PloS One 7 (3), (e30837-e30837).

Meier, J.C., Henneberger, C., Melnick, I., Racca, C., Harvey, R.J., Heinemann, U., Schmieden, V., Grantyn, R., 2005. RNA editing produces glycine receptor alpha3(P185L), resulting in high agonist potency. Nat. Neurosci. 8 (6), 736–744.

Meier, J.C., Semtner, M., Winkelmann, A., Wolfart, J., 2014. Presynaptic mechanisms of neuronal plasticity and their role in epilepsy. Front. Cell. Neurosci. 8, 164.

Ortega-Guerrero, A., Espinosa-Duran, J.M., Velasco-Medina, J., 2016. TRPV1 channel as a target for cancer therapy using CNT-based drug delivery systems. Eur. Biophys. J.: EBJ.

Pineño, O., 2014. ArduiPod Box: a low-cost and open-source Skinner Box using an iPod Touch and an Arduino microcontroller. Behav. Res. Methods 46 (1), 196–205.

Schubert, T.W., D'Ausilio, A., Canto, R., 2013. Using Arduino microcontroller boards to measure response latencies. Behav. Res. Methods 45 (4), 1332–1346.

Seyfried, G., Pei, L., Schmidt, M., 2014. European do-it-yourself (DIY) biology: beyond the hope, hype and horror. Bioessays 36 (6), 548–551.

Shannon, K.M., Gage, G.J., Jankovic, A., Wilson, W.J., Marzullo, T.C., 2014. Portable conduction velocity experiments using earthworms for the college and high school neuroscience teaching laboratory. Adv. Physiol. Educ. 38 (1), 62–70.

Spivey, E.C., Xhemalce, B., Shear, J.B., Finkelstein, I.J., 2014. 3D-printed microfluidic microdissector for high-throughput studies of cellular aging. Anal. Chem. 86 (15), 7406–7412.

Starosolski, Z.A., Kan, J.H., Rosenfeld, S.D., Krishnamurthy, R., Annapragada, A., 2014. Application of 3-D printing (rapid prototyping) for creating physical models of pediatric orthopedic disorders. Pediatr. Radiol. 44 (2), 216–221.

Stokes, T.H., Venugopalan, J., Hubbard, E.N., Wang, M.D., 2013. A pilot biomedical engineering course in rapid prototyping for mobile health. Conf. Proc. IEEE Eng. Med Biol. Soc. 2013, 2515–2518.

Talwar, S., Lynch, J.W., Gilbert, D.F., 2013. Fluorescence-based high-throughput functional profiling of ligand-gated ion channels at the level of single cells. PloS One 8 (3), e58479.

Walzik, M.P., Vollmar, V., Lachnit, T., Dietz, H., Haug, S., Bachmann, H., Fath, M., Aschenbrenner, D., Abolpour Mofrad, S., Friedrich, O., Gilbert, D.F., 2015. A portable low-cost long-term live-cell imaging platform for biomedical research and education. Biosens. Bioelectron. 64, 639–649.

Wardyn, J.D., Sanderson, C., Swan, L.E., Stagi, M., 2015. Low cost production of 3D-printed devices and electrostimulation chambers for the culture of primary neurons. J. Neurosci. Methods 251, 17–23.

Wittbrodt, J.N., Liebel, U., Gehrig, J., 2014. Generation of orientation tools for automated zebrafish screening assays using desktop 3D printing. BMC Biotechnol. 14, (36-36).

Publication 2: Kraus et al., 2019

Kraus L, Hetsch F, Schneider UC, Radbruch H, Holtkamp M, Meier JC, Fidzinski P. Dimethylethanolamine Decreases Epileptiform Activity in Acute Human Hippocampal Slices in vitro. Front Mol Neurosci. 2019

frontiers in Molecular Neuroscience

BRIEF RESEARCH REPORT
published: 06 September 2019
doi: 10.3389/fnmol.2019.00209

Dimethylethanolamine Decreases Epileptiform Activity in Acute Human Hippocampal Slices *in vitro*

*Larissa Kraus [1,2], Florian Hetsch [3], Ulf C. Schneider [4], Helena Radbruch [5], Martin Holtkamp [1,2], Jochen C. Meier [2,3] and Pawel Fidzinski [1]**

[1]*Charité-Universitätsmedizin Berlin, corporate member of Freie Universität Berlin, Humboldt-Universität zu Berlin, and Berlin Institute of Health, Department of Neurology with Experimental Neurology, Berlin, Germany,* [2]*Berlin Institute of Health (BIH), Zoologisches Institut, Technische Universität Braunschweig, Braunschweig, Germany,* [3]*Zoologisches Institut, Technische Universität Braunschweig, Braunschweig, Germany,* [4]*Charité-Universitätsmedizin Berlin, corporate member of Freie Universität Berlin, Humboldt-Universität zu Berlin, and Berlin Institute of Health, Department of Neurosurgery, Berlin, Germany,* [5]*Charité-Universitätsmedizin Berlin, corporate member of Freie Universität Berlin, Humboldt-Universität zu Berlin, and Berlin Institute of Health, Department of Neuropathology, Berlin, Germany*

Temporal lobe epilepsy (TLE) is the most common form of focal epilepsy with about 30% of patients developing pharmacoresistance. These patients continue to suffer from seizures despite polytherapy with antiepileptic drugs (AEDs) and have an increased risk for premature death, thus requiring further efforts for the development of new antiepileptic therapies. The molecule dimethylethanolamine (DMEA) has been tested as a potential treatment in various neurological diseases, albeit the functional mechanism of action was never fully understood. In this study, we investigated the effects of DMEA on neuronal activity in single-cell recordings of primary neuronal cultures. DMEA decreased the frequency of spontaneous synaptic events in a concentration-dependent manner with no apparent effect on resting membrane potential (RMP) or action potential (AP) threshold. We further tested whether DMEA can exert antiepileptic effects in human brain tissue *ex vivo*. We analyzed the effect of DMEA on epileptiform activity in the CA1 region of the resected hippocampus of TLE patients *in vitro* by recording extracellular field potentials in the pyramidal cell layer. Epileptiform burst activity in resected hippocampal tissue from TLE patients remained stable over several hours and was pharmacologically suppressed by lacosamide, demonstrating the applicability of our platform to test antiepileptic efficacy. Similar to lacosamide, DMEA also suppressed epileptiform activity in the majority of samples, albeit with variable interindividual effects. In conclusion, DMEA might present a new approach for treatment in pharmacoresistant TLE and further studies will be required to identify its exact mechanism of action and the involved molecular targets.

Keywords: epilepsy, drug development, human, hippocampus, *ex vivo*

OPEN ACCESS

Edited by:
Jaewon Ko,
Daegu Gyeongbuk Institute of Science and Technology (DGIST), South Korea

Reviewed by:
Aleksey V. Zaitsev,
Institute of Evolutionary Physiology and Biochemistry (RAS), Russia
Giuseppe Biagini,
University of Modena and Reggio Emilia, Italy

**Correspondence:*
Pawel Fidzinski
pawel.fidzinski@charite.de

Received: 19 May 2019
Accepted: 09 August 2019
Published: 06 September 2019

Citation:
Kraus L, Hetsch F, Schneider UC, Radbruch H, Holtkamp M, Meier JC and Fidzinski P (2019) Dimethylethanolamine Decreases Epileptiform Activity in Acute Human Hippocampal Slices in vitro. Front. Mol. Neurosci. 12:209. doi: 10.3389/fnmol.2019.00209

INTRODUCTION

Epilepsy is a major neurological disorder affecting up to 65 million people worldwide (Hirtz et al.,2007;Ngugi et al.,2010). The need for adequate treatment is not only given by seizures itself along with associated risks of injury and premature death but also by comorbidities and social stigmatization. Specifically in focal epilepsy, 30%–40% of patients do not respond to

currently available antiepileptic drugs (AEDs), resulting in pharmacoresistance with ongoing seizures despite treatments with multiple AEDs at high dosages (Stephen et al.,2001). Alternative therapies such as ketogenic diet or brain stimulation have been suggested to reduce seizure burden in pharmacoresistant patients (Giordano et al.,2014;Kowski et al., 2015;Dibué-Adjei et al.,2019). However, ketogenic diet has been shown to be effective in children and with modification in adults but is still rarely considered as treatment in adults (Hallböök et al.,2015;Falco-Walter et al.,2019). Ongoing investigations show promising seizure reduction in pharmacoresistant patients by deep brain stimulation (Zangiabadi et al.,2019). However, this approach requires optimal selection of targeted brain regions and prospective trials are lacking. Finally, surgical removal of the epileptic focus remains often the only treatment option for pharmacoresistant patients (Wiebe et al.,2001;Engel et al., 2007). Yet, only in a minority of patients, epilepsy is amenable to surgery, and only 60%–70% of resected patients have a positive outcome with substantial reduction of the seizure burden (International League Against Epilepsy Outcome Scale 1–2; Mohan et al.,2018). Thus, identification of new antiepileptic treatment options in focal pharmacoresistant epilepsy is of paramount importance.

Dimethylethanolamine (DMEA) has previously been investigated as a stimulant and treatment for several neurological diseases, including tardive dyskinesia (TD), Alzheimer's disease (AD) and senile dementia (Ferris et al.,1977; Penovich et al., 1978; de Montigny et al., 1979; Fisman et al., 1981; George et al.,1981). First, application of DMEA to human healthy volunteers dates back to the 1960s when DMEA was reported to exert stimulating effects comparable to amphetamine (Murphree et al.,1960; Pfeiffer et al.,1963). Murphree et al. (1960) described improved concentration, increased muscle tone and changed sleeping habits in healthy males (21–26 years) with an intake of 10–20 mg DMEA (or Deanol) daily for 2-3 weeks compared to a placebo group. In later studies, DMEA was hypothesized as an acetylcholine (ACh) precursor and therefore tested in diseases that are considered to be linked to the cholinergic system. However, results of several studies were inconclusive and a systematic review could not confirm the positive effects of DMEA or other cholinergic compounds in patients with TD (Tammenmaa et al.,2004). In addition, *in vivo* experiments showed that DMEA is not methylated to choline and does not alter brain ACh levels (Millington et al.,1978; Jope and Jenden,1979).

Interestingly, in both acute and chronic seizure models in rats, a conjugate of DMEA and valproate (DEVA) was shown to be more potent than valproate alone, potentially by facilitation of valproate transport *via* the blood brain barrier (Shekh-Ahmad et al., 2012). In this study, however, the effects of DMEA alone were not tested. To our knowledge, effects of DMEA on pathological neuronal network activity have never been investigated before.

In principle, resected human tissue of temporal lobe epilepsy (TLE) patients carries the potential to bridge the translational gap between preclinical and clinical drug development. Animal models have been instrumental in the discovery and preclinical development of novel AEDs (Löscher,2011). However, animal models cannot represent all aspects of complex neurological disorders and sometimes produce misleading results as exemplified by the neuropeptide galanin. Galanin showed robust antiepileptic effects in a mouse model of epilepsy, however, the effect could not be reproduced in resected human tissue (Ledri et al.,2015).

Here, we decided to investigate the effects of DMEA on epileptiform activity directly in *ex vivo* human tissue resected from epilepsy patients.

MATERIALS AND METHODS

Primary Rat Hippocampal Neuronal Cell Culture

Hippocampal cultures from E18 Wistar rat embryos were prepared as previously described (Winkelmann et al.,2014) according to the approval by the Animal Care Committee of the Technical University Braunschweig (Zentrale Einrichtung für Tierhaltung der TU Braunschweig, §4 10.15.R TSB TU BS) and maintained in Neurobasal medium supplemented with B27 and 1% FCS (Brewer et al.,1993). Hippocampal neurons were subjected to whole cell patch clamp analysis at DIV13–16 to ensure that the cultures were mature enough to display synaptic activity.

Electrophysiological Recordings of Cultured Hippocampal Neurons

An EPC-7 amplifier (List-Medical, Darmstadt, Germany), ITC-18 interface and Patchmaster software (both HEKA, Lamprecht, Germany) were used for patch clamp recordings and data acquisition. Patch pipettes made from borosilicate glass (Science Products, Hofheim, Germany), had resistances of 4–7 MΩ when filled with the intracellular solution containing (in mM): KCl (130), NaCl (5), $CaCl_2$ (0.5), $MgCl_2$ (1), EGTA (5) and HEPES (30), pH 7.2 (KOH). Neurons were continuously perfused with carbogenated artificial cerebrospinal fluid (aCSF) containing (in mM): NaCl (125), KCl (2), $MgCl_2$ (1), $CaCl_2$ (2), $NaHCO_3$ (25), NaH_2PO_4 (1.25) and glucose (10), pH 7.4. Extracellular solution was supplied by gravity using a perfusion pencil (Automate Scientific Inc., Berkeley, CA, USA) for fast solution exchange. The extracellular solution was supplemented with 0.5, 2, 5 or 10 mM DMEA. Series resistances (Rs) were monitored by 5 mV voltage pulses (50 ms) applied every 5 s and varied between 10 MΩ and 30 MΩ. Data were acquired with a sampling rate of 20 kHz and filtered at 2.8 kHz. All experiments were carried out at room temperature (~24°C).

The effect of DMEA on synaptic activity and excitability was tested in current-clamp mode with stepwise increase of DMEA concentration. DMEA was applied for 60 s, following 3–5 min wash-out with aCSF before applying the next drug concentration. No synaptic or intrinsic blockers were added. A steady current injected into the cell was used to hold the membrane potential around 50 mV never exceeded 150 pA. Action potential (AP) threshold was investigated by short current injections using 10 pA steps with or without the application of DMEA. AP threshold was determined as the mean between the minimum

membrane potential necessary for AP generation and membrane potential of the previous step current.

Human Tissue Transport and Preparation

Human hippocampal tissue from epilepsy surgery was collected from 12 TLE patients (10 males, two females), who all gave written consent prior to the procedure. Experiments were approved by the Ethics Committee of Charité-Universitätsmedizin Berlin on the 1st of November 2014 (EA2/111/14) and performed in agreement with the Declaration of Helsinki.

Hippocampal tissue was transferred to carbonated (95% O_2, 5% CO_2), ice-cold transport solution immediately after resection. Tissue was transported to the lab in <60 min and cut to 400 µm slices using a vibratome (Leica VT1200S, Wetzlar, Germany). N-methyl d-glucamine (NMDG)-aCSF was used for brain tissue transport and slice preparation from patients 1–7, while choline-aCSF was used to handle tissue of patient 8–12 in order to optimize transport. NMDG-aCSF contained (in mM): NMDG (93), KCl (2.5), NaH_2PO_4 (1.2), $NaHCO_3$ (30), $MgSO_4$ (10), $CaCl_2$ (0.5), HEPES (20), glucose (25), Na-L-ascorbate (5), thiourea (2), Na-pyruvate (3;Ting et al.,2014). Choline-aCSF contained (in mM): Choline chloride (110), KCl (2.5), NaH_2PO_4 (1.25), $NaHCO_3$ (26), $MgCl_2$ (7), $CaCl_2$ (0.5), glucose (10), Na-L-ascorbate (11.6), Na-pyruvate (3.1;Testa-Silva et al.,2010).

As part of the standard clinical routine, every third slice collected during the slicing procedure was fixed in 4% paraformaldehyde (PFA, pH 7.4, phosphate-buffered saline) and analyzed for pathological alterations. For electrophysiological recordings, slices were stored in an interface chamber for a recovery period of at least 5 h and continuously perfused with carbogenated aCSF containing (in mM): NaCl (129), NaH_2PO_4 (1.25), $CaCl_2$ (1.6), KCl (3.0), $MgSO_4$ (1.8), $NaHCO_3$ (21), Glucose (10; 1.6 ml/min, 35˚C, pH 7.4). All slices were studied between 6 h and 20 h after resection.

Electrophysiological Recordings of Human Tissue

For electrophysiological recordings, slices were transferred to a custom modified version of the membrane chamber (Hill and Greenfield,2011) and perfused with aCSF (10 ml/min, 32 ˚C). The membrane chamber is a submerged-type recording chamber with a high flow rate but stable slice position, guaranteeing optimal oxygen supply and fast drug applications. Field potential recordings were performed with borosilicate pipettes (1.5 mm outer diameter, Science Products, Hofheim, Germany) pulled with a vertical puller (1–2 MΩ, PC-10, Narishige, Tokyo, Japan) and filled with NaCl (154 mM). Signals were recorded from CA1 pyramidal cell layer, sampled at 10 kHz, low-pass filtered at 2 kHz by a Digidata 1550 interface and processed by PClamp10 software (Molecular Devices, Sunnyvale, CA, USA).

Induction of epileptiform activity in rodent brain slices can be achieved by a stand-alone manipulation such as inhibition of potassium channels by 4-aminopyridine (4-AP; Perreault and Avoli, 1991; Avoli et al., 2002; Heuzeroth et al., 2019). On the contrary, induction of epileptiform activity in human brain tissue *ex vivo* is less straightforward and subject to controversy. In resected human brain tissue only application of 4-AP in combination with electrical stimulation or elevated extracellular potassium was able to show stable induction of epileptiform activity, not application of 10 or 12 mM potassium or 4-AP alone (Gabriel et al.,2004;Antonio et al.,2016). Here, we used bath application of high potassium (8 mM) and 4-AP (100 µM, Sigma, Munich, Germany) for the induction of epileptiform activity in human brain tissue. Increase of osmolarity by 8 mM KCl was balanced by lowering NaCl concentration from 129 mM to 124 mM.

Baseline epileptiform activity was recorded for ≥20 min. DMEA (10 mM, Sigma, Munich, Germany) or lacosamide (LAC, 100 µM, Biozol, Eching, Germany) were then applied for ≥20 min, followed by ≥20 min of wash-out. In initial experiments we tested 5 mM and 10 mM of DMEA in the same slice, starting with 5 mM DMEA (20 min), followed by 10 mM DMEA and wash-out as described above.

Addition of DMEA increases osmolarity of aCSF possibly affecting neuronal activity. Therefore, we performed control experiments with increasing the osmolarity of aCSF up to 310 mOsm by addition of 10 mM sucrose (patients 10, 11, and 12). This approach has been used to test hyperosmolar solutions before (Rosenmund and Stevens,1996). Here, the recording sequence stated above was modified and consisted of the following steps: (1) baseline with stable epileptiform activity (≥10 min); (2) 10 mM sucrose (≥20 min); and (3) wash-out sucrose (≥10 min), 10 mM DMEA (≥20 min), wash-out DMEA (≥20 min).

Data Analysis and Statistics

Electrophysiological data recorded in single cells from primary neuronal cell cultures was quantified and measured using an IGOR Pro (Version 6.3.7.2, Wavemetrics Inc., Oregon, USA) procedure written by Dr. Marcus Semtner (MDC Berlin) and the extension PatchersPowerTools (written by Dr. Francisco Mendez and Frank Würriehausen).

Recordings in human hippocampal tissue were band pass filtered (1–1,000 Hz) and the 300 s long episodes (last 5 min of each application phase) were analyzed with Clampfit 10.7 (Molecular Devices, Sunnyvale, CA, USA) threshold analysis. All events visually identified as burst activity (defined by biphasic, positive and negative deflection and a duration ≥100 ms) were manually indicated for further analysis of event frequency (inter-event-interval, IEI), amplitude and total number of events during the analyzed time frame. Interictal spikes (defined by exclusive negative deflections and a duration <10 ms) were not analyzed. According to literature, interictal spikes, although pathologically relevant, are not significantly affected by AEDs (Spencer et al., 2008;D'Antuono et al.,2010).

All data were analyzed with GraphPad Prism 5 (GraphPad Software Inc., San Diego, CA, USA). Prior to analysis, data were subjected to D'Agostino and Pearson omnibus normality test and analyzed accordingly. In cases where sample size of tested groups was too small for evaluation of data distribution, data were analyzed using non-parametric tests.

Statistical analysis of normal distributed data was performed using repeated measurement analysis of variance (ANOVA)

and *post hoc* Tukey's comparison of all groups. Non-normal distributed data or data with small sample size was analyzed either using Friedman test and *post hoc* Dunnett's multiple comparison of individual groups or Wilcoxon signed-rank test. For all analysis, a p-value < 0.05 was considered statistically significant.

Data analyzed by parametric tests were presented as scatter plots with mean ± standard deviation (SD) while data analyzed by non-parametric tests were presented as scatterplots with median and interquartile range. Due to IEI variance during drug application (DMEA or LAC), frequency of events for all patients was summarized as number of events. IEI for individual recordings is presented as boxplots with median and Tukey whiskers (1.5 the interquartile distance) to show data distribution and inter-individual differences.

Human datasets analyzed in this study can be found in figshare repository (https://doi.org/10.6084/m9.figshare.8148572).

RESULTS

To investigate whether DMEA affects neuronal activity and to obtain information about potential molecular targets, we performed electrophysiological recordings in primary neuronal cultures. DMEA dose-dependently reduced spontaneous synaptic events and associated APs with an estimated EC50 of ~ 0.5–1.0 mM. A full block of activity was observed in all recorded cells when using 5 mM or 10 mM DMEA (**Figures 1A,B,D,E**). Neither resting membrane potential (RMP) nor AP threshold changed upon DMEA application (**Figures 1C,F, Supplementary Figures S1A,B**), suggesting that intrinsic properties do not represent the main target of DMEA action.

We also investigated the effects of DMEA on epileptiform activity in hippocampal tissue resected from 12 patients undergoing epilepsy surgery. Histopathology of resected tissue revealed distinct pathologies: malformations of cortical development (MCD) were diagnosed in two patients [mild MCD changes in one and clear focal cortical dysplasia (FCD) in the other patient], unspecific astrogliosis in three patients and clear pathological changes indicating hippocampal sclerosis (HS) in seven patients (**Supplementary Table S1**). The changes in pyramidal layers of CA1, CA3 and CA4 included <10% neuronal cell loss in three patients (Wyler grade 1), up to 50% cell loss in three patients (Wyler grade 2) and more than 50% cell loss in one patient (Wyler grade 3).

From these 12 resected samples, a total of 30 hippocampal slices was used for electrophysiological recordings. After slice recovery, we tested our experimental approach by assessing whether: (1) epileptiform activity in human slices can be induced by elevated potassium and 4-AP; (2) whether this activity is stable for prolonged periods of time; and (3) sensitive to conventional AEDs. In 27 slices from 12 patients, both interictal spikes and ictal burst activity (**Figures 2A,B**) could be induced within a few minutes (**Figures 2C,F**). In three slices from three patients, burst events did not occur within 20 min, therefore these slices were excluded from the analysis.

In control recordings without drug application, the pathologically relevant burst activity was stable for at least 60 min (tested in three slices from three patients), suggesting good viability of human slices in our experimental setting. In more detail, both frequency and amplitude of burst activity did not change in most cases during the recording as indicated by stable IEI, amplitude and number of burst events (**Figures 2D,E**).

To test whether burst activity was sensitive to conventional AEDs, we investigated the effect of the sodium channel blocker LAC. During application of LAC, IEI increased in all recorded slices, which was reversible in three out of four patients (**Figure 2G**). Number of events of all recordings decreased during LAC application when compared to baseline activity, while amplitude of burst activity did not change (**Figure 2H**). In conclusion, we were able to induce stable epileptiform activity that can be inhibited by clinically approved AEDs.

Next, we investigated the effects of DMEA in 14 hippocampal slices from 10 TLE patients. In initial experiments, we tested the effects of 5 mM and 10 mM DMEA within one experiment (**Supplementary Figure S2**). As the inhibitory effect was more robust when using 10 mM DMEA (**Supplementary Figure S2B**, $p < 0.05$, $n = 6$; tested in patients 2–7), we decided to perform subsequent experiments with this effective concentration. In contrast to LAC, DMEA effects varied considerably between samples ranging from no effect (patient 8, **Figure 3A**) or only a moderate effect observed in slices of patient 7 (**Figure 3B**) to a full block of burst activity (**Figure 3C**) in four slices from patients 9, 10 and 11. Irrespective of the effect variability, DMEA displayed antiepileptic effects in 10 out of 11 patients (**Figure 4A**), as indicated by the increase of IEI and a significant decrease of number of events during application of DMEA (**Figure 4B**, $p < 0.01$, $n = 10$). In eight patients, these effects were clearly reversible upon wash-out of DMEA. Amplitude of epileptiform bursts was not affected (**Figure 4C**).

Addition of DMEA at 10 mM increases osmolarity of the extracellular environment (here, aCSF) which could possibly decrease epileptiform activity simply by osmotic effects (Traynelis and Dingledine,1989;Dudek et al.,1990).
To test whether DMEA effects are mediated by mechanisms beyond pure change in osmolarity, we investigated how sucrose and DMEA affect epileptiform activity in the same slice when applied sequentially. In six slices of three patients increase of osmolarity by sucrose (310 ± 5 mOsm) to match osmolarity of solutions containing 10 mM DMEA resulted in a weak increase of IEI and a weak decrease of number of events (**Supplementary Figure S3**). This decrease matched the observed decrease without intervention over time as shown in **Figure 2E** and was likely due to a slow decay in activity in the course of *in vitro* experiments. The mild effect of sucrose application stood in contrast to a full block of activity during subsequent application of DMEA in patients 10 and 11 and a strong decrease of activity in patient 12 (**Supplementary Figures S3A,B**).

In summary, in human brain slices DMEA exerted antiepileptic effects presented as an overall decrease in frequency

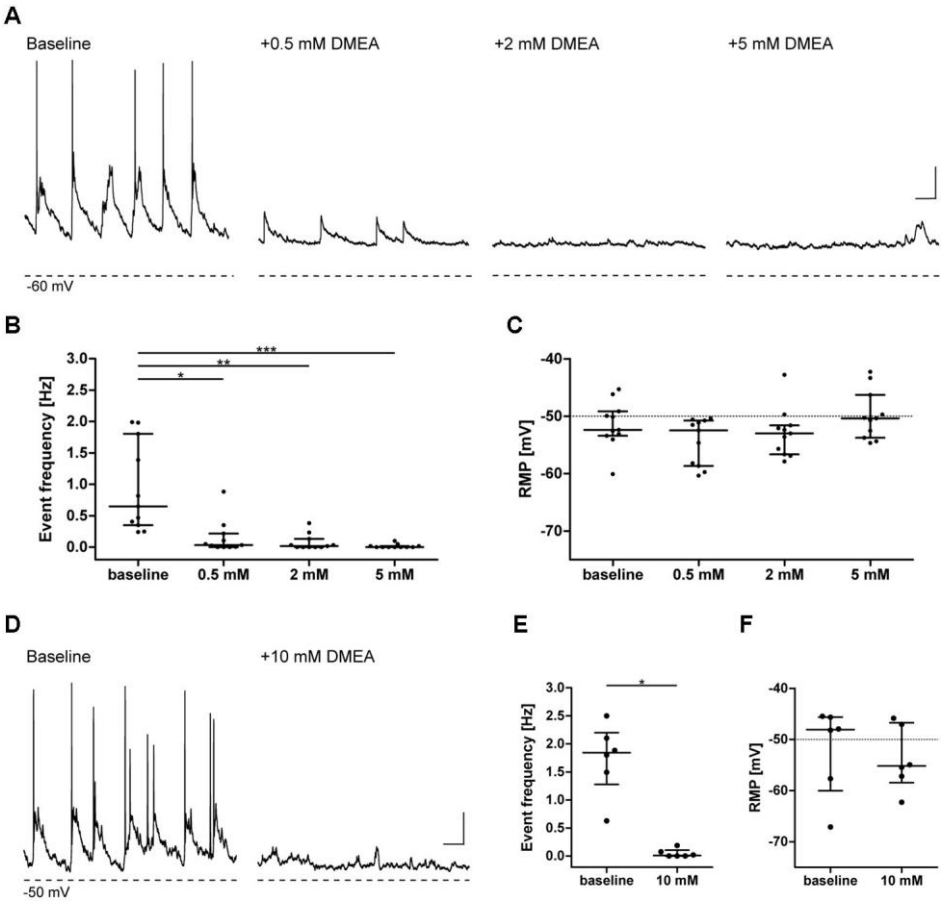

FIGURE 1 | Dimethylethanolamine (DMEA) decreases spontaneous neuronal activity in neuronal cultures in a concentration-dependent manner. Activity of cultured hippocampal neurons (DIV 13–16) was investigated in current-clamp mode in the absence or presence of DMEA. During baseline conditions, all neurons displayed excitatory synaptic events with associated action potentials (APs) at a frequency of ~1 Hz. Both AP, as well as large amplitude synaptic event frequency, decreased with increasing DMEA concentration to reach a full block with 5 mM DMEA. (A,D) Exemplary recordings in neurons with application of 0.0, 0.5, 2.0 and 5.0 mM DMEA (A) or 10 mM DMEA (D); note that due to experimental setup we could not perform repeated measurement in one cell including all concentrations and present the results here separately; Dashed lines below recordings indicate resting membrane potential (RMP, in mV) of cells. (B,E) DMEA significantly decreases event frequency in a concentration-dependent manner. (C,F) Application of DMEA does not affect RMP. All data are shown as scatter plots with median and interquartile range. Asterisks mark significant differences as assessed by Friedman test and *post hoc* by Dunnett's multiple comparison of groups (B,C) or by Wilcoxon signed-rank test (E,F; $^{*}p < 0.05$, $^{**}p < 0.01$, $^{***}p < 0.001$). Scale bar: 10 mV, 0.5 s.

of burst events, which were not due to osmotic changes. A summary of all results is presented in Supplementary Table S2.

DISCUSSION

In the present study, we investigated the effect of DMEA on spontaneous activity in neuronal cultures and on epileptiform activity in human hippocampal tissue *ex vivo*. We were able to show a decrease of spontaneous activity in rodent neuronal cultures. In the majority of investigated human slices, DMEA displayed strong antiepileptic effects including full block of burst activity in slices of three patients. The effect of DMEA in human tissue varied considerably, implying interindividual differences in expression patterns of molecular DMEA targets.

The mechanism of DMEA action is not known. Our preliminary experiments in neuronal cultures showing dose-dependent inhibition of spontaneous neuronal activity without altering RMP or AP threshold suggest that DMEA likely affects synaptic but not intrinsic excitability. In previous clinical studies, DMEA was tested as a potential ACh precursor but did not improve disease symptoms in TD or AD. DMEA increased choline concentrations in plasma and brain though this did not affect brain ACh concentrations, questioning a beneficial effect of DMEA in diseases involving the cholinergic system (Millington et al., 1978; Jope and Jenden, 1979). Nevertheless, due to structural similarities of DMEA, ACh and choline, muscarinic ACh receptors (mAChRs) present possible targets of DMEA action. ACh and choline are both ligands of M2 and M3 mAChRs (Shi et al., 2004; Moreno-Galindo et al., 2016), which upon activation increase the open probability of G-protein coupled inwardly rectifying potassium (GIRK) channels, specifically GIRK1 and GIRK4 (Nemec et al.,1999). GIRK1 and

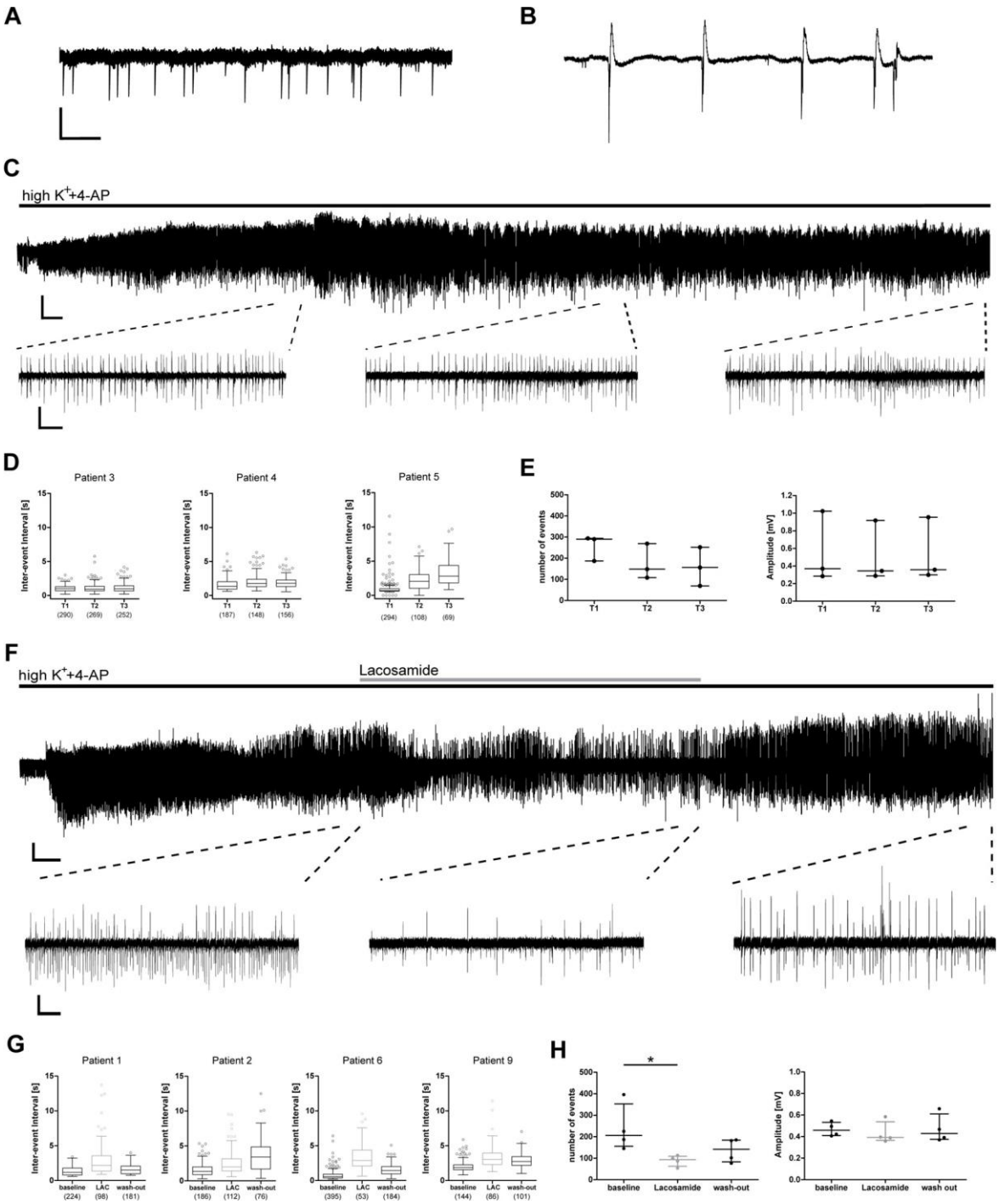

FIGURE 2 | Epileptic burst activity in human slices is stable over long time periods and decreases during application of lacosamide. Application of 8 mM K^+ and 100 μM 4-aminopyridine (4-AP) induces two patterns of network activity recorded by field potential electrodes in the CA1 area of human hippocampal slices: interictal spikes (A) and burst activity (B). (C–E) Burst activity is induced a few minutes after application and stable for at least 60 min. (F–H) Induced burst activity decreases during application of lacosamide (LAC). (C,F) Exemplary recording with excerpts of regions used for analysis. (D,G) Inter-event intervals (IEI) of individual recordings shown as box plots with mean and 1.5× interquartile distance. Each dot represents data point outside the 1.5× interquartile distance. Total number of IEI during analyzed time frame are indicated in brackets. (E,H) Summarized results for all patients [number of events and amplitude as mean ± standard deviation (SD)]; each dot indicates one patient. Asterisks mark significant differences as assessed by Friedman test and *post hoc* with Dunnett's multiple comparison of groups ($p < 0.05$). T1, T2, T3 in (D,E) are periods analyzed for each patient, comparable to analyzed times in (G,H) and Figure 3. Scale bars: 0.2 mV, 500 ms (A,B), 5 min (full recording, C), 2 min (full recording, F), 5 s (excerpts, C,F).

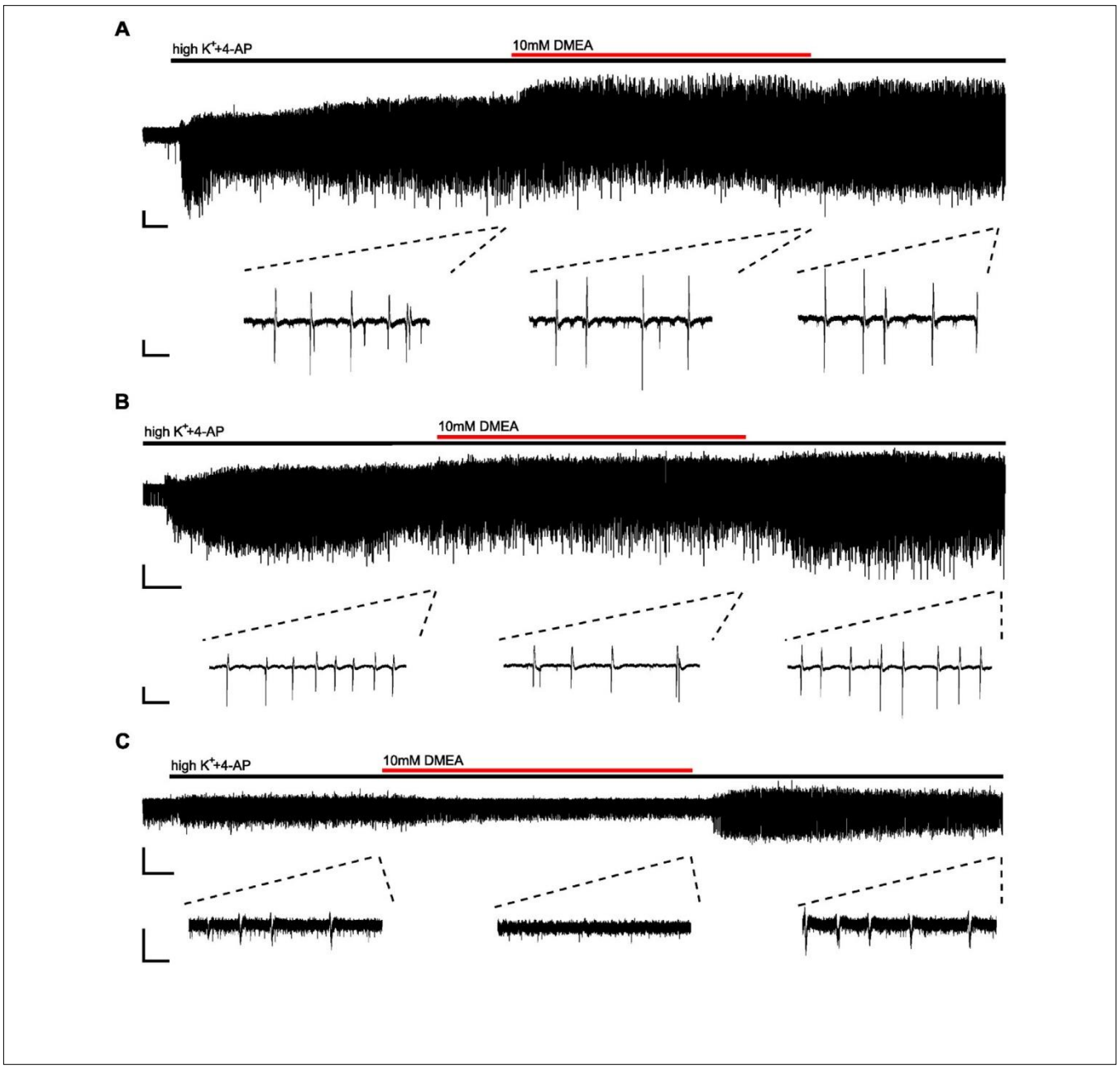

GIRK4 are expressed in the hippocampus (Miyashita and Kubo,1997;Murer et al.,1997;Cea-del Rio et al.,2010) and pharmacological activation of GIRK results in antiepileptic effects *in vitro* and *in vivo* (Kaufmann et al.,2013). Thus, M2 or M3 mAChRs and GIRK channels present a possible mechanism for DMEA action.

Another possible candidate are glycine receptors (GlyR). In a separate project, our group analyzed the effects of DMEA on GlyR, which has been described as subject to increased RNA editing in TLE (Krestel et al.,2013;Winkelmann et al., 2014;Meier et al.,2016;Srivastava et al.,2017). Presynaptic RNA-edited GlyR facilitates neurotransmitter release resulting in increased neuronal gain and, depending on the neuronal subtype, network hyper- or hypoexcitability (Winkelmann et al.,2014;Caliskan et al.,2016). In an initial screen for antagonists against RNA-edited GlyR (data not shown), DMEA was considered as a candidate giving an additional incentive to test this substance in human brain slices. However, confirmatory experiments were not able to reproduce DMEA specificity against RNA-edited GlyR. Overall, the molecular targets of DMEA and its mechanism of action in brain tissue remain indeterminate.

The main goal of our study was to demonstrate a possibly clinically relevant effect of DMEA. DMEA has been tested in patients and healthy volunteers since 1960s (Murphree et al., 1960; Pfeiffer et al., 1963). In healthy males,

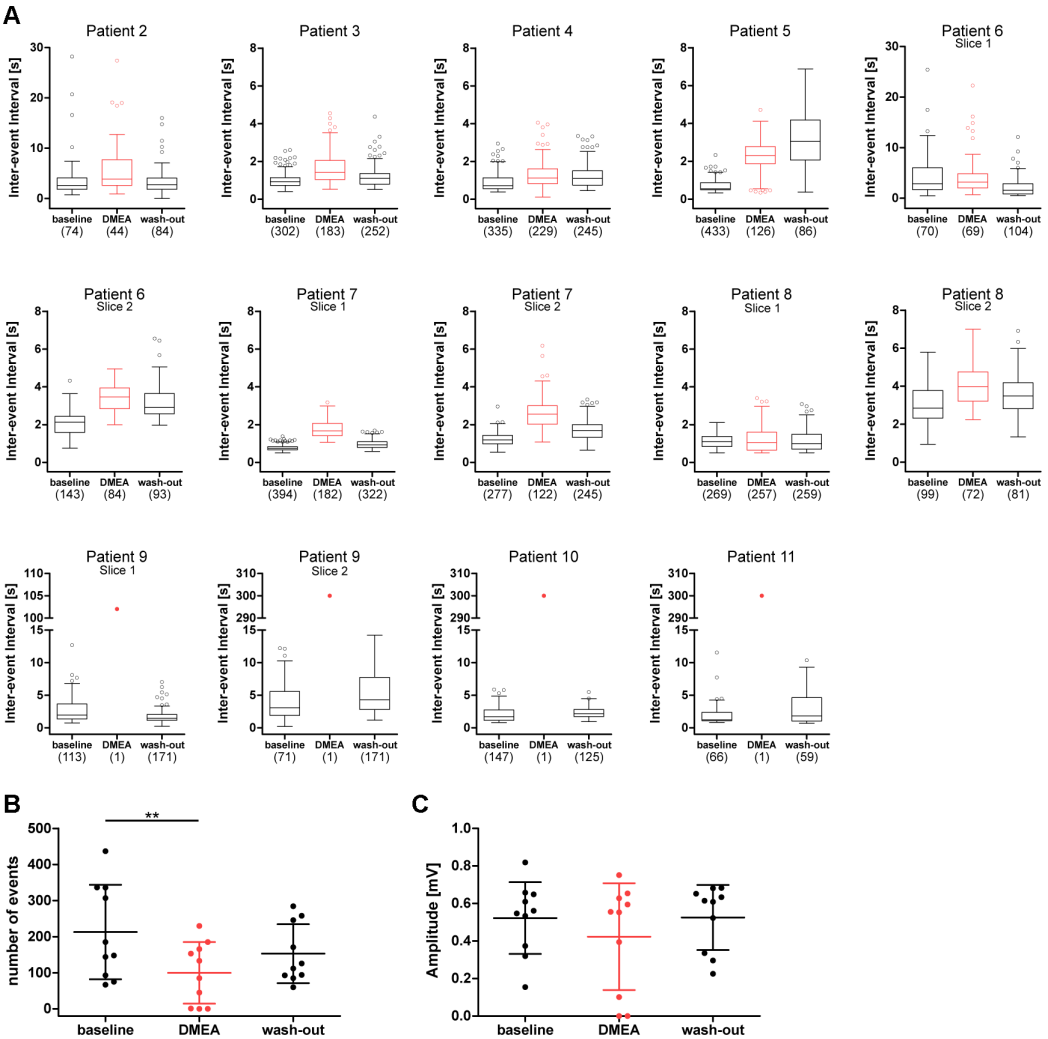

FIGURE 4 | DMEA reduces epileptiform activity in human hippocampal slices. Summary of DMEA effects on burst activity recorded in CA1 pyramidal cell layer of resected human hippocampus. (A) Box plots of IEIs with mean and 1.5× interquartile distance before, during and after DMEA application for each patient are shown for all recorded slices ($n = 10$ patients). Dots represent data points outside the 1.5× interquartile distance. Total number of IEI during analyzed time frame are indicated in brackets. (B) Summary of DMEA effects on number and (C) amplitude of burst events for all patients; each dot indicates one patient. Data is presented as scatter plots with mean ± SD, asterisks mark significant differences as assessed by repeated measurement analysis of variance (ANOVA) and *post hoc* with Tukey's comparison ($^{**}p < 0.01, n = 10$).

Murphree et al. (1960) reported no change in heart rate, body weight, muscle power, hand steadiness or vital capacity with an intake of 10–20 mg DMEA (or Deanol) daily for 2–3 weeks. In two double-blinded, placebo-controlled studies of TD, DMEA led to side effects such as lethargy, drowsiness and a mild but significant increase in the schizophrenia score (de Montigny et al., 1979; George et al., 1981), although a systematic review was not able to confirm an increased risk for psychosis (Tammenmaa et al.,2004).Fisman et al. (1981)detected severe neurological and cardiovascular effects (apathy, motor retardation, increased confusion associated with rise in systolic and diastolic blood pressure) in two patients with AD when treated with 1,800 mg DMEA daily. In these studies, as compared to Murphree et al. (1960), DMEA was administered in a 100-fold higher daily dosage (10–20 mg vs. 1,000–2,000 mg). A dose of 2,000 mg DMEA corresponds to a molar amount of 22 mM and a final *in vivo* concentration of 0.44 mM assuming a distribution across all compartments and a body water content of approximately 50 l for an adult male. This concentration is lower by a factor of 20 when compared to 10 mM tested to be effective in human brain tissue *ex vivo* in our study, and this difference is rather underestimated when taking into account oral bioavailability. Of note, in neuronal cultures, the effective concentration to inhibit neuronal activity was lower by a factor of 10, implying that differences in microenvironment, neuronal connectivity and drug diffusion in different preparations and species might influence the effective concentration.

Addition of DMEA to our experimental solution increased the osmolarity by ~10 mOsm. In previous studies, application of hyperosmolar solutions decreased neuronal excitability and epileptiform activity, but in most cases, an increase of 30 mOsm and more was necessary to induce these effects (Traynelis and Dingledine, 1989; Dudek et al., 1990; Rosen and Andrew, 1990). According to Rosen and Andrew (1990), an increase of extracellular osmolarity by 10 mOsm might result in a 10% decrease of EPSC amplitude in CA1 pyramidal neurons, but the effects of such EPSC alteration on network activity have not been investigated. Here, increase of aCSF osmolarity by application of 10 mM sucrose did not alter epileptiform activity, indicating that the antiepileptic effects of DMEA are not primarily mediated by changes in osmolarity.

Although our study clearly demonstrated an antiepileptic effect of DMEA, the large concentration difference between our work and previous clinical studies and the variability of underlying pathologies represent substantial limitations. The results suggest heterogeneous expression of DMEA targets, however, also differences in neuronal survival and the degree of HS could possibly contribute. An additional limitation is given by different transport solutions used in our study, namely either NMDG or choline aCSF (Testa-Silva et al., 2010; Eyal et al., 2018; Ting et al., 2018). Although we were unable to detect differences in tissue quality as seen by stable induction and properties of epileptiform activity, we cannot exclude differences in neuronal survival between these solutions.

The predictive value of brain activity for drug development in an *ex vivo* setting is still unclear. In our approach using a modified submerged chamber, we mostly observed burst activity (spike and burst activity) described before as interictal-like (Remy et al., 2003; Gabriel et al., 2004; Sandow et al., 2015; Reyes-Garcia et al., 2018) and standing in contrast to ictal discharges lasting >10 s. Brückner and Heinemann (2000) suggested that AEDs applied in brain slices (of non-epileptic animals) rather inhibit ictal but not interictal activity. Other animal studies *in vitro*, however, demonstrated a robust decrease in interictal activity in the hippocampus upon AED application (Fueta and Avoli, 1992; Holtkamp et al., 2017; Taing et al., 2017), which was comparable to our results with LAC and DMEA. We show that burst activity was sensitive to the approved antiepileptic LAC, indicating that our experimental setting is capable of validating and possibly predicting antiepileptic efficacy for drug development.

Taken together, our work identified the antiepileptic effect of DMEA in human hippocampal tissue from TLE patients. Interindividual effect variability, differences in the effective concentration range and previously reported side effects call for future, more detailed investigation of cell-type specific effects and molecular targets of DMEA.

DATA AVAILABILITY

All datasets generated for this study are included in the manuscript and/or the Supplementary Files. Human datasets analyzed in this study can be found in figshare repository (https://doi.org/10.6084/m9.figshare.8148572).

ETHICS STATEMENT

The studies involving human participants were reviewed and approved by Charité-Universitätsmedizin Berlin (EA2/111/14). The patients/participants provided their written informed consent to participate in this study. The animal study was reviewed and approved by Animal Care Committee of the Technical University Braunschweig (Zentrale Einrichtung für Tierhaltung der TU Braunschweig, §4 10.15.R TSB TU BS).

AUTHOR CONTRIBUTIONS

JM and PF designed the study. MH selected patients for operation. US operated patients. HR performed histopathological analysis. LK performed and analyzed recordings in human tissue. FH performed neuronal experiments. LK and FH analyzed neuronal experiments. LK and PF wrote the manuscript, which all authors edited and finalized.

FUNDING

JM thanks the Deutsche Forschungsgemeinschaft (DFG; Priority Programme SPP1784 ME2075/7-1).

ACKNOWLEDGMENTS

We thank Mandy Marbler-Pötter (Charite Unversitätsmedizin, Berlin) for excellent technical assistance and Tabea Tito for assistance with clinical data on patients.

SUPPLEMENTARY MATERIAL

The Supplementary Material for this article can be found online at:https://www.frontiersin.org/articles/10.3389/fnmol.2019.00209/full#supplementary-material

FIGURE S1 | DMEA does not change action potential threshold. Application of 10 mM DMEA does not change threshold for AP generation. (A) Exemplary recordings of patch-clamp recordings in current-clamp mode with step current without AP (first for each) and with AP generation (second); dashed lines below recordings show −60 mV value to indicate RMP of cells. (B) Quantified effect of DMEA on AP threshold in neurons. Data are shown as median with interquartile range and was subjected to Wilcoxon signed-rank test; $n = 6$.

FIGURE S2 | Dose-dependent effects of DMEA on epileptiform activity in human hippocampal slices. (A) Box plots of inter-event intervals (IEI) during baseline, 5 mM DMEA, 10 mM DMEA and wash-out for each patient given for all recorded slices ($n = 6$ patients). In all experiments, both concentrations were applied in the same brain slice. Box plots are shown with mean and Tukey whiskers (1.5× interquartile distance). Each dot represents a data point outside the 1.5× interquartile distance. Total number of IEI during analyzed time frame are indicated in brackets. (B) Summary of DMEA effects on the number and amplitude of burst

events for all tested patients; each dot indicates one patient. Data are presented as scatter plots with median ± interquartile range. Asterisks mark significant differences as assessed by Friedman test and *post hoc* with Dunnett's multiple comparison of groups ($^*p < 0.05$).

FIGURE S3 | Increase of osmolarity by 10 mOsm does not affect epileptiform activity. For control purposes, sucrose was used to increase osmolarity and applied in the same slice before DMEA application. (A) Full time course and detailed excerpts of exemplary recording used for the analysis of potential hyperosmotic effects of DMEA on epileptiform activity. Note that sucrose application leading to the same osmotic change as DMEA does not significantly alter epileptiform activity, while DMEA application in the same slice clearly exerts an antiepileptic effect. (B) Inter-event intervals of individual recordings shown as box plots with a total number of IEI during analyzed time frames indicated in brackets. (C) Summarized number of events and amplitudes for all patients presented as scatterplots with median and interquartile range; each dot indicates one patient. Scale bars: 0.2 mV, 5 min (full recordings), 5 s (excerpts).

TABLE S1 | Clinical data of patients, who provided tissue for electrophysiological assessment of the effects of DMEA on epileptic activity.

TABLE S2 | Summarized results of burst activity in human tissue during application of DMEA, LAC, no intervention or sucrose as control for osmolarity effects.

REFERENCES

Antonio, L. L., Anderson, M. L., Angamo, E. A., Gabriel, S., Klaft, Z. J., Liotta, A., et al. (2016). *In vitro* seizure like events and changes in ionic concentration. *J. Neurosci. Methods* 260, 33–44.doi: 10.1016/j.jneumeth.2015.08.014

Avoli, M., D'Antuono, M., Louvel, J., Köhling, R., Biagini, G., Pumain, R., et al. (2002). Network and pharmacological mechanisms leading to epileptiform synchronization in the limbic system *in vitro*. *Prog. Neurobiol.* 68, 167–207. doi: 10.1016/s0301-0082(02)00077-1

Brewer, G. J., Torricelli, J. R., Evege, E. K., and Price, P. J. (1993). Optimized survival of hippocampal neurons in B27-supplemented Neurobasal, a new serum-free medium combination. *J. Neurosci.* 35, 567–576.doi: 10.1002/jnr.490350513

Brückner, C., and Heinemann, U. (2000). Effects of standard anticonvulsant drugs on different patterns of epileptiform discharges induced by 4-aminopyridine in combined entorhinal cortex-hippocampal slices. *Brain Res.* 859, 15–20. doi: 10.1016/s0006-8993(99)02348-3

Caliskan, G., Müller, I., Semtner, M., Winkelmann, A., Raza, A. S., Hollnagel, J. O., et al. (2016). Identification of parvalbumin interneurons as cellular substrate of fear memory persistence. *Cereb. Cortex* 26, 2325–2340. doi: 10.1093/cercor/bhw001

Cea-del Rio, C. A., Lawrence, J. J., Tricoire, L., Erdelyi, F., Szabo, G., and McBain, C. J. (2010). M3 muscarinic acetylcholine receptor expression confers differential cholinergic modulation to neurochemically distinct hippocampal basket cell subtypes. *J. Neurosci.* 30, 6011–6024.doi: 10.1523/JNEUROSCI.5040-09.2010

D'Antuono, M., Köhling, R., Ricalzone, S., Gotman, J., Biagini, G., and Avoli, M. (2010). Antiepileptic drugs abolish ictal but not interictal epileptiform discharges *in vitro*. *Epilepsia* 51, 423–431.doi: 10.1111/j.1528-1167.2009.02273.x

de Montigny, C., Chouinard, G., and Annable, L. (1979). Ineffectiveness of deanol in tardive dyskinesia: a placebo controlled study. *Psychopharmacology* 65, 219–223.doi: 10.1007/bf00492207

Dibué-Adjei, M., Brigo, F., Yamamoto, T., Vonck, K., and Trinka, E. (2019). Vagus nerve stimulation in refractory and super-refractory status epilepticus—a systematic review. *Brain Stimul.* doi: 10.1016/j.brs.2019.05.011[Epub ahead of print].

Dudek, F. E., Obenaus, A., and Tasker, J. G. (1990). Osmolality-induced changes in extracellular volume alter epileptiform bursts independent of chemical synapses in the rat: importance of non-synaptic mechanisms in hippocampal epileptogenesis. *Neurosci. Lett.* 120, 267–270.doi: 10.1016/0304-3940(90)90056-f

Engel, J., Wiebe, S., French, J., Sperling, M., Williamson, P., Spencer, D., et al. (2007). Practice parameter: temporal lobe and localized neocortical resections for epilepsy. *Contin. Lifelong Learn. Neurol.* 13, 225–234.doi: 10.1212/01.CON.0000284531.20401.00

Eyal, G., Verhoog, M. B., Testa-Silva, G., Deitcher, Y., Benavides-Piccione, R., DeFelipe, J., et al. (2018). Human cortical pyramidal neurons: from spines to spikes *via* models. *Front. Cell. Neurosci.* 12:181.doi: 10.3389/fncel.2018.00181

Falco-Walter, J. J., Roehl, K., Ouyang, B., and Balabanov, A. (2019). Do certain subpopulations of adults with drug-resistant epilepsy respond better to modified ketogenic diet treatments? Evaluation based on prior resective surgery, type of epilepsy, imaging abnormalities, and vagal nerve stimulation. *Epilepsy Behav.* 93, 119–124.doi: 10.1016/j.yebeh.2019.01.010

Ferris, S. H., Sathananthan, G., Gershon, S., and Clark, C. (1977). Senile dementia: treatment with deanol†. *J. Am. Geriatr. Soc.* 25, 241–244.doi: 10.1111/j.1532-5415.1977.tb00407.x

Fisman, M., Mersky, H., and Helmes, E. (1981). Double-blind trial of 2-dimethylaminoethanol in Alzheimer's disease. *Am. J. Psychiatry* 138, 970–972.doi: 10.1176/ajp.138.7.970

Fueta, Y., and Avoli, M. (1992). Effects of antiepileptic drugs on 4-aminopyridine-induced epileptiform activity in young and adult rat hippocampus. *Epilepsy Res.* 12, 207–215.

Gabriel, S., Njunting, M., Pomper, J. K., Merschhemke, M., Sanabria, E. R. G., Eilers, A., et al. (2004). Stimulus and potassium-induced epileptiform activity in the human dentate gyrus from patients with and without hippocampal sclerosis. *J. Neurosci.* 24, 10416–10430.doi: 10.1523/jneurosci.2074-04.2004

George, J., Pridmore, S., and Aldous, D. (1981). Double blind controlled trial of deanol in tardive dyskinesia. *Aust. New Zeal. J. Psychiatry* 15, 68–71. doi: 10.3109/00048678109159413

Giordano, C., Marchiò, M., Timofeeva, E., and Biagini, G. (2014). Neuroactive peptides as putative mediators of antiepileptic ketogenic diets. *Front. Neurol.* 5:63.doi: 10.3389/fneur.2014.00063

Hallböök, T., Sjölander, A., Åmark, P., Miranda, M., Bjurulf, B., and Dahlin, M. (2015). Effectiveness of the ketogenic diet used to treat resistant childhood epilepsy in Scandinavia. *Eur. J. Paediatr. Neurol.* 19, 29–36.doi: 10.1016/j.ejpn.2014.09.005

Heuzeroth, H., Wawra, M., Fidzinski, P., Dag, R., and Holtkamp, M. (2019). The 4-aminopyridine model of acute seizures *in vitro* elucidates efficacy of new antiepileptic drugs. *Front. Neurosci.* 13:677.doi: 10.3389/fnins.2019.00677

Hill, M. R. H., and Greenfield, S. A. (2011). The membrane chamber: a new type of *in vitro* recording chamber. *J. Neurosci. Methods* 195, 15–23.doi: 10.1016/j.jneumeth.2010.10.024

Hirtz, D., Thurman, D. J., Gwinn-Hardy, K., Mohamed, M., Chaudhuri, A. R., and Zalutsky, R. (2007). How common are the ''common'' neurologic disorders? *Neurology* 68, 326–337.doi: 10.1212/01.wnl.0000252807.38124.a3

Holtkamp, D., Opitz, T., Niespodziany, I., Wolff, C., and Beck, H. (2017). Activity of the anticonvulsant lacosamide in experimental and human epilepsy *via* selective effects on slow Na^+ channel inactivation. *Epilepsia* 58, 27–41. doi: 10.1111/epi.13602

Jope, R. S., and Jenden, D. J. (1979). Dimethylaminoethanol (deanol) metabolism in rat brain and its effect on acetyicholine synthesis1. *J. Pharmacol. Exp. Ther.* 211, 472–479.

Kaufmann, K., Romaine, I., Days, E., Pascual, C., Malik, A., Yang, L., et al. (2013). ML297 (VU0456810), the first potent and selective activator of the GIRK potassium channel, displays antiepileptic properties in mice. *ACS Chem. Neurosci.* 4, 1278–1286.doi: 10.1021/cn400062a

Kowski, A. B., Voges, J., Heinze, H.-J., Oltmanns, F., Holtkamp, M., and Schmitt, F. C. (2015). Nucleus accumbens stimulation in partial epilepsy-A randomized controlled case series. *Epilepsia* 56, e78–e82.doi: 10.1111/epi.12999

Krestel, H., Raffel, S., von Lehe, M., Jagella, C., Moskau-Hartmann, S., Becker, A., et al. (2013). Differences between RNA and DNA due to RNA editing in temporal lobe epilepsy. *Neurobiol. Dis.* 56, 66–73.doi: 10.1016/j.nbd.2013.04.006

Ledri, M., Sørensen, A. T., Madsen, M. G., Christiansen, S. H., Ledri, L. N., Cifra, A., et al. (2015). Differential effect of neuropeptides on excitatory

synaptic transmission in human epileptic hippocampus. *J. Neurosci.* 35, 9622–9631.doi: 10.1523/JNEUROSCI.3973-14.2015

Löscher, W. (2011). Critical review of current animal models of seizures and epilepsy used in the discovery and development of new antiepileptic drugs. *Seizure* 20, 359–368.doi: 10.1016/j.seizure.2011.01.003

Meier, J. C., Kankowski, S., Krestel, H., and Hetsch, F. (2016). RNA editing-systemic relevance and clue to disease mechanisms? *Front Mol. Neurosci.* 9:124. doi: 10.3389/fnmol.2016.00124

Millington, W. R., McCall, A. L., and Wurtman, R. J. (1978). Deanol acetamidobenzoate inhibits the blood brain barrier transport of choline. *Ann. Neurol.* 4, 302–306.doi: 10.1002/ana.410040403

Miyashita, T., and Kubo, Y. (1997). Localization and developmental changes of the expression of two inward rectifying K^+-channel proteins in the rat brain. *Brain Res.* 750, 251–263.doi: 10.1016/s0006-8993(96)01365-0

Mohan, M., Keller, S., Nicolson, A., Biswas, S., Smith, D., Osman Farah, J., et al. (2018). The long-term outcomes of epilepsy surgery. *PLoS One* 13:e0196274. doi: 10.1371/journal.pone.0196274

Moreno-Galindo, E. G., Sanchez-Chapula, J. A., Tristani-Firouzi, M., and Navarro-Polanco, R. A. (2016). Pharmacological conversion of a cardiac inward rectifier into an outward rectifier potassium channel. *Mol. Pharmacol.* 90, 334–340.doi: 10.1124/mol.116.104950

Murer, G., Adelbrecht, C., Lauritzen, I., Lesage, F., Lazdunski, M., Agid, Y., et al. (1997). An immunocytochemical study on the distribution of two G-protein-gated inward rectifier potassium channels (GIRK2 and GIRK4) in the adult rat brain. *Neuroscience* 80, 345–357.doi: 10.1016/s0306-4522(97)00001-8

Murphree, H. B. Jr., Pfeiffer, C. C., and Backerman, I. A. (1960). The stimulant effect of 2-dimethylaminoethanol (deanol) in human volunteer subiects. *Clin. Pharmacol. Ther.* 1, 303–310.doi: 10.1002/cpt196013303

Nemec, J., Wickman, K., and Clapham, D. E. (1999). Gβγ binding increases the open time of IKACh: kinetic evidence for multiple Gβγ binding sites. *Biophys. J.* 76, 246–252.doi: 10.1016/s0006-3495(99)77193-6

Ngugi, A. K., Bottomley, C., Kleinschmidt, I., Sander, J. W., and Newton, C. R. (2010). Estimation of the burden of active and life-time epilepsy: a meta-analytic approach. *Epilepsia* 51, 883–890.doi: 10.1111/j.1528-1167.2009.02481.x

Penovich, P., Morgan, J. P., Kerzner, B., Karch, F., and Goldblatt, D. (1978). Double-blind evaluation of deanol in tardive dyskinesia. *JAMA J. Am. Med. Assoc.* 239, 1997–1998.doi: 10.1001/jama.1978.03280460065020

Perreault, P., and Avoli, M. (1991). Physiology and pharmacology of epileptiform activity induced by 4-aminopyridine in rat hippocampal slices. *J. Neurophysiol.* 65, 771–785.doi: 10.1152/jn.1991.65.4.771

Pfeiffer, C. C., Goldstein, L., Munoz, C., Murphree, H. B., and Jenney, E. H. (1963). Quantitative comparisons of the electroencephalographic stimulant effects of deanol, choline, and amphetamine. *Clin. Pharmacol. Ther.* 4, 461–466. doi: 10.1002/cpt196344461

Remy, S., Gabriel, S., Urban, B. W., Dietrich, D., Lehmann, T. N., Elger, C. E., et al. (2003). A novel mechanism underlying drug resistance in chronic epilepsy. *Ann. Neurol.* 53, 469–479.doi: 10.1002/ana.10473

Reyes-Garcia, S. Z., Scorza, C. A., Araújo, N. S., Ortiz-Villatoro, N. N., Jardim, A. P., Centeno, R., et al. (2018). Different patterns of epileptiform-like activity are generated in the sclerotic hippocampus from patients with drug-resistant temporal lobe epilepsy. *Sci. Rep.* 8:7116.doi: 10.1038/s41598- 018-25378-9

Rosen, A. S., and Andrew, R. D. (1990). Osmotic effects upon excitability in rat neocortical slices. *Neuroscience* 38, 579–590.doi: 10.1016/0306-4522(90)90052-6

Rosenmund, C., and Stevens, C. F. (1996). Definition of the readily releasable pool of vesicles at hippocampal synapses. *Neuron* 16, 1197–1207. doi: 10.1016/s0896-6273(00)80146-4

Sandow, N., Kim, S., Raue, C., Päsler, D., Klaft, Z.-J., Antonio, L. L., et al. (2015). Drug resistance in cortical and hippocampal slices from resected tissue of epilepsy patients: no significant impact of p-glycoprotein and multidrug resistance-associated proteins. *Front. Neurol.* 6:30.doi: 10.3389/fneur.2015.00030

Shekh-Ahmad, T., Bialer, M., and Yavin, E. (2012). Synthesis and anticonvulsant evaluation of dimethylethanolamine analogues of valproic acid and its tetramethylcyclopropyl analogue. *Epilepsy Res.* 98, 238–246.doi: 10.1016/j.eplepsyres.2011.10.005

Shi, H., Wang, H., Yang, B., Xu, D., and Wang, Z. (2004). The M_3 receptor-mediated K^+ current (I_{KM3}), a G_q protein-coupled K^+ channel. *J. Biol. Chem.* 279, 21774–21778.doi: 10.1074/jbc.C400100200

Spencer, S. S., Goncharova, I. I., Duckrow, R. B., Novotny, E. J., and Zaveri, H. P. (2008). Interictal spikes on intracranial recording: behavior, physiology, and implications. *Epilepsia* 49, 1881–1892.doi: 10.1111/j.1528-1167.2008.01641.x

Srivastava, P. K., Bagnati, M., Delahaye-Duriez, A., Ko, J.-H., Rotival, M., Langley, S. R., et al. (2017). Genome-wide analysis of differential RNA editing in epilepsy. *Genome Res.* 27, 440–450.doi: 10.1101/gr.210740.116

Stephen, L. J., Kwan, P., and Brodie, M. J. (2001). Does the cause of localisation-related epilepsy influence the response to antiepileptic drug treatment? *Epilepsia* 42, 357–362.doi: 10.1046/j.1528-1157.2001.29000.x

Taing, K. D., O'Brien, T. J., Williams, D. A., and French, C. R. (2017). Anti-epileptic drug combination efficacy in an *in vitro* seizure model—phenytoin and valproate, lamotrigine and valproate. *PLoS One* 12:e0169974. doi: 10.1371/journal.pone.0169974

Tammenmaa, I. A., Sailas, E., McGrath, J. J., Soares-Weiser, K., and Wahlbeck, K. (2004). Systematic review of cholinergic drugs for neuroleptic-induced tardive dyskinesia: a meta-analysis of randomized controlled trials. *Prog. Neuropsychopharmacol. Biol. Psychiatry* 28, 1099–1107.doi: 10.1016/j.pnpbp.2004.05.045

Testa-Silva, G., Verhoog, M. B., Goriounova, N. B., Loebel, A., Hjorth, J., Baayen, J. C., et al. (2010). Human synapses show a wide temporal window for spike-timing-dependent plasticity. *Front. Synaptic Neurosci.* 2:12. doi: 10.3389/fnsyn.2010.00012

Ting, J. T., Daigle, T. L., Chen, Q., and Feng, G. (2014). Acute brain slice methods for adult and aging animals: application of targeted patch clamp analysis and optogenetics. *Methods Mol. Biol.* 1183, 221–242.doi: 10.1007/978-1-4939-1096-0_14

Ting, J. T., Kalmbach, B., Chong, P., de Frates, R., Keene, C. D., Gwinn, R. P., et al. (2018). A robust *ex vivo* experimental platform for molecular-genetic dissection of adult human neocortical cell types and circuits. *Sci. Rep.* 8:8407. doi: 10.1038/s41598-018-26803-9

Traynelis, S. F., and Dingledine, R. (1989). Role of extracellular space in hyperosmotic suppression of potassium-induced electrographic seizures. *J. Neurophysiol.* 61, 927–938.doi: 10.1152/jn.1989.61.5.927

Wiebe, S., Blume, W. T., Girvin, J. P., Eliasziw, M., and Effectiveness and Efficiency of Surgery for Temporal Lobe Epilepsy Study Group. (2001). A randomized, controlled trial of surgery for temporal-lobe epilepsy. *N. Engl. J. Med.* 345, 311–318.doi: 10.1056/nejm200108023450501

Winkelmann, A., Maggio, N., Eller, J., Caliskan, G., Semtner, M., Häussler, U., et al. (2014). Changes in neural network homeostasis trigger neuropsychiatric symptoms. *J. Clin. Invest.* 124, 696–711.doi: 10.1172/jci71472

Zangiabadi, N., Ladino, L. D., Sina, F., Orozco-Hernández, J. P., Carter, A., and Téllez-Zenteno, J. F. (2019). Deep brain stimulation and drug-resistant epilepsy: a review of the literature. *Front. Neurol.* 10:601.doi: 10.3389/fneur.2019.00601

Conflict of Interest Statement: The authors declare that the research was conducted in the absence of any commercial or financial relationships that could be construed as a potential conflict of interest.

Publication 3: Le Duigou et al., 2018

Le Duigou C, Savary E, Morin-Brureau M, Gomez-Dominguez D, Sobczyk A, Chali F, Milior G, **Kraus L**, Meier JC, Kullmann DM, Mathon B, de la Prida LM, Dorfmuller G, Pallud J, Eugène E, Clemenceau S, Miles R. Imaging pathological activities of human brain tissue in organotypic culture. J Neurosci Methods. 2018
https://doi.org/10.1016/j.jneumeth.2018.02.001

11. Curriculum Vitae

My curriculum vitae is not published in the electronic version of my work for reasons of data protection.

Complete list of own publications

1. Agostinho, A. S., Mietzsch, M., Zangrandi, L., Kmiec, I., Mutti, A., **Kraus, L**., Fidzinski, P., Schneider, U. C., Holtkamp, M., Heilbronn, R. & Schwarzer, C. Dynorphin-based 'release on demand' gene therapy for drug-resistant temporal lobe epilepsy. EMBO Mol. Med. 11, e9963 (2019).

2. Böttcher, C., Schlickeiser, S., Sneeboer, M. A. M., Kunkel, D., Knop, A., Paza, E., Fidzinski, P., **Kraus, L.**, Snijders, G. J. L., Kahn, R. S., Schulz, A. R., Mei, H. E., Hol, E. M., Siegmund, B., Glauben, R., Spruth, E. J., de Witte, L. D. & Priller, J. Human microglia regional heterogeneity and phenotypes determined by multiplexed single-cell mass cytometry. Nat. Neurosci. 22, 78–90 (2019).

3. Jurek, B., Chayka, M., Kreye, J., Lang, K., **Kraus, L.**, Fidzinski, P., Kornau, H., Dao, L., Wenke, N. K., Long, M., Rivalan, M., Winter, Y., Leubner, J., Herken, J., Mayer, S., Mueller, S., Boehm-Sturm, P., Dirnagl, U., Schmitz, D., Kölch, M. & Prüss, H. Human gestational N-methyl-d-aspartate receptor autoantibodies impair neonatal murine brain function. Ann. Neurol. 86, 656–670 (2019).

4. **Kraus, L.**, Hetsch, F., Schneider, U. C., Radbruch, H., Holtkamp, M., Meier, J. C. & Fidzinski, P. Dimethylethanolamine Decreases Epileptiform Activity in Acute Human Hippocampal Slices in vitro. Front. Mol. Neurosci. 12, 209 (2019).

5. Le Duigou, C., Savary, E., Morin-Brureau, M., Gomez-Dominguez, D., Sobczyk, A., Chali, F., Milior, G., **Kraus, L.**, Meier, J. C., Kullmann, D. M., Mathon, B., de la Prida, L. M., Dorfmuller, G., Pallud, J., Eugène, E., Clemenceau, S. & Miles, R. Imaging pathological activities of human brain tissue in organotypic culture. J. Neurosci. Methods 298, 33–44 (2018).

6. Schneidereit, D., **Kraus, L.**, Meier, J. C., Friedrich, O. & Gilbert, D. F. Step-by-step guide to building an inexpensive 3D printed motorized positioning stage for automated high-content screening microscopy. Biosens. Bioelectron. 92, 472–481 (2017).

12. Acknowledgments

I would like to thank my supervisors, who all helped shape this PhD thesis in their individual ways.

Prof. Martin Holtkamp, I would like to thank you for giving me the opportunity to work in the group of experimental epileptology and giving me the opportunity to learn more about the clinical aspect of neuroscience.

Prof. Jochen Meier, thank you for all your scientific input and drafting the project. Without your spontaneous ideas and enthusiasm would have not gotten the results or the thesis I have now.

PD Pawel Fidzinski, your supervision was the key to finishing this project. You have been a great teacher in the lab and taught me how to be more diplomatic. Thank you for never losing patience in our many discussions and having the patience to explain to me (sometimes) why I was wrong. Thank you for all the laughs we had and believing in me and what I can do.

Thanks to the people of my lab: Mandy, without you at my back, I would have never been able to do any experiments. Thanks to Matthias for always explaining Matlab to me and watching funny videos together instead of working. Laura, I have found a friend in you that I hope to keep for the rest of my life. I will miss our seemingly endless discussions and making sarcastic jokes that you never get.

Thanks to all my friends, old and new who have been a constant source of fun and inspiration during some of the hardest times of my PhD: Eileen, Stephie, Betty, Anniki, Cami, Lisa, Moni, Ina, Claudia and the famous Marc!

Finally, I thank my family. I know every one of you has my back and would jump in to help me whenever I need it! Most of all, my sister Natascha, who not only fed me for 2 whole years, but has been nothing but supportive during this long 5 years!